Optimization-based Microgrid Energy Management Systems

OPTIMIZATION-BASED MICROGRID ENERGY MANAGEMENT SYSTEMS

BY

ADHITHYA RAVICHANDRAN, M.Sc.,

McMaster University, Hamilton, Canada

A THESIS

SUBMITTED TO THE DEPARTMENT OF ELECTRICAL & COMPUTER ENGINEERING

AND THE SCHOOL OF GRADUATE STUDIES

OF MCMASTER UNIVERSITY

IN PARTIAL FULFILMENT OF THE REQUIREMENTS

FOR THE DEGREE OF

DOCTOR OF PHILOSOPHY

Doctor of Philosophy (2016) McMaster University

(Electrical & Computer Engineering) Hamilton, Ontario, Canada

TITLE:	Optimization-based Microgrid Energy Management Systems
AUTHOR:	Adhithya Ravichandran B.Eng., (Electronics & Communication Engineering) Anna University, Chennai, India
SUPERVISOR:	Dr. Shahin Sirouspour & Dr. Ali Emadi
NUMBER OF PAGES:	xvi, 197

To my parents Dr. P. Ravichandran & Dr. T. Rajarajeswari, who supported me from across the world

And to many a friend from McMaster & Hamilton who gave me a community throughout my doctoral studies

Abstract

Energy management strategies for microgrids, containing energy storage, renewable energy sources (RES), and electric vehicles (EVs); which interact with the grid on an individual basis; are presented in Chapter 3. An optimization problem to reduce cost, formulated over a rolling time horizon, using predicted values of load demand, EV connection/disconnection times, and charge levels at time of connection, is described. The solution provides the on-site storage and EV charge/discharge powers. For the first time, both bidirectional and unidirectional charging are considered for EVs and a controller which accommodates uncertainties in EV energy levels and connection/disconnection times is presented. In Chapter 4, a stochastic chance constraints based optimization is described. It affords significant improvement in robustness, over the conventional controller, to uncertainties in system parameters. Simulation results demonstrate that the stochastic controller is at least twice as effective at meeting the desired EV charge level at specific times compared to the non-stochastic version, in the presence of uncertainties.

In Chapter 5, a network of microgrids, containing RES and batteries, which trade energy among themselves and with the utility grid is considered. A novel distributed energy management system (EMS), based on a central EMS using a Multi-Objective (MO) Rolling Horizon (RH) scheme, is presented. It uses Alternating Direction

Method of Multipliers (ADMM) and Quadratic Programming (QP). It is inherently more data-secure and resilient to communication issues than the central EMS. It is shown that using an EMS in the network provides significant economic benefits over MGs connected directly to the grid. Simulations demonstrate that the distributed scheme produced solutions which are very close to those of the central EMS. Simulation results also reveal that the faster, less memory intensive distributed scheme is scalable to larger networks —more than 1000 microgrids as opposed to a few hundreds for the central EMS.

Acknowledgements

I am grateful to my supervisors Dr. Ali Emadi & Dr. Shahin Sirouspour for their support, encouragement, advice, guidance, and faith during my studies towards my Ph.D. I thank them for providing an excellent environment and facilities for performing my academic research. Their patience and guidance through difficulties in my early academic career has been invaluable.

I would like to thank my supervisory committee, which included, at various times, Dr. Mohamed Bakr, Dr. Hassan Kojori, Dr. T. Kirubarajan, for providing advice when needed, and helping me keep my progress towards the completion of my doctoral studies on track.

My colleagues in my research group at various times, Dr. Pawel Malysz, Dr. Yanbo Xue, Eric Yu, Abdul Lateef, Guotao Lin, Mohsen Rafiee Sandgani, and Raheleh Khodabaksh were influential in various ways from laying foundations for my research, to contributing valuable insights and ideas in group discussions. I thank all of them.

Dr. Tim Davidson in the Department of Electrical and Computer Engineering, was helpful in the early discussions during the development of some of the optimization algorithms which form the core of my thesis. Dr. Nigel Schofield was very generous in his provision of time, friendly advice and support, which helped me handle the travails of graduate studies. Cheryl Gies, the graduate assistant, has been invaluable

with her help and wisdom in dealing with the everyday life as a graduate student. I thank all of them.

I thank my colleagues from all across the McMaster Engineering graduate community—some of whom worked with me in the early years of the Engineering Graduate Society; and the rest of whom shared office space with me over the large part of the past 4 years—for their friendship, sharing of their knowledge, and for making graduate work a bit more fun.

Lastly, this research was undertaken, in part, thanks to funding from the Canada Excellence Research Chairs (CERC) Program. I appreciate the program's generosity.

Contents

List of Tables

List of Figures

Chapter 1

Introduction

1.1 Motivation

Microgrids (MGs) are localized collections of Distributed Generators (DGs), loads, Energy Storage Systems (ESS), and Electric Vehicles (EVs) in the power distribution network; which present to the utility grid as a single entity. They are capable of operating disconnected from the utility grid, a capability known as 'islanding'. As originally defined by Consortium of Electric Reliability Technology Solutions (CERTS), a MG contains a semi-autonomous collection of distributed generators and controllable loads acting together, to provide reliable and secure electric power and heating to a local community [1].

Microgrids are expected to play a significant role in achieving the objectives of the smart grid (SG) concept [2, 3]. They provide viable solutions to integrate renewable energy sources (RES) and grid energy storage into the electric power system, both of which are important to enhance the reliability and capacity of the grid. Integrating EVs to the grid using MGs might accelerate their market uptake.

The ESS used in a MG could be of any type—it could be flywheels, super capacitors, batteries, or a hybrid containing a combination of storage technologies. EVs connecting to a MG could also be a plug-in hybrid electric vehicle (PHEV) or Battery electric vehicle (BEV). Some EVs are capable of taking advantage of Vehicle-to-Grid (V2G) technologies to facilitate bidirectional power flow between the EV and the utility grid. A survey of the literature on the connection of ESS and EVs is discussed in Chapter 2.

Electrified vehicles include Hybrid Electric Vehicles (HEVs), which use a combination of an internal combustion engine and an electric drive; BEVs; or PHEVs, which are HEVs which have an energy storage element that can be charged by plugging into the electric power grid. Among these categories, we discuss those which can plug into the utility grid, viz. BEVs and PHEVs.

Electric drive vehicles, and PHEVs in particular, have several advantages over fossil fuel powered vehicles, such as, reduction in petroleum imports, thereby reducing the dependence on oil producing countries, improving the quality of the environment by reducing noise and particulate emission levels, etc. However, there are several challenges,—technical, social, infrastructure, and policy—that are to be overcome, if we are to realize widespread adoption of PHEVs by consumers. In addition, the impact that such widespread adoption of PHEVs will have on the environment, the electric power system, user driving behaviour, etc. are hitherto unclear. In this thesis, the term Electric Vehicles (EVs) shall hereinafter refer to BEVs and PHEVs.

Some of the technical challenges for integrating electric vehicles include an increase in total load capacity at the distribution level of the electric power system,

non-deterministic connection and disconnection times of EVs to and from the electric power grid, among others. In addition, V2G technologies, which enable EVs to supply power to the grid, pose the additional challenge of bi-directional power flow. Infrastructure challenges related to EV integration are planning and implementation of a network of charging stations for EVs, utilizing V2G capabilities of numerous vehicles to perform ancillary services like voltage regulation, etc.

In [4], Lasseter describes three critical control functions in MGs. They are low-level, fast-acting controllers based on power electronics; the Energy Manager, which decides the set points of MG components, minimizing costs and losses; system protection network comprised of isolation circuits and relays, working to protect the MG in the event of faults within and outside the MG. Energy management systems (EMS) and control in microgrids are important topics which have gained increased attention from the smart grid research community in recent years [5, 6, 7, 8, 9].

MGs considered in this thesis are those that provide only electric power. The work presented in this thesis concerns the development of Energy Management Systems (EMS) which utilize optimization solvers to determine *time-averaged* charging and discharging power rates of the energy storage devices, including EVs, in the MG, in order to minimize costs, sometimes under uncertainty in system parameters, while ensuring system constraints are met. The EMS-s proposed in this work are applicable to a generic MG containing DGs, EVs, and ESS. The DGs could be renewable sources of power such as wind turbines or photovoltaic (PV) panels; the EVs could be those with or without V2G capabilities; and the ESS could be of any kind—lithium ion batteries, super capacitors, flywheel storage, hybrid storage, etc. The system under consideration is modelled to be a consumer on a utility distribution network, such as

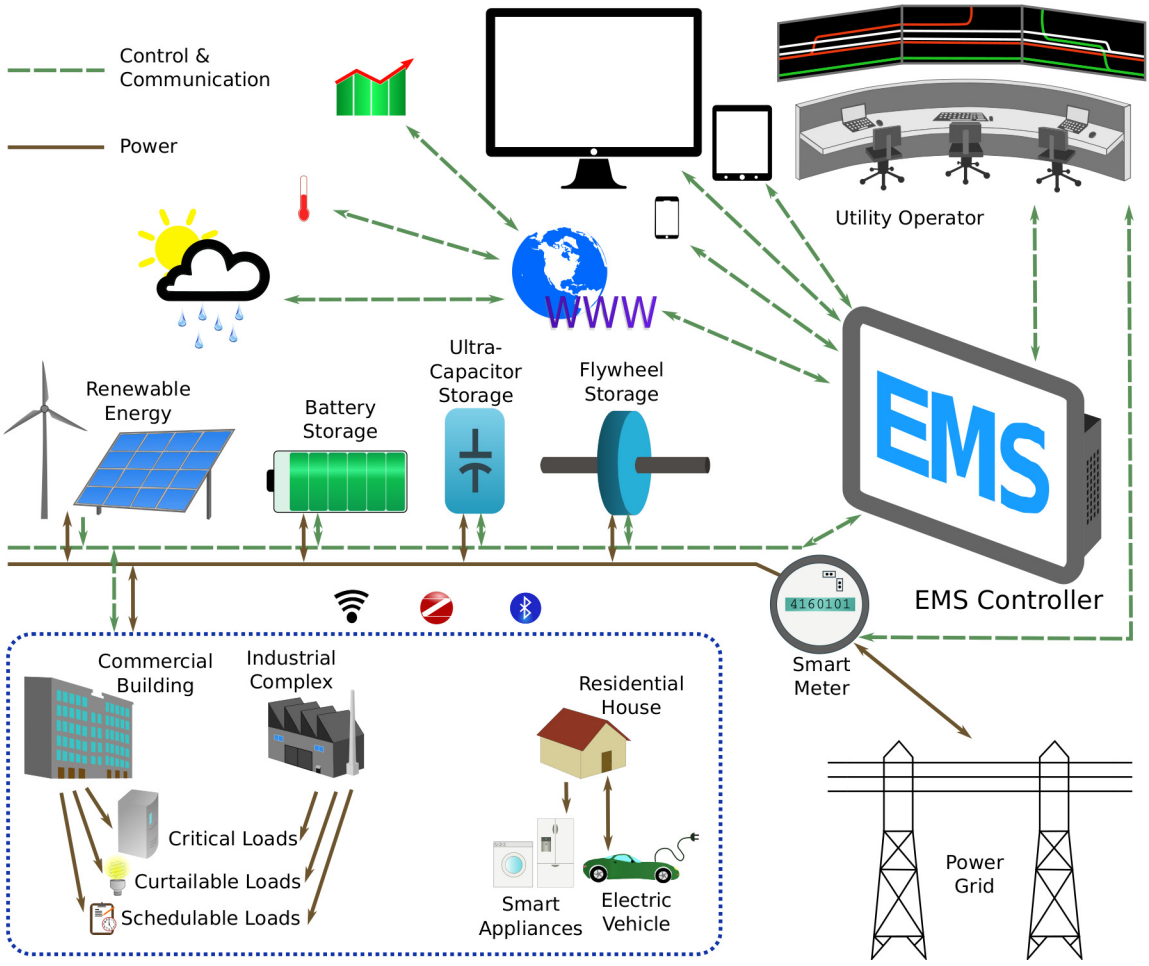

Figure 1.1: Generic system model of a microgrid considered in this thesis.

an industrial complex, commercial, or residential building. A generic system model of a typical MG considered in this thesis is shown in Figure 1.1.

Some of the main smart grid objectives include improved reliability, promote high penetration of renewables, islanding, and improving the efficiency of power generation. As suggested by [2], microgrids have a the potential to play a significant role in the realization of smart grid goals at the distribution level. Thinking beyond individual MGs connected to the grid, networks of MGs are envisioned. EMSs which enable

MGs to save costs by trading energy among each other could incentivize the adoption of MGs in the coming decade.

When energy is traded within a network of MGs—at the distribution level—the losses and infrastructure costs associated with long distance power transmission does not come into play, thus enabling cost incentives for local trade of energy. A network of MGs also enables a better overall use of energy storage within the network to meet wider 'community' energy needs, by allowing storage and use of energy by virtually any MG in the network. Further, conceptually, networks of MGs offer another layer of decentralization of the energy infrastructure, on top of distributed generators and storage devices.

Challenges in the development of EMSs for a network of MGs are multi-fold. The sheer size and number of controllable elements may require vast computational resources. The need for coordination and cooperation among the MGs in a network requires reliable a data communication backbone. Further, data privacy concerns arise, since information regarding the state of the MGs and the values of the system variables being controlled may need to leave the physical boundaries of individual MGs.

The problems solved by the different EMSs consider variations of the MG system model described above; the descriptions of the EMSs are provided along with those of the problems considered and contributions to the state-of-the-art, in the rest of this chapter.

1.2 Problem Statement

In this thesis, the following problems are addressed. Firstly, a microgrid with PV generators and an on-site battery storage system is considered. Multiple EVs are assumed to connect to it over different time periods. The goal is to develop an EMS for this system. A number of challenges arise when developing an EMS for such MGs with integrated EVs:

- the vehicles connect and disconnect intermittently to and from the MG
- the energy level of the storage in the EVs at the times of connection is unknown
- the EV needs to be charged/discharged to specific desired minimum energy levels by specific times, so as to guarantee a minimum driving range
- the times of connection and disconnection of EVs, the values of which could be uncertain, need to be known by the EMS

Secondly, networks of MGs with PV generators and on-site batteries are considered. The aim is to develop an EMS for these networks such that energy trade within networks is incentivized. This poses several challenges:

- fair economic incentives should be guaranteed for all MGs participating in the network
- the EMS should not necessitate investment in additional computational resources
- Communication of critical microgrid data should be limited to reduce risks to data security

- the EMS should allow for the network to scale and expand, while ensuring control decisions are made within a reasonable time duration

Given these issues, two different solutions were devised and were successfully proven to be effective. They are briefly introduced below.

1.2.1 Solutions

EV Integration Under Uncertainty

In a system with PV generators, on-site batteries, and EVs; the EMS is expected to make optimal or sub-optimal decisions on power rate values of on-site batteries and EVs, such that electricity costs are minimized and all system requirements are met. However, uncertainties are present in several system parameters, such as the times of connection and disconnection of EVs; energy level at time of connection; value of power demand; and value of power generated. A stochastic optimization control framework which guarantee a minimum probability of failure[1] is devised to function as the EMS for this system. The optimizer considers a future rolling time horizon for making current decisions

Distributed EMS for Network of Microgrids

In a network of MGs with on-site batteries and PV generators, the EMS has to ensure that the decisions on the charge/discharge power rates of the batteries, the buy/sell power rates within the network, and those with the utility grid are optimal in a way that the economic benefits of individual microgrids are maximized at the same time

[1]The word failure is used in the context of the stochastic optimization. This will be expounded upon in Chapter 3

as maximizing the utilization of energy resources from within the network. A rolling horizon control framework based on a multi-objective (MO) optimization formulation, in which the decisions are computed in a distributed fashion, is developed to operate as the EMS in a network of MGs.

1.3 Contributions

An optimal control framework for the flow of time-averaged power in microgrids, formulated using chance constraints optimization, over a rolling time horizon, is described. The present work has a number of significant features:

- It presents an *online* optimal controller for microgrids with renewable sources, on-site storage, and EVs.
- The controller accommodates various EV charging scenarios, namely adjustable power bidirectional, single-level unidirectional, and unidirectional block charging.
- It also accounts for changes in the system at every time step and uncertainties in
  - Predicted load demand
  - Renewable power generated
  - EV to microgrid connection/disconnection times
  - EV state of charge at time of the connection

  by using stochastic chance constraints optimization. In particular, solution to energy management in microgrids in presence of uncertainties in EV connection

and disconnection times to microgrid, which poses big technical challenges, has not been addressed in the literature.

- Stochastic optimization techniques have been employed in tandem with rolling horizon control to overcome uncertainties in magnitude of uncertain parameters and uncertainties in time. This has shown to significantly improve robustness of the system response over conventional rolling horizon control.

One of the main contributions of this work is the consideration of a more complete system with renewable power generation, on-site energy storage, and electric vehicles, whose presence in the system is intermittent; along with the use of an online model predictive controller which makes new decisions at every time step while considering uncertain system parameters over a future rolling time horizon. Another contribution is the accommodation of different types of EV charging: bidirectional, unidirectional On/Off, and One Block charging. A third contribution is the use of stochastic optimization techniques used along with rolling horizon control to overcome uncertainties in magnitude of uncertain parameters and uncertainties in time.

In the case of the system with a network of MGs, a scalable, distributed, MO control scheme, which constitutes an EMS and outperforms its centralized counterpart, is presented. This work contains several significant contributions:

- A distributed optimization formulation is derived, using Alternating Direction Method of Multipliers (ADMM). This formulation guarantees economic benefits for all the MGs participating in the network.

- It enables the decisions pertaining to each MG to be made locally, does not require significant computing power, and has the following advantages over the

centralized framework:

  - **Scalability:** Given limited computational resources, the distributed algorithm can be applied to networks of sizes which are multiples of the largest networks for which the centralized algorithm can be applied
  - **Computational Efficiency:** By making decisions and storing variables locally at each MG, the computational resources at each MG is utilized efficiently
  - **Speed:** Using distributed computational resources enables computations to be performed faster
  - **Data privacy and resilience:** The Distributed EMS makes decisions regarding individual MGs locally. In comparison to a central EMS, the communication of data critical to each MG is minimal, thus improving data privacy and security

- Results of numerical simulations which demonstrate the cost effectiveness of the optimization framework and the efficacy of the distributed formulation are presented

1.4 Summary

In this chapter, the motivation and significance of the problems being addressed in this thesis were explained. In addition, the problems that are addressed in this thesis and brief descriptions of the proposed solutions were discussed. Two distinct systems are in focus. The first system is one in which a MG integrates renewable energy

sources, on-site battery, and EVs. The biggest challenge in devising an EMS for this system is uncertainty in system parameters. A stochastic optimization framework is proposed as a solution.

The second system contains a network of MGs which trade energy amongst themselves. The most significant challenges in the formulation of an EMS for this system are the computational requirements and scalability. A distributed algorithm is proposed as a solution. The contributions of the work presented in the thesis to the literature were clearly stated.

1.4.1 Organization of the Thesis

In Chapter 2, a survey of the literature pertinent to the core topics of the thesis is presented. The Adaptive Energy Management System (A-EMS), which solves the problem of controlling a MG while integrating renewable energy, on-site battery, and EVs is discussed in Chapter 3. In Chapter 4, a stochastic version of the A-EMS and numerical simulations which demonstrate the performance of the A-EMS are presented. Chapter 5 presents the Distributed Energy Management System for a network of MGs. In Chapter 6, a summary of the work presented in the thesis is presented along with a detailed discussion on the scope of future research stemming from it. The notations used in the mathematical formulations in Chapters 3 and 5 are listed for reference in appendices at the end of the thesis.

Chapter 2

Literature Survey

In the previous chapter, the problems addressed in this thesis were introduced along with brief descriptions of the solutions and contributions to the literature. This chapter comprises a survey of the literature related to the problems addressed and solutions suggested. The work presented in this thesis centres around MGs. As alluded to in the previous chapter, smart grid functions viz. improved reliability, high penetration of renewable energy sources, self healing, reconfigurable grid, active load control, and improved generation efficiency can be achieved by breaking down the grid into multiple MGs [2]. MG initiatives in the US are described in [10] and the role of customer driven MGs, supporting energy storage, in the realization of smart grid is discussed. However, the articles surveyed in this chapter cover systems that vary in size—ranging from entire electric power system networks, to small microgrids. Papers discussing types, methods, and impacts of integrating various microgrid components viz., EVs, batteries, renewable sources of energy, etc. into the electric power system are also reviewed.

Advances in battery technologies and those of other types of energy storage have

created new opportunities for addition of significant storage capacity in the electric grid through their integration in microgrids. All MG systems considered in this thesis include energy storage systems. Numerous research efforts have focussed on the integration of storage into the grid—methods to integrate them in MGs, impacts on grid operation, socio-economic impacts, etc. In Section 2.1, a number of works available in the literature which concern grid integration of storage are reviewed.

A large proportion of the contributions in this thesis are in the topic of integration of EVs in microgrids. Grid integration of EVs has received ever-increasing attention with the rapid increase in availability of electric drive vehicles, capable of plugging into the grid (PHEVs and BEVs). This is the result of governmental regulations and incentives; increased awareness of climate change; etc. Integration of EVs in the grid poses several technical and socio-economic challenges. Their impact on the current electric power system is, as yet unknown. In relation to microgrids, an EV can represent a significant portion of the load when charging. Additionally, Vehicle-to-Grid (V2G) technologies might allow microgrids to communicate with EVs, which in turn might facilitate demand response functionality. The idea of EVs as backup storage or as ancillary service providers has also been explored in the literature. An overview of the different layers of controls in microgrids, types of EVs, V2G technologies, and suggestion for research in control of microgrids with integrated V2G is presented in [11]. A detailed survey of the literature on the topic of EV integration into the grid is discussed in Section 2.2. It includes topics such as impacts of EVs, control techniques while integrating into the grid—directly, through aggregators, or as part of microgrids.

The work discussed in this paper makes use of various optimization techniques.

Linear Programs, Mixed-Integer Linear Programs, and Quadratic Programs are used primarily. In Section 2.3, a brief introduction to each of these classes of optimization problems is given, along with references to literature which discuss the theory behind them and their corresponding solution techniques.

Solutions developed in the work presented in this thesis are the control frameworks designed to function as the energy management systems of microgrids. Control frameworks discussed in the literature vary on several criteria: the power system for which they are designed, components that are controlled, the main objective of the controller, computational resources available, speed at which the controller is expected to operate, etc. Section 2.4 surveys the literature on control solutions for power systems—primarily single microgrids connected to the the grid at the distribution level—containing various components, with different objectives, and control schemes chosen, including some which are commercially available.

Lastly, a significant portion of the contributions in this thesis concerns energy management in a network of microgrids. Solutions for such systems usually involve multi-objective optimization problems, solved either centrally or in a distributed fashion. Several examples of energy management in and among multiple microgrids are available in the literature; works on multiples of systems similar to microgrids, variously referred to as 'green communities', 'nanogrids', etc., are also available. A wide selection of these are surveyed in Section 2.5. Further, MO optimization problems have been formulated to solve energy management problems for systems other than multiple microgrids, such as single microgrids and aggregators. Literature pertaining to the use of MO optimization problems in electric power systems is also reviewed.

The research surveyed in Sections 2.4 and 2.5 represent the works which are similar

or relevant to the ideas and solutions developed in this thesis. Therefore, in these sections, commentary on the differences and disadvantages of these methods to the work described in this thesis is presented.

2.1 Energy Storage in Microgrids

The ever-increasing penetration of power electronics interfaced and intermittent (in the case of RES) distributed generators necessitates the integration of Energy Storage Systems, in order to mitigate the ill-effects of power imbalances, voltage and frequency fluctuations resulting from load transients, etc. Further, the use of energy storage will alleviate the burden on the utility by enabling demand response, peak reduction, and ancillary services such as frequency regulation. Power electronics interfaces for integrating energy storage elements into the grid are surveyed in [12], in addition to those suited for decentralized generators. Different energy storage systems such as Flywheel Energy Storage Systems (FESSs), Battery Energy Storage Systems (BESSs), Ultracapacitors (UCs) and Supercapacitors (SCs), Vanadium Redox Batteries (VRBs), Superconducting Magnetic Energy Storage (SMES), Hybrid Energy Storage Systems (HESSs), etc. are surveyed, their configurations and topologies discussed, and their suitability for integration in MGs investigated in [13, 14]. The economic feasibility of using re-purposed PHEV batteries in MGs is discussed in [15].

2.1.1 FESS and BESS in Microgrids

Flywheels store energy mechanically and the feasibility of their use in MGs has been verified experimentally in [16]. Decentralized control strategies for control of FESS connected to MGs are proposed and their performances analyzed in [17, 18]. [19] proves the feasibility of integrating BESSs in MGs through experimental results from operating a grid-connected microgrid test bench. An Artificial Neural Network (ANN) controller for a BESS connected to MGs in order to inject power into the microgrid bus to stabilize the system during power imbalance is presented in [20]. Sizing of energy storage systems connected to MGs is an important problem to consider. The size of storage required for an MG depends on the capacity of the load connected to the MG and the capital available for investment. Sizing of FESS for MG applications is discussed in [21], whereas an optimal method for sizing BESS for MGs is proposed in [22].

2.1.2 HESS in Microgrids

Grid energy storage elements can be broadly classified as high energy density and high power density storage elements. An example for the former is BESS and that for the latter is Ultracapacitors. While high energy density storage can store a lot of energy, their output cannot ramp up or down as fast as high power density storage. Hybrid Energy Storage Systems usually contain at least one storage element from each of these categories in order to take advantage of their individual benefits. However, they need complex controllers for managing charging and discharging, and power balance of the constituent storage elements.

Most HESSs used in microgrids utilize a combination of supercapacitor or ultra-capacitor and a battery. The suitability and feasibility of HESS for use in MGs is analyzed in [23, 24]. Several structures and charging and discharging schemes are considered. It is found that these schemes result in prolonging of the battery's life. A literature review and simulations of the different topologies and energy management algorithms for HESS in MGs, and their comparison are presented in [25, 26]. Control methods for power balancing and compensation in AC and AC-DC microgrids by controlling HESS are presented in [27, 28, 29].

2.1.3 Control of Microgrids with Energy Storage

The presence of energy storage elements connected to a microgrid affords it to add a higher proportion of intermittent RES to its bus without relying heavily on the utility grid and conventional sources for power balancing and voltage and frequency stabilization. In fact, with proper control and protection mechanisms, such MGs can operate isolated from the utility grid. In addition, such MGs can be operated in an optimal fashion to minimize energy and operating costs, emissions, and damage to battery. A plethora of research papers [30, 31, 32, 33, 34, 35, 36, 37, 38, 39, 40, 41, 42, 43, 44, 45, 46, 47, 48, 49] are available on the topic of controlling microgrids containing energy storage elements, such as UC, SC, BESS, FESS, HESS, VRB and SMES, some of them using optimization techniques, such as dynamic programming and genetic algorithms. Prediction of solar irradiation, wind profile, photvoltaic (PV) power, and load demand are also performed in [36, 48], while Demand Side Management (DSM) by load shedding is performed in [41, 42]. References [50, 51, 9] present comprehensive reviews of different types of control techniques used for MGs with storage. Concepts

like decentralized, distributed and hierarchical controls for AC and AC-DC hybrid microgrids, methods for mitigating effects of uncertainties due to RES, etc. are also discussed in these papers. While most of the research discussed in this section consider MGs with energy storage and their control, the use of a combination of RES and storage to maximize economic benefits, using optimization is not discussed.

2.2 Electric Vehicles Connected to Microgrids

Governments across the world have introduced economic incentive programs, such as tax incentives and price rebates, in a bid to increase the consumer adoption of vehicles which have an electric drive in them. These topics have been well studied in the literature. Techno-economic issues, and socio-technical issues, such as impediments to consumer acceptance, resistance from stake holders in existing infrastructure, related to integrating V2G into the grid are discussed in [52, 53] respectively, and solutions are suggested. A regional, income-based incentive policy for Plug-in Hybrid Electric Vehicle (PHEV) adoption, in place of existing policies is suggested in [54]. Using a micro-level electric demand model for determining household electricity consumption in California, in the presence of a PHEV, it is determined in [55] that time-of-use (TOU) pricing is best suited for PHEV competitiveness, as opposed to tiered pricing.

A number of research groups have focussed their efforts on aiding the integration of electric drive vehicles into the electric power system, in part, by solving these challenges; some of this work is discussed here.

2.2.1 Grid Integration of EVs

The financial risks associated with battery lifetime degradation in fleets of electric vehicles, which are expected to perform ancillary services, in addition to their regular drive cycles are determined in [56]. The total number of regulation cycles of the EV's battery which make it profitable is calculated. In [57], simulations are performed to investigate the potential profits of PHEVs in the frequency regulation markets in Sweden and Germany. In the series of articles [58, 59], the types of EVs and the electricity markets that they are suited to participate in are determined using calculations. In addition, long-term strategies, business models, and steps needed for V2G infrastructure implementation are discussed. A technical solution, by defining PHEV operation states, is proposed in [60] to enable rapid integration of EVs into existing power system infrastructure. References [61, 62] describe a framework for integrating EVs in the electric power system and suggest using V2G to maximize integration of intermittent Renewable Energy Sources (RES) such as wind turbines. EV charging station technologies around the world are reviewed in [63] and a network of EV charging stations, which has three levels of control, is proposed.

2.2.2 Impact of EVs

A methodology for calculating fuel consumption and emission factors, in order to compare different vehicle technologies is proposed in [64], aimed at giving good insight on impact on electric grid and CO_2 life cycle emissions. The impact of PHEVs on the distribution grid are studied with the help of simulation models in [65, 66]. The latter also suggests that coordinated charging strategies aid local grid stabilization, in addition to supporting RES. Analyzing the effects of PHEV fleets in Ohio, while

considering controlled and uncontrolled charging scenarios, it is found in [67] that, PHEVs result in a major reduction in gasoline consumption and in emission levels, despite the high penetration of coal in Ohio electricity generation.

2.2.3 Role of Aggregators

In terms of connecting V2G to grid, [68] compares a direct vehicle connection architecture to an aggregative vehicle command architecture. It is found that an aggregator improves the scale and reliability of V2G ancillary services and makes it more compatible with current ancillary services markets. Simulation studies in [69] find that an aggregator for V2G minimizes the need for conventional sources for power balancing, in the presence of a large scale RES with large fluctuations in production. A technical framework for implementing aggregators for V2G along with an incentive program is proposed in [70]. An optimal charge control mechanism for individual EVs, using Dynamic Programming, for grid-scale frequency regulation in the presence of an aggregator is presented in [71]. Interactions between EV aggregators and market regulations are simulated in [72]. It is found that use of aggregators can increase profits for its operator and consumers, and can enhance market efficiency.

2.2.4 EV Charging Strategies

Analyses of simulations of different charging strategies, viz. controlled, uncontrolled, and V2G discussed in [73], while considering external factors like weather, holidays, and electricity price, show that intelligent charging strategies can increase the battery lifetime while reducing charging costs. Reference [74] studies the effect of combined driving and V2G on the lifetime performance of commercial Lithium-ion cells. It finds

that vehicle motive cycling degraded the cells faster than V2G cycling. The effects of different charging behaviours of PHEVs on electricity demand, demand profiles and energy use in the US are assessed in [75]. The results suggest that, when it comes to peak shaving, a delayed charging option in the charging station is sufficient, avoiding the need for complex optimization and smart charging strategies.

2.2.5 EVs in Microgrids

A few papers have focused on integration of PHEVs in microgrids. Design of robust controllers for microturbines (MTs), electrolyzer, and heat pump, in the presence of RES and PHEV in MGs is presented in [76, 77]. V2G and remote demand response capabilities of a small residential level MG comprising a PHEV are demonstrated in [78].

In the discussion above, it is evident that several papers consider various methods for EV charging and integrating EVs into the grid. However, a solution wherein MGs containing a combination of storage, RES, and EVs, where the charging of the storage and EV are controlled optimally, in the presence of uncertainties is not available.

2.3 Optimization Techniques

In this section, the three different classes of optimization problems that are primarily used in the work presented in this thesis are introduced. Literature relevant to these problems are also referenced.

2.3.1 Linear Program

Linear program (LP), a class of convex optimization problems, forms the basis of the optimization formulations presented in this thesis. The objective function and constraints in linear programs take the form of a linear or affine function. A typical LP problem with n decision variables is of the form

$$\min_{\mathbf{x}} \mathbf{c}^T\mathbf{x} \tag{2.1a}$$

$$\mathbf{A}\mathbf{x} \leq \mathbf{b} \tag{2.1b}$$

$$\mathbf{A}_{eq}\mathbf{x} = \mathbf{b}_{eq} \tag{2.1c}$$

where

$\mathbf{c} \in \mathbb{R}^n$	is the linear cost function vector
$\mathbf{x} \in \mathbb{R}^n$	is the optimization variable vector
$\mathbf{A} \in \mathbb{R}^{p\times n}$	is the coefficients matrix for the p linear inequality constraints
$\mathbf{b} \in \mathbb{R}^p$	is the right hand side vector for the p linear inequality constraints
$\mathbf{A}_{eq} \in \mathbb{R}^{q\times n}$	is the coefficients matrix for the q linear equality constraints
$\mathbf{b}_{eq} \in \mathbb{R}^q$	is the right hand side vector for the q linear equality constraints

Linear program solvers typically make use of Simplex or Interior point algorithms to solve problems of the form shown in (2.1). Theoretical background on LP and related solution algorithms can be found in [79], [80], [81], and [82].

2.3.2 Mixed-Integer Linear Program

Mixed-Integer Linear Programs (MILPs) are identical to LPs, except for the fact that some of the decision variables are integer-valued, rather than real-valued. A typical

MILP is of the form

$$\min_{\mathbf{x},\boldsymbol{\delta}} \mathbf{c}_{\mathbf{x}}^T\mathbf{x} + \mathbf{c}_{\boldsymbol{\delta}}^T\boldsymbol{\delta} \tag{2.2a}$$

$$\mathbf{A}_{\mathbf{x}}\mathbf{x} + \mathbf{A}_{\boldsymbol{\delta}}\boldsymbol{\delta} \leq \mathbf{b} \tag{2.2b}$$

$$\mathbf{A}_{eq,\mathbf{x}}\mathbf{x} + \mathbf{A}_{eq,\boldsymbol{\delta}}\boldsymbol{\delta} = \mathbf{b}_{eq} \tag{2.2c}$$

Here, $\boldsymbol{\delta} \in \mathbb{Z}^m$ is the vector of m integer variables. The cost and constraint coefficients are similar to those described in (2.1). Solvers for MILP optimization problems utilize fast implementations of *branch and bound* techniques, which were developed in the 1960s [83], along with algorithms used for solving LP problems.

2.3.3 Quadratic Program

Quadratic Programs (QP) are similar to LP, with the addition of a quadratic term in the objective function. A typical QP is of the form

$$\min_{\mathbf{x}} \mathbf{c}^T\mathbf{x} + \mathbf{x}^T\mathbf{Q}\mathbf{x} \tag{2.3a}$$

$$\mathbf{A}\mathbf{x} \leq \mathbf{b} \tag{2.3b}$$

$$\mathbf{A}_{eq}\mathbf{x} = \mathbf{b}_{eq} \tag{2.3c}$$

All variables and coefficients above are defined identically to those described in the LP formulation, with the addition of the symmetric matrix $Q \in \mathbb{R}^{n\times n}$. The theory behind the solutions to QPs and its different applications are discussed in detail in [84].

2.4 Microgrid Energy Management

In the early descriptions of microgrid structure [4], it was proposed to have three different layers of controls in MGs: power electronic controllers, protection system, and energy manager. The coordinated control of bidirectional converters in an AC-DC hybrid microgrid, detailed in [85] is an example of power electronic control in MGs. Another example is an approach proposed in [86], to control interactions between multiple energy sources in an islanded MG bus in a decentralized manner, without mutual communication between them. A smart protection scheme based on Controller Area Network (CAN), presented in [87] is an example for protection systems in MGs.

An optimal dispatch problem of microCHPs, which constitute a Virtual Power Plant (VPP) is the focus of the research described in [88]. A method called column generation is utilized in this EMS. The work in [89] elucidates on the use of short-term and mid-term prediction of wind generation for optimal control of State of Charge (SOC) of batteries for power balancing. DSM by intelligent load shedding in rural, autonomous MGs, in order to maintain grid stability, is the topic of concern in [90]. A multi agent-based hierarchical control structure for MG, in order to achieve economical and environmental benefit is presented in [91].

The EMSs presented in this thesis make use of *Rolling Horizon* (RH) and *Model predictive Control* (MPC) techniques. There are several works available in the literature which make use of one or both of these for the dispatch problem in power systems. A multi-level approach for controlling distributed sources and storage is taken by Delfino et al. [92] using receding horizon model predictive control (MPC). A distributed economic dispatch problem for microgrids with renewable generation, storage, and DSM is proposed by Yu Zhang et.al. [93]; uncertainties are dealt with by

minimizing worst case transaction costs between the microgrid and the utility grid.

2.4.1 Use of Mixed Integer Linear Program

Studies in optimally scheduling the dispatch of microgrid resources have been carried out in different contexts. A two-horizon scheduling algorithm using mixed-integer-linear-program (MILP) to optimally schedule energy resources in a residential microgrid is presented by Beaudin et al. [94]. Fakhrazari et al. [95] propose a MILP-based optimal shrinking horizon scheduling algorithm for smart entities to reduce energy costs for given time-varying electricity prices.

Methods for optimal microgrid scheduling in the presence of uncertainty are also available. Malysz et al. [96] propose optimal power management strategies using MPC and MILP, for microgrids connected to the grid, considering uncertainties in the usage demand. Several novel control features for preservation of battery life, grid and battery signal shaping, etc. are also presented in this work. Xiaohong Guan et al. [97] optimize the efficiency of building microgrid operation using MILP and Scenario Tree Method.

2.4.2 Systems with EVs

Techniques have been developed for controlling systems containing EVs in combination with renewable sources; charging strategies for multiple EVs, when Vehicle-to-Grid (V2G) services are available; and charging strategies in the presence of uncertainties. Su et al. [98] propose a 2-stage stochastic method based on MILP for scheduling in microgrids with EVs, in presence of uncertainties in renewable energy

generation. An optimal EMS using MILP for residential microgrids with V2G enabled EVs and renewable sources was devised by Igualada et al. [99]. Li Zhu et al. [100] formulate the problem of optimal charging control of EVs in microgrids with renewable resources as a semi Markov decision process. An optimal joint scheduling scheme for EVs and home appliances in a microgrid is discussed by Tushar et al. in [101]. Tan and Wang [102] propose a two-layer intelligent optimization to integrate plug-in EVs to a distribution grid using a fuzzy logic model to deal with uncertainties in their arrival times.

Optimal energy delivery for V2G systems is addressed from the viewpoint of both the aggregator and owner by Liang et al. in [103] using the stochastic inventory theory. Uncertainties in vehicle mobility and time-of-use (TOU) electricity prices are considered. While this work considers a problem similar to the one discussed in this thesis, the use of distributed RES and storage with local MG control is not discussed. Zhang and Chen [104] compare microgrid energy management and optimal scheduling of EVs and battery swapping stations in both grid-connected and islanded modes of operation. Sortomme and El-Sharkawi propose an optimal energy and ancillary services scheduling scheme for EVs with V2G services, to be used by an aggregator in [105]. Shaaban et al. [106] propose a system for real-time coordination of plug-in EV charging in a distribution network. A two-step solution is proposed by Yifeng He et al. [107], to overcome difficulties of creating a scalable, globally optimal EV charging scheme. Many of the above works consider systems or solutions, aspects of which overlap with the system considered and techniques used to solve problems in this thesis. However literature on an EMS for a system with EVs, storage, and RES, where uncertainties in demand, EV connection/disconnection times, and energy

levels are considered, is not available.

2.4.3 Use of Stochastic Methods

Stochastic methods which use "scenarios" (alternatively called "particles" or "samples") are well known. Calafiore and Campi [108] present a scenario based approach for robust control design, which can be applied to chance constraints based problems. An approach whereby samples are drawn only in the boundary region of the uncertainty set, in order to reduce computational costs and conservativeness, is presented by Margellos et al. [109]. Several other efforts have focussed on solving stochastic optimization problems with chance constraints, approximated by samples, and the theory is well-known [110], [111], [112], [113] and [114].

Chance constraints have been employed to solve Optimal Power Flow (OPF) and scheduling problems at the transmission level. Zhang and Li [115] solve a chance constrained OPF problem involving load uncertainties in load power using a sequential quadratic program. While this work utilizes chance constraints to solve OPF problems, the control of time-averaged power in a microgrid with local generation, storage, and EVs is not considered. A cutting plane method is employed to solve an OPF problem with uncertain renewable sources, formulated using chance constraints by Bienstock et al. [116]. A framework to address the reserve scheduling problem in presence of intermittent wind generation is presented by Vrakopoulou et al. in [117]. A component of the framework consists of a scenario based solution to a chance constraints based optimization formulation. However, this work does not address the problem of integrating PV generators and EVs within a microgrid while ensuring electricity costs are reduced.

2.4.4 Commercial Energy Management Systems

The economic viability of EMSs and the benefits they promise for consumers and businesses have resulted in the development of several EMS products, mostly in Japan, targeting various types of markets. Kyocera's Home Energy Management System (HEMS) [118], targets homes which already have PV panels installed. The system consists of a Lithium-ion battery with a bidirectional converter, enabling the system to store energy and buy or sell power from the electricity grid. Nissan's Vehicle to Home system [119] can use Nissan Leaf EV's battery to power a home when connected. The Denso HEMS [120], which can be monitored and controlled through a touch panel or a smart phone app, works with several appliances, incorporates Vehicle-to-Home (V2H) technology. It comes with an optional battery, with which it can quick charge an EV. Panasonic's array of energy solutions for a home includes a a smart HEMS [121], which brings together generation technologies, appliance management, monitoring and optimal control, in one HEMS. The use of a hybrid AC-DC architecture for home MG in this system is being explored. Eaton [122] and Intel [123] have each developed a touch screen EMS control dashboard. Both of them can connect to the home thermostat wirelessly. NEST [124], although not strictly an EMS, has the potential to be expanded to function as one. It is a thermostat, which utilizes occupancy sensors and adaptive learning algorithms to intelligently control the heating system to achieve economic benefits for the owner. Nokia-Siemens [125] has developed a system, which can incorporate fuel cells, batteries, RESs, while Lockheed Martin's [126] solutions are highly fault tolerant and autonomous, thus suitable for use in the armed forces. Enbala Power Networks [127] is a company which provides DSM solutions, which include touch screen monitoring and control panels, to larger electricity consumers. A

number of of start-up companies; such as Vivint [128], alarm.com [129], Opower [130], iControl [131], and tendril [132]; have emerged providing solutions which enable capabilities for remote monitoring and control, demand side management, home automation, etc., to enable energy savings for the consumer. While all of these works present proof-of-concept systems, the use of advanced stochastic optimization-based control methods to integrate PV and EVs in a microgrid, while ensuring economic benefits under uncertain system parameters, has not been addressed.

2.5 Network of Microgrids

With research on microgrids gathering momentum, one can expect networks of microgrids to be operational in the foreseeable future. When considering multiple microgrids, problems concerning coordination and management of many such microgrids arise. In order to achieve overall environmental and economic benefits, system stability, and reliability, coordination among microgrids might be sought. Such coordination would require a layer of control above the controllers within individual microgrids, resulting in multiple layers of control.

Feasibility and economic profitability of multiple microgrids (MMGs) are discussed in [133]. A study to assess the pros and cons of the MMG concept using multi criterion decision aids is presented in [134]. Technical aspects of providing frequency control reserves (FCR) and profitability of MMG participation in FCR markets are investigated in [135]. Communication aspects under different market conditions are focused upon. It is learnt from the results that centralized coordination of MMG, requiring a communication infrastructure, performs better than a decentralized approach, in terms of economic profitability.

The work in [136] explores a hierarchical control architecture for frequency control in MMG in islanded mode. Automated load control, with load shedding, using contributions from local storage and PHEVs are explored. Simulation results show that this centralized control approach is feasible and is capable of dealing with large numbers of distributed energy sources. Impact of communications in such hierarchically controlled MMGs are assessed in [137]. A model to support optimal decisions in a network of MG is proposed in [138] where instantaneous power flow in the MG network is optimized. The objective is to minimize variation of energy stored in each device and minimize exchange of power between MGs. Communications can introduce difficulties like delays, and in the case of an islanded MG, loss of signal. Results show that the control actions of the hierarchical controller reduces the impact of communication difficulties in most scenarios, especially in more demanding scenarios like both delays and losses in communication. Another hierarchical control strategy, making use of the communication, control and advanced metering infrastructure of smart grids is discussed in [139]. Highest priority is given to grid stability, at the same time as incorporating storage devices, dispatchable energy units and controllable loads. In the above works, the feasibility or control methods for optimizing a network of microgrids is presented. However, a distributed solution to control the time-averaged power flow within a network, where microgrids exchange power among themselves to reduce cost of electricity paid to the grid, while ensuring economic benefits for all microgrids in the network, is not discussed.

Shi et. al [140] proposed a distributed technique for solving an optimal power flow (OPF) to reduce operating costs in microgrids. Shi et. al also prestented a stochastic OPF problem in [141]. This method has the objective of balancing demand and supply

in real time, as opposed to electricity cost reduction considered in the current work. In both of these papers, the solution method calculates instantaneous power values for a single microgrid systems, while in the work presented in this paper, time averaged power flow values are calculated in networks of MGs. Wouters et. al [142] proposed an optimization-based approach for a multi-MG residential system. Their objective is distribution system planning rather than power dispatch to reduce electricity cost.

2.5.1 Use of Multi-Agent System

A multi-microgrid control system using multi agent system concepts for control and communication is presented in [143]. References [144, 145] also propose multi agent system based control for operating multiple microgirds. While the former proposes a decentralized, communication-less strategy, the latter presents a two-level architecture for Distributed Energy Resource (DER) management.

2.5.2 Multi-Objective Optimization

Several schemes for power dispatch in multi MGs are available in the literature. Chen et. al [146] proposed a cloud-based energy management system (EMS) for multiple 'green communities'. Ouammi et. al [147] investigated a problem similar to the one described here, wherein optimization is used to control the charge and discharge activities of the storage systems in the MGs. They developed a model predictive controller (MPC) to determine power exchanges that would minimize cost. Some of the existing methods utilize random search techniques. In particular, Nikmehr et. al [148] introduced a multi-MG dispatch scheme using particle swarm optimization, while Chiu et. al [149] presented the artificial immune system method, to design a market operator

and a distributed network operator. A two-microgrid system was considered by Rahbar et. al [150] where central controller was proposed to minimize electricity cost. Wang et. al [151] proposed a two-step heuristic method for non-cooperative multi-MG system to minimize cost. The problem was solved centrally and scalability of the system was not discussed. While these papers investigate somewhat similar problems to the one considered in this paper, their proposed solutions are based on centralized optimization, rather than a distributed commuting scheme, which in principle, could afford better scalability, speed, computational efficiency, and security/reliability.

2.5.3 Hierarchical Methods

Hierarchical methods exist for control in power distribution systems. Manshadi et. al [152] introduced a two-level optimizer using mixed integer programming (MIP) in multi-MG systems. The objective of this controller was to ensure resilient operation of vulnerable components in the system, rather than minimization of electricity cost of the MGs involved. Wang et. al [153] proposed a bi-level decentralized algorithm for coordinated operation of a network of MGs in a distributed system to minimize operation cost of the Distribution Network Operator (DNO) and MGs in grid-connected mode, and to maintain reliable power in islanded mode. The algorithm involves solving optimization problems at both levels, whereas in the method presented in this paper only the local controllers solve optimization problems. The authors also introduced a similar stochastic bi-level approach to control a network of MGs in [154]. The objective of the proposed algorithm is to minimize the combined cost of electricity traded by the network of MGs with the utility grid. Che et. al [155] proposed a method for hierarchical coordination in a community of AC and DC MGs. The work

focuses on economic operation of the MGs by controlling instantaneous power flow among them, without considering energy storage.

2.5.4 Game Theory

A number of papers have employed concepts from the game theory for energy management in multiple microgrids. Despite the fact that game theoretic methods are different to the methods employed in the current work, the system considered and the objectives of the controllers presented are similar in scope in the following works. Belhaiza and Baroudi [156] developed a game theoretic-based optimization model for multiple MGs, considering impairments in communication in the form of a Mixed Integer Linear Program (MILP). Sheiki et. al [157] solved a non-cooperative game among "smart energy hubs" using a distributed, projected gradient method, to perform demand side management (DSM). Whereas the objective of the work in the current paper is to enable electricity cost reduction for MGs in the network, the objectives in [156] and [157] are to perform demand response. Du et. al [158] also discussed a game theoretic formulation for energy dispatch in multi-MG configurations, which facilitates economic gains by controlling the power output in distributed generators (DGs). In contrast, the entity controlled in the current paper is the charge/discharge power of the integrated energy storage systems.

2.5.5 Distributed Algorithms

Distributed solutions to multi-MG energy management problem have been presented before. Mahmoodi et. al [159] proposed an optimal economic dispatch of microgrids, viewed as multiple 'nanogrids', decomposed into several problems, managed

by a central controller. Worthmann et. al [160] presented centralized and decentralized MPCs for energy management in a network of MGs, in order to mitigate the effects of integrating residential photovoltaic installations on grid voltage and frequency. Werth et. al [161] proposed a conceptual study of a heuristic strategy with distributed decision makers for a network of nanogrids, designed to facilitate exchange of intermittent energy between houses in a local community. Mou et. al [162] developed a scalable Rolling Horizon (RH) based decentralized optimizer, performing DSM to 'flatten' the load at Low Voltage (LV) transformers. Lu et. al [163] proposed a distributed multi-objective energy consumption scheduling for demand response using Tchebycheff decomposition. Sharma et. al [164] presented a decentralized, multi-objective, multi-agent approach to solve a service restoration problem using controlled distributed generator islanding. McNamara et. al [165] introduced a decentralized method for demand response in aggregated loads using Dantzig-Wolfe decomposition. Liu and Chu [166] proposed augmented Lagrangian-based distributed algorithms for active transfer capability in multi-area power systems. Srikantha and Kundur [167] proposed a scalable power dispatch strategy for distributed generators using dual decomposition.

Khan et. al [168] proposed a distributed algorthim for reactive power control in power grids. However they did not consider PV and storage their system, their objective was control of reactive power rather than cost minimization. Nguyen et. al [169] presented a distributed model for scheduling generators in a multi-MG system to minimize cost and to curtail load during islanding; energy storage was not addressed in this work. Wu and Guan [170] introduced a decentralized distribution management system to reduce the operating cost of distributed generation network

consisting of coupled MGs. Their aim was to reduce the overall cost of the distribution network, rather than attempting to reduce the electricity cost of individual MGs. The research papers discussed above utilize distributed methods in a variety of systems, i.e. distributed generators, home DC grids, and nanogrids to achieve a number of different objectives. These include demand response, distributed generator dispatch, and load balancing. They generally achieve these goals by controlling demand power, generator power, or by load shedding.

ADMM Based Methods

ADMM has previously been applied for control in power systems. Ma et. al [171] proposed a distributed online ADMM-based energy management approach for a network of MGs. However their system is different from the one considered in this paper in that it has no energy storage, and their objective is cost minimization from the perspective of the DNO as opposed to the MGs. While Tsai et. al [172] proposed an ADMM-based approach for real-time distributed demand response in a neighbourhood with loads and renewable sources, their system cannot be considered as a network of MGs. Verschae et. al [173] presented coordinated energy management of groups of loads in order to minimize inter-group imbalance using ADMM. Doostizadeh [174] utilized ADMM in a decentralized parallel method, for multi- area energy and reserve clearing under wind generation uncertainty. However, the controller objectives in both these papers are different from the one considered in the current work and they do not address energy storage.

2.5.6 Cooperative Control

Methods based on cooperation and consensus are also available in the literature. Hug et. al [175] presented a distributed EMS based on a consensus based technique in order to balance demand and supply, where the distributed decision makers agree on a common value for the control variables. This paper considered only a single MG system. Xu et. al [176] proposed a method to cooperatively control multiple energy storage systems to maximize charge/discharge efficiency. Meng et. al [177] proposed an iterative multi-objective MPC to cooperatively control batteries in an interconnected network to minimize changes to control variables over time. It is to be noted that none of these papers consider minimizing the electricity cost. Ahmadi et. al [178] developed a multi-objective optimization model to cooperatively control residential MGs with storage, based on prioritized loads. The model facilitates demand response by informing consumers about their power consumption behaviour; estimated economic benifits are presented. The work did not utilize a distributed algorithm and aims to enable economic benefits by controlling loads, i.e. demand response rather than by controlling charge and discharge of storage systems. Fathi and Bevrani [179] proposed a power dispatchnig method in interconnected MGs. Their system did not include PV generators or storage and power dispatch functionality is achieved using DSM, as opposed to control of storage charge and discharge powers.

2.6 Summary

An extensive review of the state of the art in several MG topics was presented in this chapter. In particular works on the impacts on the current infrastructure, technical

solutions to enable integration of new technologies, and their control were surveyed. In Section 2.1, research related to types, impacts, and technical challenges in the integration of storage technologies into the grid were discussed. Integration of EVs into the grid and their control was the focus of Section 2.2. Research efforts on Energy Management at different levels of the electric power infrastructure, and at the microgrid level in particular were discussed in Section 2.4. Section 2.5 presented a survey of the available research work on central and distributed energy management, using varied techniques, in microgrids and in the wider the power system infrastructure.

It can be surmised from examining Section 2.5, that control frameworks which operate centrally are available for networks of MGs. Those which operate in a distributed fashion do not account for data privacy issues and increase in communication needs. A scalable distributed EMS for a network of microgrids, with low computational and communication requirements, is not available currently.

The review of literature in Section 2.4 reveals several papers which have considered control of microgrids in combination with one or more components. Several different types of controllers were used in these papers: day ahead controllers, receding horizon controllers, some of which consider uncertainties in system parameters while some do not. However, there is a need for an EMS designed considering a more complete system with RES, storage, and EVs; accommodating different EV charging scenarios; and accounting for uncertainties in magnitude and times of occurrence of events. These issues are addressed in the following chapter through the proposed *Adaptive Energy Management system.*

Chapter 3

Adaptive Energy Management System

3.1 Introduction

In the last chapter, the available literature on systems and related control frameworks, which integrate RES, energy storage, and EVs into the electric power system—microgrids in particular—were reviewed. In this chapter, a microgrid control framework called the Adaptive Energy Management System (A-EMS) is introduced and described. The work presented in this chapter places a strong emphasis on the design of the A-EMS control framework while integrating EVs. The MG system model assumed for developing the theory behind A-EMS is illustrated in Figure 3.1. The model includes PV panels and on-site battery energy storage. A generic electric load, such as a commercial building, is assumed. EVs are assumed to connect and disconnect to the system at undetermined instances in time. The flow of power between the MG and EVs could either be *unidirectional* or *bidirectional*.

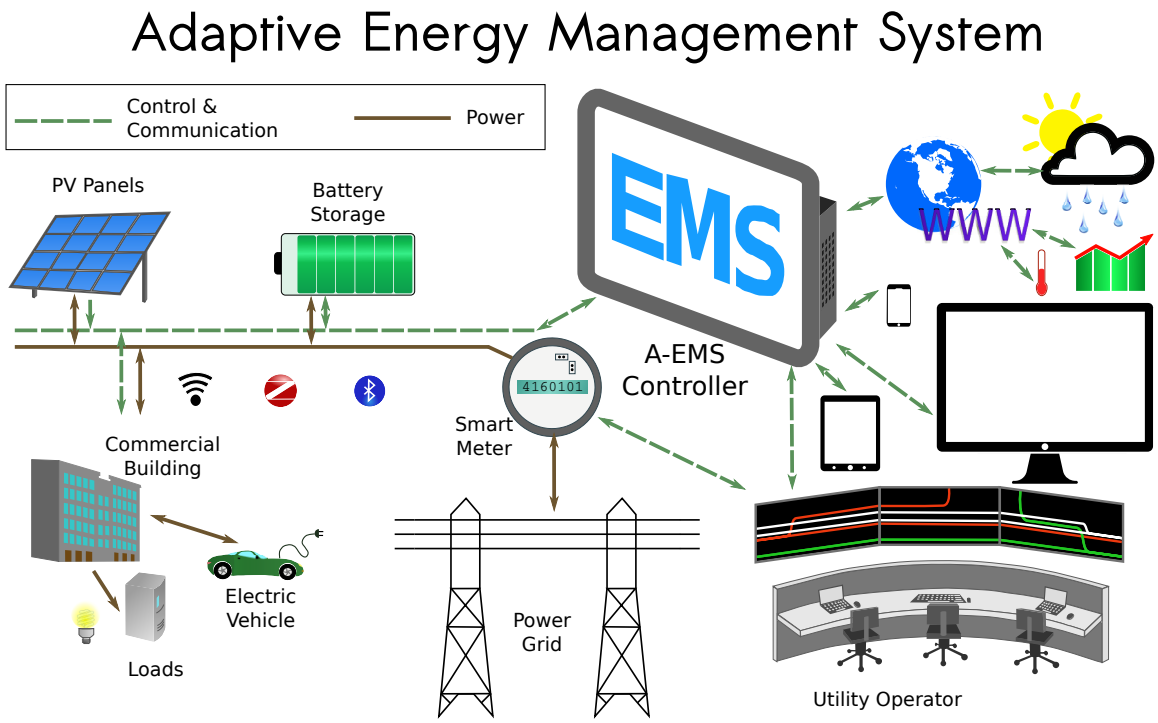

Figure 3.1: System Model used in the development of A-EMS

The proposed control framework constituting the A-EMS calculates optimal values of time-averaged power flow, which maximize economic benefits to the microgrid owner, while ensuring that the energy stored in EVs connected to the microgrid reach specific values by user specified times. Achievement of the latter task poses difficult technical challenges since the EVs connect to the MG intermittently at time instances which cannot be predicted with certainty. In many jurisdictions, electricity prices can vary within a day, depending on the time of day and the season. It is assumed that TOU prices are levied for the energy flowing between the utility grid and the microgrid. EVs connected to the microgrids can also be treated as energy storage devices, when bidirectional flow of power is facilitated through V2G services. MGs with a combination of the A-EMS, EVs, and on-site energy storage—and at

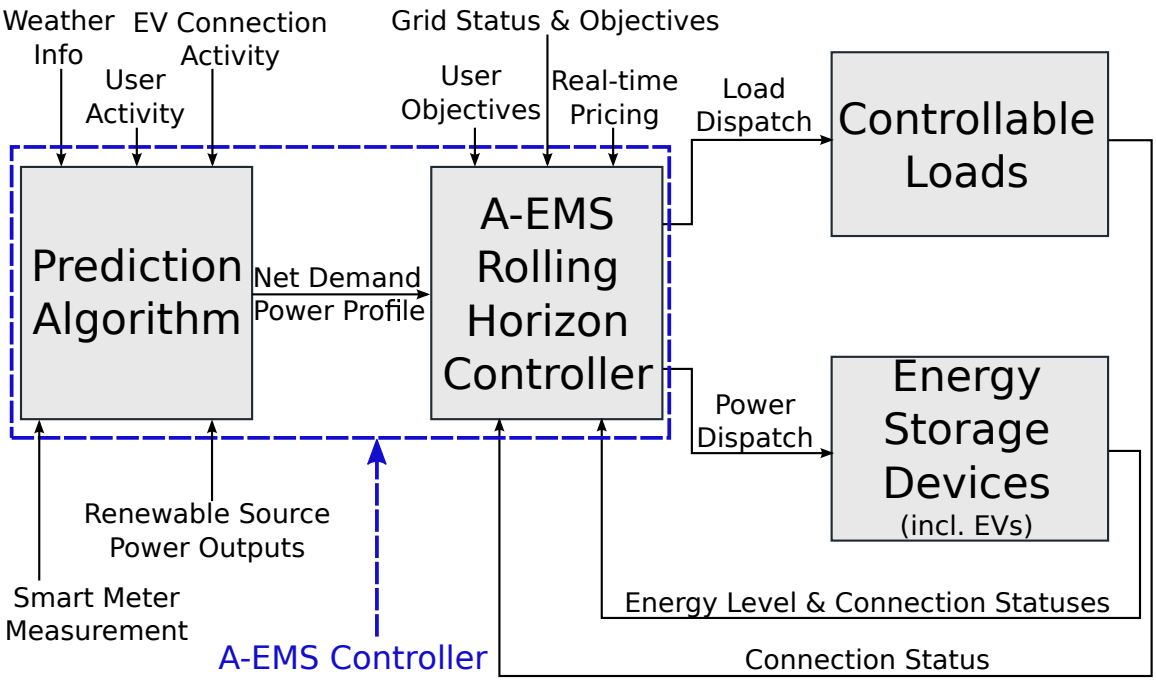

Figure 3.2: Control System Architecture of the A-EMS

times, EVs—have the flexibility of storing energy, to be used when needed or when the prices are higher. This flexibility enables the possibility of reaping economic benefits while being transparent to the customer.

The control system architecture of the A-EMS is shown in Figure 3.2. A Rolling Horizon (RH) controller is employed in the A-EMS. It makes use of predicted future values of the microgrid's system parameters, viz. net power demand, which is an aggregate of the load demand and power generated by renewable sources; the connection and disconnection times of EVs; and the energy levels of the EVs at times of connection to the microgrid. The control decisions are made over a future time horizon, i.e. the prediction window. The discussion in this chapter centres around the development of the RH control framework. A prediction algorithm is presumed, which learns the behaviour of the uncertain system parameters in order to aid the

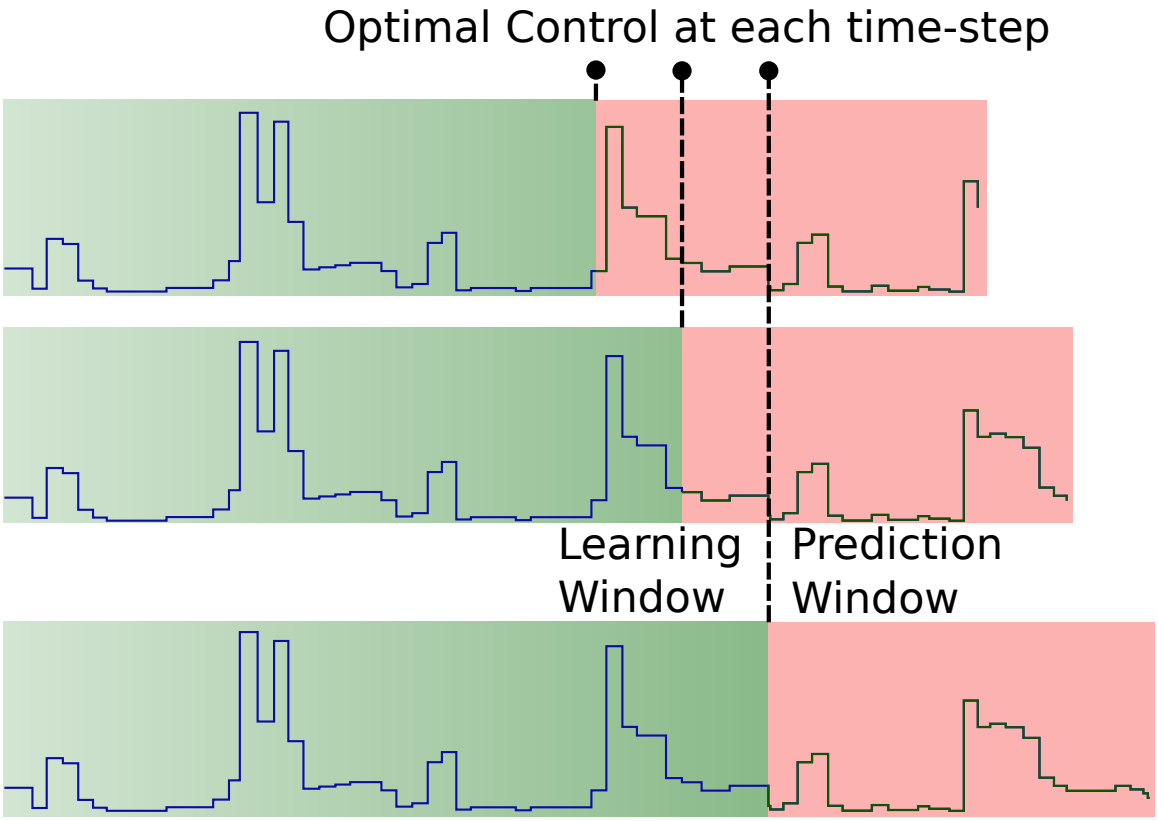

Figure 3.3: Illustration of a Rolling Control Horizon

decision making process in the A-EMS. The design of a prediction algorithm is not discussed in this thesis.

In the RH control framework, the prediction values are updated every time the prediction window rolls to the next time step as shown in 3.3. Thus, the A-EMS can adapt to changes in system parameters and predictions at each time step. This adaptability of the A-EMS is one of its salient features. The flow of control in A-EMS is shown in 3.4, showing the sequence of processes which are executed at each RH time step. It can be seen that type of optimizater used is either a *Linear Program* (LP) or a *Mixed-Integer Linear Program* (MILP) optimization solver. Only the decision variables corresponding to the first time step of the prediction window are used for

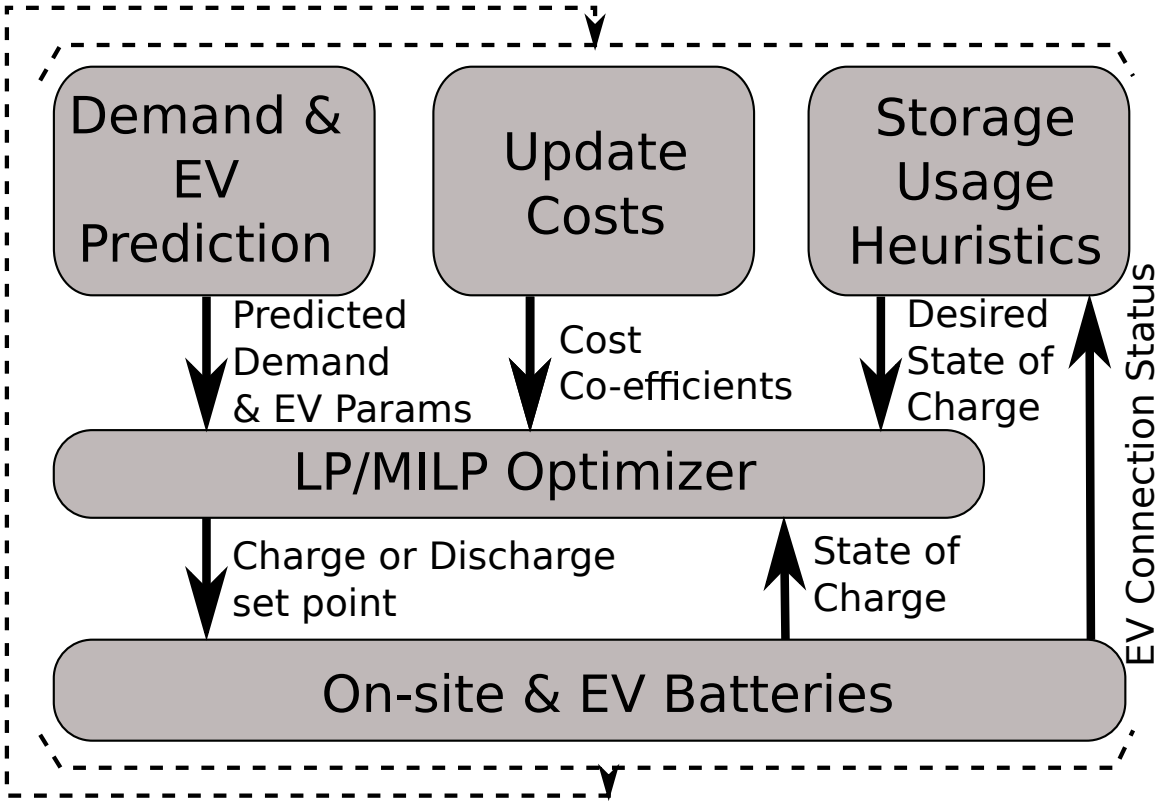

Figure 3.4: Rolling Horizon Control Flow

control in the current time step.

3.1.1 Energy Storage Model

The optimization decision variables in the A-EMS are the time-averaged charging or discharging power values of the on-site battery or the EV(s) connected to the microgrid. For both the battery and EV(s), the following linear, dynamic, discrete-time model is assumed

$$E_{i+1} = E_i + \eta_c h_i p_i^c + \frac{1}{\eta_d} h_i p_i^d - P^{loss} h_i \tag{3.1}$$

where E_i energy level[1] at time step i in kW h, η_c and η_d are the charging and discharging efficiencies, h_i is the duration of the time step i in hours, p_i^c and p_i^d are the charging and discharging power, and P^{loss} is a self-discharge power loss expressed in $\frac{\text{kW}}{\text{h}}$; p_i^d is negative or 0. Defining the power value of the battery or EV as $p_i = p_i^c + p_i^d$, (3.1) can be rewritten as

$$E_{i+1} = E_i + h_i\big(\eta_c p_i^c + \frac{1}{\eta_d}(p_i - p_i^c) - P^{loss}\big) \tag{3.2}$$

3.2 EV Integration: A First Attempt

An earlier version of the A-EMS control framework was originally proposed by Malysz et. al [96] for a microgrid system with RES and storage, but without EVs. The objectives of the controller described in this work include cost savings, demand smoothing and flattening, a 2-level charging and discharging paradigm for batteries, etc. The design accounted for uncertainties in the magnitude of the predicted load demand and PV power generation in the system model assumed. Extending this framework to enable control decisions for EVs was attempted; this work is described in this section. Electric Vehicles are mobile, i.e., they are physically present within the MG only during certain periods of time on a given day. The times at which they are present in a given location, where the MG operates, will depend on the driving characteristics of the vehicles' owner(s), traffic and weather conditions, etc.

Additionally, the EVs' batteries would have to be charged—and/or discharged, if

[1] In addition to expressing energy level in kW h, the term *state of charge* (SOC) is used in the literature to denote the energy level of the battery as a percentage of its maximum energy capacity.

components with technologies which enable bidirectional power flow and V2G services are installed—such that the EVs' storage elements attain certain desired energy levels at particular times during the day, so that the owners are able to use their vehicles according to their needs. For example, a particular EV might need to have enough energy to be driven 60 km at 7 A.M. on workdays, for its owner to complete his/her round-trip commute to his/her work place. Depending on the type and capacity of the EV's energy storage, this desired value of energy would be represented by a parameter called the desired SOC of the vehicle's energy storage element. The exact amount of energy will depend on the efficiency characteristics of the EVs' powertrains, EVs' energy storage capacities, the owner's driving characteristics, etc.

In addition, whenever the vehicle gets connected to the MG, it will have a certain amount of energy stored in it, which is unknown to the A-EMS. The A-EMS would need some information on the times of connection and disconnection of EVs to and from a MG, the desired final SOC of the vehicle's storage, the unknown SOC at the time of connection, etc. These can either be predicted based on historical data, a computer model, or a combination of the two, or this information can be obtained from the user remotely.

In summary, when integrating EVs in MGs, the following details need to be considered when re-designing the A-EMS:

- EVs are connected to the MGs intermittently
- EVs' storage elements have an unknown initial SOC at the time of connection to MG
- EVs' storage elements need to be charged and/or discharged to particular desired SOCs at particular times

- Times of connection and disconnection, initial SOCs, and desired final SOCs need to be known for the A-EMS to perform its functions; values of these parameters can either be predicted or obtained from the EVs' owner(s)

3.2.1 EV Models, Variables, Cost Terms, & Constraints

Models, optimization cost terms, and constraints, which have been added to the A-EMS framework described by Malysz et. al [96], are discussed here. The relevant formulation from the earlier A-EMS framework is described in Appendix A[2].

The rate at which an EV's energy storage element—a battery in most cases—can charge or discharge, is limited by the battery chemistry. In discussions shown here, it is assumed that an EV's battery has two ranges of power rates at which they can be charged or discharged: the *green zone* range, in which, charging or discharging does not have considerable undesirable effects on the battery's lifetime performance; and the *red zone* range, which if utilized results in detrimental effects on the battery's lifetime performance. The A-EMS may choose to charge or discharge an EV's battery in the red zone range if it would result in economic benefits, or if a certain energy level has to be reached within a limited time period. The following discussions on variables, cost terms, and constraints will expound further on this idea.

[2]The resulting complete optimization formulation has not been discussed, since it would entail discussing and describing terms, variables, equations, etc. which would distract from the discussion undertaken in this section, i.e., integration of EVs in the A-EMS framework presented in [96].

EV storage model

The discrete-time model described in (3.1) is adapted for EVs as follows.

$$E_{EV,i+1} = E_{EV,i} + \eta_{c,EV} h_i p^c_{EV,i} - \frac{1}{\eta_{d,EV}} h_i p^d_{EV,i} - P^{loss}_{EV} h_i \tag{3.3}$$

where $E_{EV,i}$ is the energy in the EV at time step k, typically measured in kW h, h_i is the length of time step i in the prediction horizon, measured in hours, P^{loss}_{EV} is a self discharge loss of the EV's storage element, expressed as kW h per hour, $p^c_{EV,i}$ and $p^d_{EV,i}$ EV charging and discharging power rates at time step i, $\eta_{c,EV}$ and $\eta_{d,EV}$ are charging and discharging efficiencies respectively. The frequency at which the A-EMS Rolling Horizon controller operates is dictated by h_1, i.e. the first element of horizon time step duration vector $\mathbf{h}$. Note that since EV charging/discharging are mutually exclusive events, the vector property $(\mathbf{p}^c_{EV})^T \mathbf{p}^d_{EV} = 0$ must hold.

EV Variables & Cost Terms

The following is a list of optimization variables that were added to the A-EMS, in order to facilitate the integration of EVs into the framework:

$\mathbf{p}^{gc}_{EV} \in \mathbb{R}^{Nh}$	green zone EV battery charging power rate
$\mathbf{p}^{rc}_{EV} \in \mathbb{R}^{Nh}$	red zone EV battery charging power rate
$\mathbf{p}^{gd}_{EV} \in \mathbb{R}^{Nh}$	green zone EV battery discharging power rate
$\mathbf{p}^{rd}_{EV} \in \mathbb{R}^{Nh}$	red zone EV battery discharging power rate
$\mathbf{u}_{EV} \in \mathbb{R}^{Nh}$	auxiliary vector for EV battery signal smoothing
$\boldsymbol{\delta}_{cd_{EV}} \in \mathbb{Z}^{Nh}$	binary vector for EV battery charging/discharging
$\boldsymbol{\delta}_{r_{EV}} \in \mathbb{Z}^{Nh}$	binary vector for EV battery red zone power rate usage

Here, Nh represents the number of discrete time steps in a time horizon.

In order to avoid unnecessary EV battery activity, which would reduce battery life, it is desired to impose an EV battery usage cost $\mathbf{c}_{EV}$. In order to calculate a realistic value for this cost, one may use a simple method similar to the one described in A.1.1. The EV battery signal can be smoothed by penalizing the difference in charge rates between time steps. In the optimization variable vector $\mathbf{u}_{EV}$, each element is defined by the relation

$$u_{EV,i} = p^{gc}_{EV,i} + p^{rc}_{EV,i} - p^{gd}_{EV,i} - p^{rd}_{EV,i} - p^{gc}_{EV,i-1} - p^{rc}_{EV,i-1} + p^{gd}_{EV,i-1} + p^{rd}_{EV,i-1} \tag{3.4}$$

where, subscripts i and $i-1$, represent the current and previous time steps, respectively. Note that at $i = 1$, the EV battery activity from the previous iteration of the rolling time horizon controller is needed and are treated as constants.

From the above discussion, it follows that the additional cost terms in the A-EMS' optimization formulation are:

$$\mathbf{c}^T_{EV}\left(\mathbf{p}^{gc}_{EV} + \mathbf{p}^{rc}_{EV} - \mathbf{p}^{gd}_{EV} - \mathbf{p}^{rd}_{EV}\right) + \mathbf{c}^T_{smEV}\mathbf{u}_{EV} \tag{3.5}$$

where, $\mathbf{c}_{EV} \in \mathbb{R}^{Nh}$ and $\mathbf{c}_{smEV} \in \mathbb{R}^{Nh}$ are the battery usage cost and the battery signal smoothing penalty, respectively. Thus, these are also the additional *Rolling Horizon Control Variables* associated with EVs in the A-EMS.

EV Constraints

Additional constraints which were added to the A-EMS formulation with the integration of EVs into the framework are described below.

State Decision Constraints When an EV is connected, the A-EMS rolling horizon controller makes decisions on whether to charge or discharge the EV battery. The following constraints were applied to enforce this behaviour:

$$\mathbf{0} \leq \mathbf{p}_{EV}^{gc} \leq p_{EV}^{gc,max} \boldsymbol{\delta}_{cd_{EV}} \tag{3.6}$$

$$\mathbf{0} \leq \mathbf{p}_{EV}^{rc} \leq p_{EV}^{rc,max} \boldsymbol{\delta}_{cd_{EV}} \tag{3.7}$$

$$\mathbf{0} \leq \mathbf{p}_{EV}^{gd} \leq p_{EV}^{gd,max} \left(\mathbf{1} - \boldsymbol{\delta}_{cd_{EV}}\right) \tag{3.8}$$

$$\mathbf{0} \leq \mathbf{p}_{EV}^{rd} \leq p_{EV}^{rd,max} \left(\mathbf{1} - \boldsymbol{\delta}_{cd_{EV}}\right) \tag{3.9}$$

$$\mathbf{0} \leq \boldsymbol{\delta}_{cd_{EV}} \leq \mathbf{1} \tag{3.10}$$

where $\boldsymbol{\delta}_{cd_{EV}}$ is a binary vector such that, for the i^{th} element, $\delta_{cd_{EV},i} = 1$ indicates charging and $\delta_{cd_{EV},i} = 0$ indicates discharging. The scalar constants $p_{EV}^{gc,max}$, $p_{EV}^{gd,max}$ represent maximum green zone charging/discharging power rates, while $p_{EV}^{rc,max}$ and $p_{EV}^{rd,max}$ represent maximum incremental red zone charging/discharging power rates.[3]

EV Battery Energy & Power Rate Change Constraints As discussed earlier in this section, the EV is connected to the MG only during certain time periods in a given day. $\boldsymbol{\varpi} \in \{0,1\}^{Nh}$ is a vector which represents the state of EVs connection to the MG. At time step i, a value of $\varpi_i = 1$ indicates that the EV is connected to the MG , while $\varpi_i = 0$ indicates that the EV is not connected to the MG.

Given the fact that the connection of the EV to the MG is intermittent, it is

[3]It is to be noted that Equations (A.17), (A.19), (A.21), and (A.22) in Appendix A will have to be changed slightly, due to the addition of EV variables and constraints. However, these changes are easy to understand.

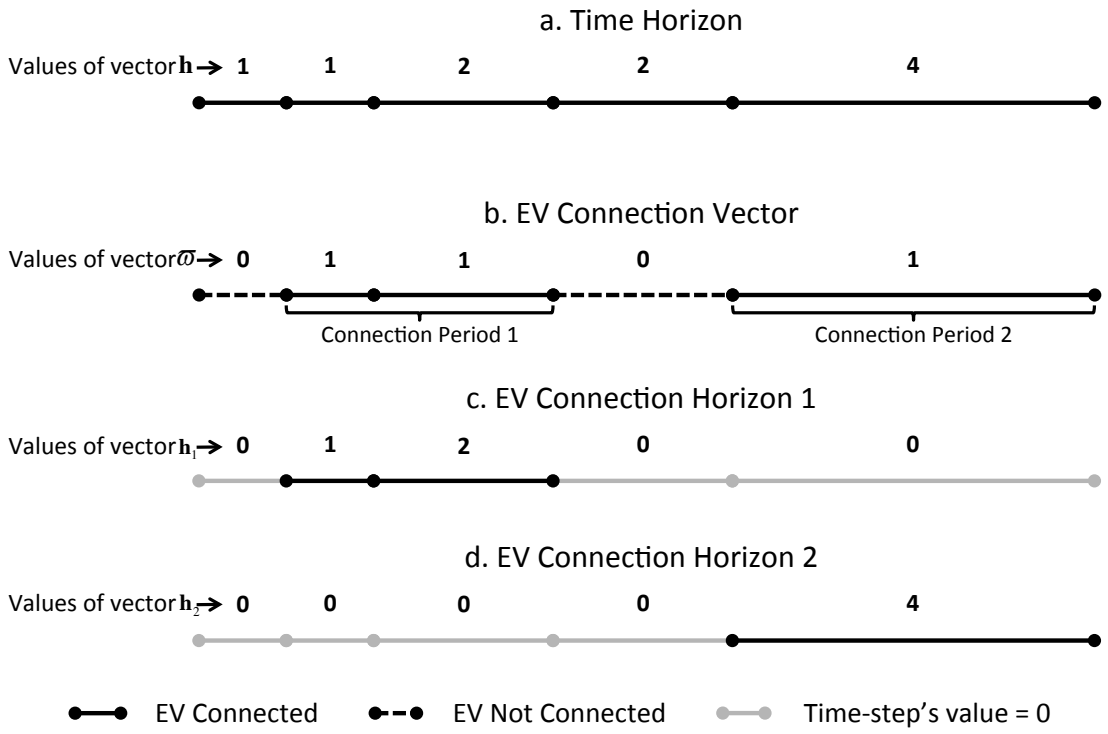

Figure 3.5: An illustrated example of multiple EV time horizons

possible that within one time horizon $\mathbf{h}$, we may have more than one time period, each of different durations, during which the EV is connected to the MG. In order to conveniently define the constraint which maintains the energy level of the EV battery within allowed limits, and another which ensures that the desired final SOC is attained before the EV is disconnected from the MG, we define new time horizons $\mathbf{h}_j$, called EV Connection Horizons, where index j runs through the number of time periods within a time horizon, during which the EV is connected to the MG. Elements of $\mathbf{h}_j$, take the same values as those of $\mathbf{h}$, for the time steps within a time duration j when an EV is connected. Values of all other time steps outside time duration j are

set to 0. For example, in Figure 3.5, the number of time durations over which the EV is connected to the MG, i.e. the number of EV connection periods is 2. Therefore, j takes values 1,2. The new time horizon vectors $\mathbf{h}_1$ and $\mathbf{h}_2$ have 0s at time steps which are outside the 1st and 2nd EV connection periods respectively.

Within each EV connection horizon $\mathbf{h}_j$, it needs to be ensured that the EV battery energy levels remain within certain bounds. Therefore we have,

$$\begin{aligned} E_{EV}^{min} \leq \eta_{c,EV} \sum_{\iota=1}^{i} h_{\iota,j}(p_{EV,\iota}^{gc}+p_{EV,\iota}^{rc}) - P_{EV}^{loss} \sum_{\iota=1}^{i} h_{\iota,j} \\ -\frac{1}{\eta_{d,EV}} \sum_{\iota=1}^{k} h_{\iota,j}(p_{EV,\iota}^{gd}+p_{EV,\iota}^{rd}) + E_{EV,j}^{o} \leq E_{EV}^{max},\ i \in [1, Nh],\ \forall j \end{aligned} \tag{3.11}$$

where $h_{i,j}$ denotes the i^{th} element of EV connection horizon $\mathbf{h}_j$; $E_{EV,j}^{o}$ is the energy level at the start of $\mathbf{h}_j$, corresponding to the initial SOC at the time of connection; and E_{EV}^{min} and E_{EV}^{max} are the lower and upper bounds on EV battery energy level, respectively.

At the end of each EV connection horizon, $\mathbf{h}_j$, we would like the EV battery energy level to be at least equal to a certain desired energy level, corresponding to the desired final SOC. This is ensured by the following inequality constraint:

$$\eta_{c,EV}\mathbf{h}_j^T\left(\mathbf{p}_{EV}^{gc}+\mathbf{p}_{EV}^{rc}\right) - \frac{1}{\eta_{d,EV}}\mathbf{h}_j^T\left(\mathbf{p}_{EV}^{gd}+\mathbf{p}_{EV}^{rd}\right) - P_{EV}^{loss}\mathbf{h}_j^T\mathbf{1} \geq E_{EV,j}^{final} - E_{EV,j}^{o}, \forall j \tag{3.12}$$

The above constraint might render the entire optimization problem infeasible for certain js if the bounds on EV charging power rates, $p_{EV}^{gc,max}$ and $p_{EV}^{rc,max}$ prohibit the optimization from reaching the desired $E_{EV,j}^{final}$ within a given EV connection horizon, $\mathbf{h}_j$. In order to overcome this, once infeasibility is detected, the desired $E_{EV,j}^{final}$ value is

changed such that the problem is feasible again. The resulting solution is, inevitably, one in which, the EV battery is charged at the maximum allowable power rate at all time steps during which the EV is connected to the MG in EV connection horizon $\mathbf{h}_j$.

The constraint related to EV battery signal smoothing and power rate change limits is represented by

$$\begin{aligned} -\Delta p_{EV} h_i \leq -u_{EV,i} \leq p^{gc}_{EV,i} + p^{rc}_{EV,i} - p^{gd}_{EV,i} - p^{rd}_{EV,i} \\ -p^{gc}_{EV,i-1} - p^{rc}_{EV,i-1} + p^{gd}_{EV,i-1} + p^{rd}_{EV,i-1} \leq u_{EV,i} \leq \Delta p_{EV} h_i \end{aligned} \tag{3.13}$$

for $i \in [1, Nh]$ and $\mathbf{u}_{EV} \geq \mathbf{0}$. The term Δp_{EV} represents the maximum allowed EV battery power rate change typically given in units of $\mathrm{kW\,h^{-1}}$.

EV Battery Red-zone Power Rate Constraints The optimization can decide when to enable/disable EV battery red zone incremental power rates by using the following

$$\mathbf{0} \leq \mathbf{p}^{rc}_{EV} \leq p^{rc,max}_{EV} \boldsymbol{\delta}_{r_{EV}} \tag{3.14}$$

$$\mathbf{0} \leq \mathbf{p}^{rd}_{EV} \leq p^{rd,max}_{EV} \boldsymbol{\delta}_{r_{EV}} \tag{3.15}$$

$$\mathbf{0} \leq \boldsymbol{\delta}_{r_{EV}} \leq \mathbf{1} \tag{3.16}$$

where the elements of binary vector $\boldsymbol{\delta}_{r_{EV}}$ indicate when incremental red-zone power rates are active. To ensure green-zone power rates are first used the following constraints are needed

$$p^{gc,max}_{EV} \boldsymbol{\delta}_{r_{EV}} - p^{gc,max}_{EV} (\mathbf{1} - \boldsymbol{\delta}_{cd_{EV}}) \leq \mathbf{p}^{gc}_{EV} \tag{3.17}$$

$$p_{EV}^{gd,max}\boldsymbol{\delta}_{r_{EV}} - p_{EV}^{gd,max}\boldsymbol{\delta}_{cd_{EV}} \leq \mathbf{p}_{EV}^{gd} \tag{3.18}$$

It is assumed the red-zone power rates can be active for a limited amount of time and thus have a maximum on-time denoted by T_{EV}^{maxon}. Moreover it is also assumed that a minimum cool down like time period is required before the red-zone power rates can be reactivated, this minimum off-time is denoted by T_{EV}^{minoff}. The maximum on-time and minimum off-time constraints considering variable time steps in the horizon are formulated as

$$\sum_{i=q}^{q+T_{EV,q}^{maxon}} h_i\delta_{r_{EV,i}} \leq T_{EV}^{maxon}, \forall q \in [q_{min}, q_{max}] \tag{3.19a}$$

$$q_{min,EV} = 2 - \min_{h_1\ell > T_{EV}^{maxon}} \ell \in \mathbb{Z} \tag{3.19b}$$

$$q_{max,EV} = \max_{\sum_{i=\gamma}^{Nh} h_i > T_{EV}^{maxon}} \gamma \in \mathbb{Z} \tag{3.19c}$$

$$T_{EV,q}^{maxon} = \min_{\sum_{i=q}^{q+\tau} h_i > T_{EV}^{maxon}} \tau \in \mathbb{Z} \tag{3.19d}$$

$$\delta_{r_{EV,q-i-1}} - \delta_{r_{EV,q-i}} \leq 1 - \delta_{r_{EV,q}}, \forall i \in [1, T_{EV,q}^{minoff} - 1] \tag{3.20a}$$

$$\forall q \in \left\{ [1, Nh] \middle| T_{EV,q}^{minoff} \geq 2 \right\} \tag{3.20b}$$

$$T_{EV,q}^{minoff} = \min_{\sum_{i=q-\tau}^{q-1} h_i \geq T_{EV}^{minoff}} \tau \in \mathbb{Z}, \ \tau \geq 1 \tag{3.20c}$$

where the first element $h_i = h_1$ is used when $i \leq 0$. Note that a history of previous red-zone activity is needed, the time length of which is dictated by T_{EV}^{maxon} and T_{EV}^{minoff}. These past binary values are treated as constants in the inequality constraints. The maximum on-time constraints are given in 3.19, these constraints function by scanning

rolling windows of time length just greater than T_{EV}^{maxon}. In 3.20, the minimum off-time constraints are shown, they operate by scanning sufficiently back such that the last time red-zone activity was disabled does not occur within the last T_{EV}^{minoff} hours. The terms in 3.19b-3.19d and 3.20c are used to find the correct range of integer indices in the variable time step horizon; they can be precomputed by using only $\mathbf{h}$, T_{EV}^{maxon} and T_{EV}^{minoff}. Note that in 3.20b, only indices that satisfy $T_{EV,q}^{minoff} \leq 2$ are included.

3.2.2 Changes to The Time Horizon

In order to accommodate EVs into the existing A-EMS framework, two significant changes are to be made to the optimization time horizon at each iteration. Previously, the A-EMS used time horizons of the same length in each iteration, even though the time steps within a time horizon were not constant. However, when one considers a case wherein an EV is connected to the MG beyond the end of the current time horizon, the A-EMS will not have a value or a method to find the value of the desired E_{EV}^{final} at the last time step of the time horizon. The solution to this issue is to extend the length of the time horizon so that its last time step coincides with the next instance of EV disconnection from the MG, assuming that the future EV connection and disconnection times are known without uncertainty.

An example for this is illustrated in Figure 3.6. It is important to note that although the length of new time horizon $\bar{\mathbf{h}}$ is greater than that of $\mathbf{h}$, the number of time steps remains the same. The significance of this is that, the number of optimization variables, which is a function of the number of time steps does not change at every iteration. It is to be noted that if the next time of disconnection is unknown or if it is too far away in the future, the extent to which the length of the

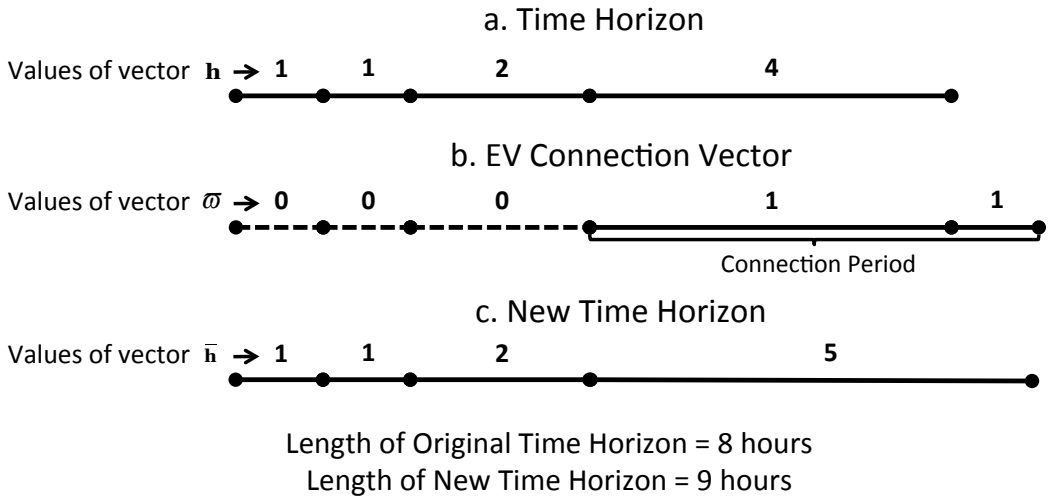

Figure 3.6: An illustrated example of changing the length of the optimization time horizon

time horizon can be increased must be restricted. In the current implementation, the maximum length of any time horizon is set to be 48 hours.

In the A-EMS, each time horizon is structured such that, its first element, i.e. time step is that of the shortest duration, with the duration increasing progressively from the first to the last element. It is assumed that one chooses the first time step to be small enough, such that no EV connection or disconnection event occurs within the time step. However, such events might occur within the duration of most other time steps. This is undesirable, since, in order to implement the inequality constraints represented by Equations 3.11 and 3.12, EV connection and disconnection events must coincide with the beginning and ending of time steps, respectively.

Let us consider the example illustrated in Figure 3.7. It can be seen that within the 4^{th} time step in horizon $\mathbf{h}$, there is a disconnection event occurring. The way this situation is avoided is by splitting the time step within which an EV event occurs,

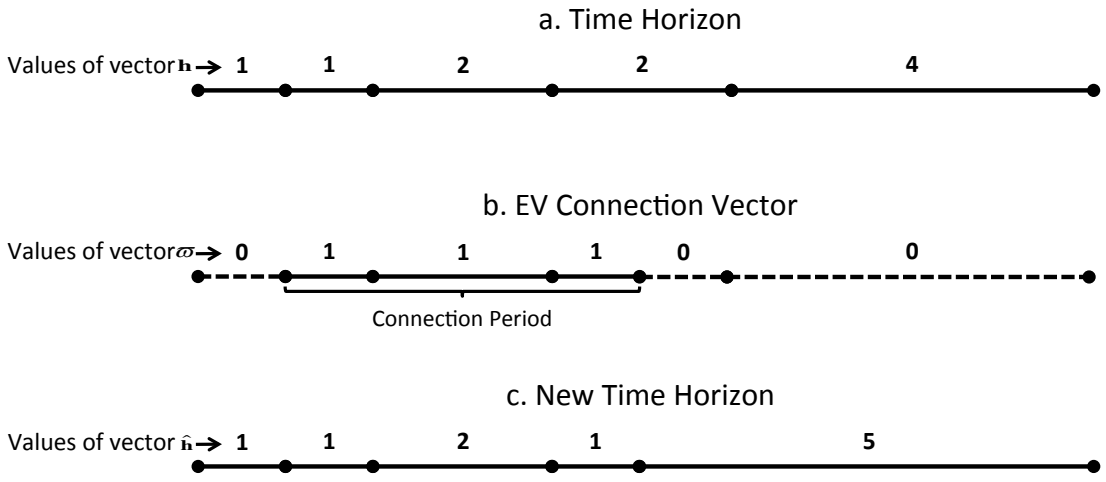

Figure 3.7: An illustrated example of splitting time steps when an EV connection or disconnection event occurs within a time step

and retaining that part of the time step which is closest to the beginning of the time horizon, while adding the remaining part of the split time step to the next time step. This can be seen clearly in the new time horizon $\hat{\mathbf{h}}$ in Figure 3.7. This strategy preserves the number of optimization variables in all but one of the cases: when the last time step is to be split.

3.2.3 Simulation Results

Once the aforementioned changes to the A-EMS formulation in Appendix A were implemented, several different simulations were conducted, some of which gave ideas as to what the future research directions should be. Here, some interesting results, observations, and inferences from some of these results are presented.

In order to be able to execute these simulations, data for EV connection and initial SOC at time of connection were generated synthetically. Information from the

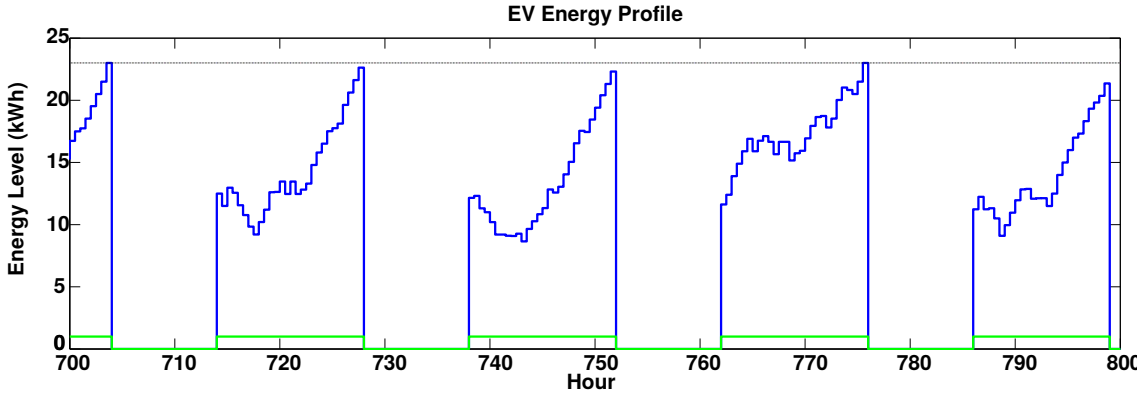

Figure 3.8: Relaxed Problem: A plot of the EV Energy Level Profile over 100 hours of simulation

Canadian Annual Vehicle Survey, 2009 [180], was utilized to aid data generation. An EV with a maximum storage capacity of 23 kWh (comparable to a Nissan Leaf) was assumed. An EV owner who is required to commute 60 kms round-trip to work, at specific times on a weekday, and travels locally, with certain probability during weekends was considered. In all EV connection horizons, the desired final SOC was set to be 100%, i.e., fully charged state.

Effect of Relaxing Binary Variables

In the original A-EMS implementation, the binary decision variables for charging and discharging of the battery $\boldsymbol{\delta}_{cs}$, red zone charging and discharging $\boldsymbol{\delta}_{r}$, and those for buying and selling electric power $\boldsymbol{\delta}_{bs1}$ and $\boldsymbol{\delta}_{bs2}$ were relaxed in such a way that all variables except those which corresponded to the first time step were allowed to take real values in the interval $[0, 1]$. This was done in order to reduce the computational complexity of the optimization problem. However, applying the same strategy to the A-EMS with EVs integrated resulted in the following problem: Within a given EV

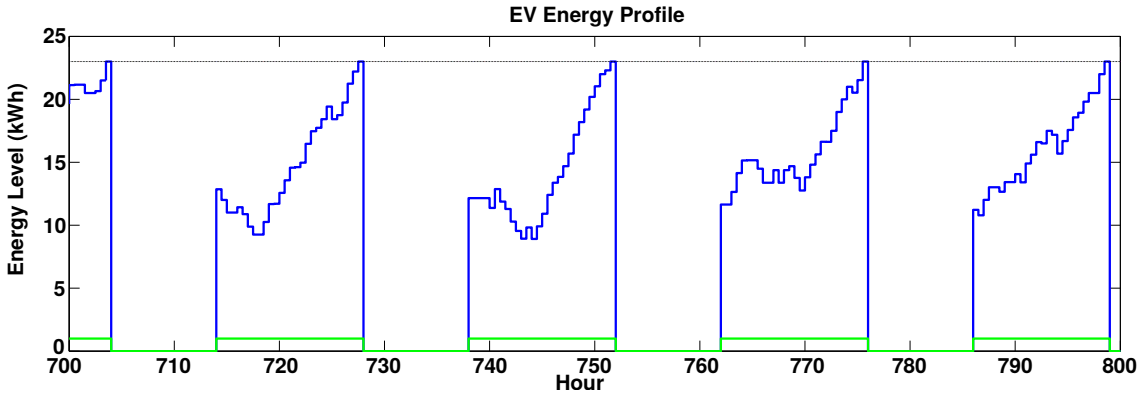

Figure 3.9: No Relaxation: A plot of the EV Energy Level Profile over 100 hours of simulation

connection horizon $\mathbf{h}_j$, the desired $E_{EV,j}^{final}$ was not attained at the time of disconnection, even though there were several instances of discharge over the duration of $\mathbf{h}_j$ and the optimizer found feasible solutions at each iteration.

This behaviour can be observed in Figure 3.8, which shows the EV energy profile over 100 simulation hours. It is understood that such behaviour results from the fact that, at each iteration of the rolling horizon A-EMS optimization, the decisions made did not consider the fact that some of these decisions, corresponding to the time steps farther in the future, were not feasible in reality. Once the optimizer rolls to these time instances, it finds the desired $E_{EV,j}^{final}$ unattainable, and in turn, the optimization problem at that iteration is infeasible. The optimizer will then adjust the $E_{EV,j}^{final}$ value so that the problem is feasible again, as described in 3.2.1. This behaviour can be observed and inferred from the fact that there is a steady increase in energy level towards the end of the first two $\mathbf{h}_j$s in Figure 3.8, corresponding to successive decisions to charge the EV battery, and yet being unable to attain the original $E_{EV,j}^{final}$ value. This effect was remedied by removing all relaxations on the values that the binary decision variables can take. Figure 3.9 shows the EV energy profile for the

same simulation over the same simulation time period, however, with no relaxations on the binary variables. It can be seen that $E_{EV,j}^{final}$ is reached in all the instances in which it wasn't reached in Figure 3.8.

Effect of Changing Values of Control Variables

In the current A-EMS formulation, some of the control variables which appear in the cost function are $\mathbf{c}_{bat}, \mathbf{c}_{EV}, \mathbf{c}_{smb}, \mathbf{c}_{smEV}, \mathbf{c}_{smg}, \mathbf{c}_{dem}$,and $\mathbf{c}_{flat}$. In the current implementation of A-EMS, except for $\mathbf{c}_{bat}, \mathbf{c}_{EV}$, the values of these variables are not determined through real world data or realistic models. Most of these variables are thought of as enable/disable switches, used to test the effect of penalizing a particular set of optimization variables. However, some of the simulation results obtained such as, relative contributions of cost terms to the value of the objective function at the optimal solution, effect of relative values of these variables on the charge/discharge decisions, amount of money that could be saved by varying values of these variables, etc. show conclusively that the value of these variables need to be determined through either through realistic models or real world data. Here, for the purpose illustrating this need, results of simulation experiments affecting charging and discharging profiles of a battery and an EV connected to a MG are shown.

Let us consider the following cases, with different combinations of values for the aforementioned decision variables:

Case 1 $\mathbf{c}_{bat} = 0.1, \mathbf{c}_{EV} = 0.1, \mathbf{c}_{smb} = 0.1, \mathbf{c}_{smEV} = 0.1, \mathbf{c}_{smg} = 1, \mathbf{c}_{dem} = 0$, and $\mathbf{c}_{flat} = 0.1$

Case 2 $\mathbf{c}_{bat} = 0.1, \mathbf{c}_{EV} = 0.1, \mathbf{c}_{smb} = 0.1, c_{smEV} = 0.1, \mathbf{c}_{smg} = 1, \mathbf{c}_{dem} = 0$, and $\mathbf{c}_{flat} = 0$

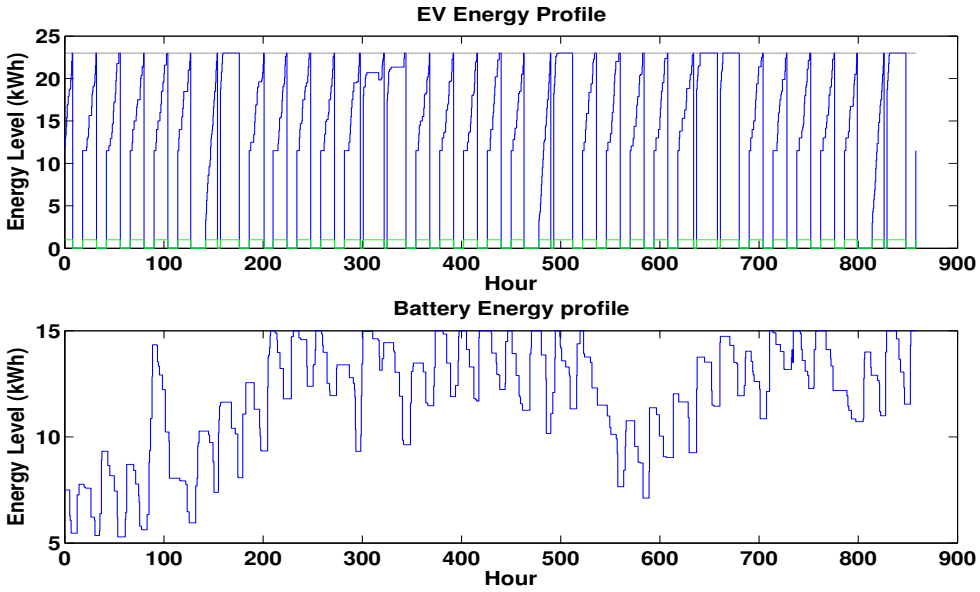

Figure 3.10: Plot of EV and Battery Energy Profiles over Simulation Time for Case 1

Case 3 $\mathbf{c}_{bat} = 0.001, \mathbf{c}_{EV} = 0.001, \mathbf{c}_{smb} = 0.1, \mathbf{c}_{smEV} = 0.1, \mathbf{c}_{smg} = 1, \mathbf{c}_{dem} = 0$, and $\mathbf{c}_{flat} = 0.1$

Figures 3.10 to 3.15 show the battery and EV energy and power profiles over the entire simulation time period, with all other parameters being the same for all three cases. It can be seen that the only difference between Cases 1 and 2 is the value of c_{flat}. However, observing and comparing, Figures 3.10, 3.11 and Figures 3.12, 3.13, one can see that there are significant differences in the charging and discharging patterns of both the battery and the EV. In Case 2, there is no discharging event for the EV. In the case of the battery, the differences between the two cases are even more dramatic, with the battery seeing no activity at all in Case 2, compared to significant charging and discharging events in case 1. The inference here, is that, since in case 1, the grid signal flattening variable is penalised, the battery is utilized to a certain extent

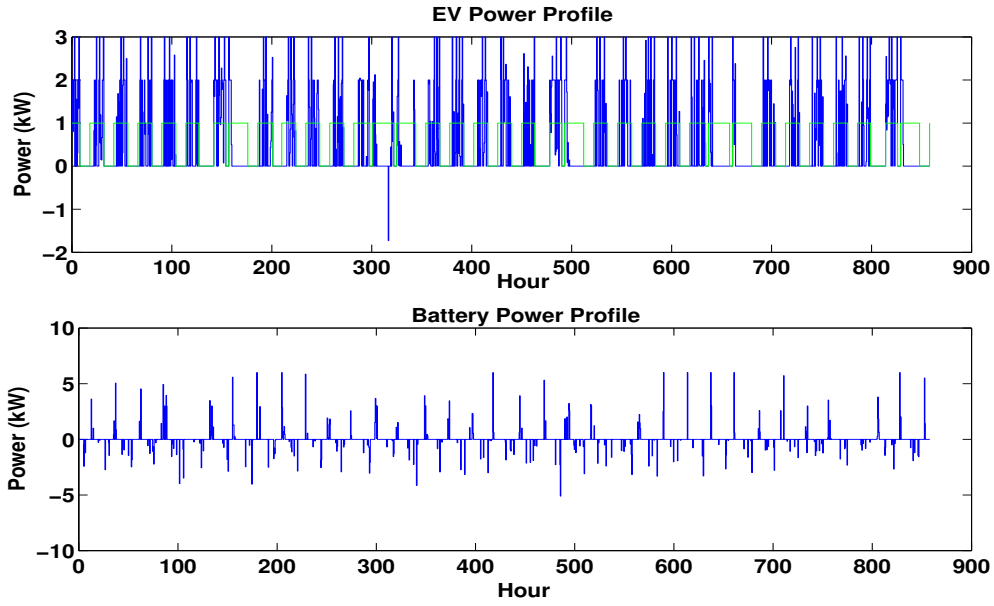

Figure 3.11: Plot of EV and Battery Power Profiles over Simulation Time for Case 1. Negative values indicate discharging; bidirectional charging is considered.

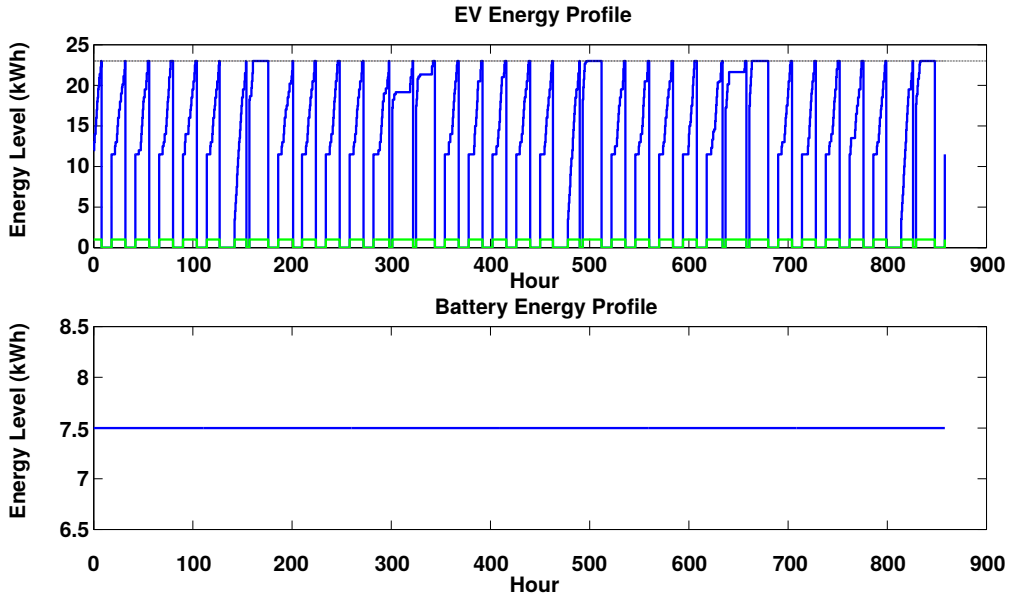

Figure 3.12: Plot of EV and Battery Energy Profiles over Simulation Time for Case 2

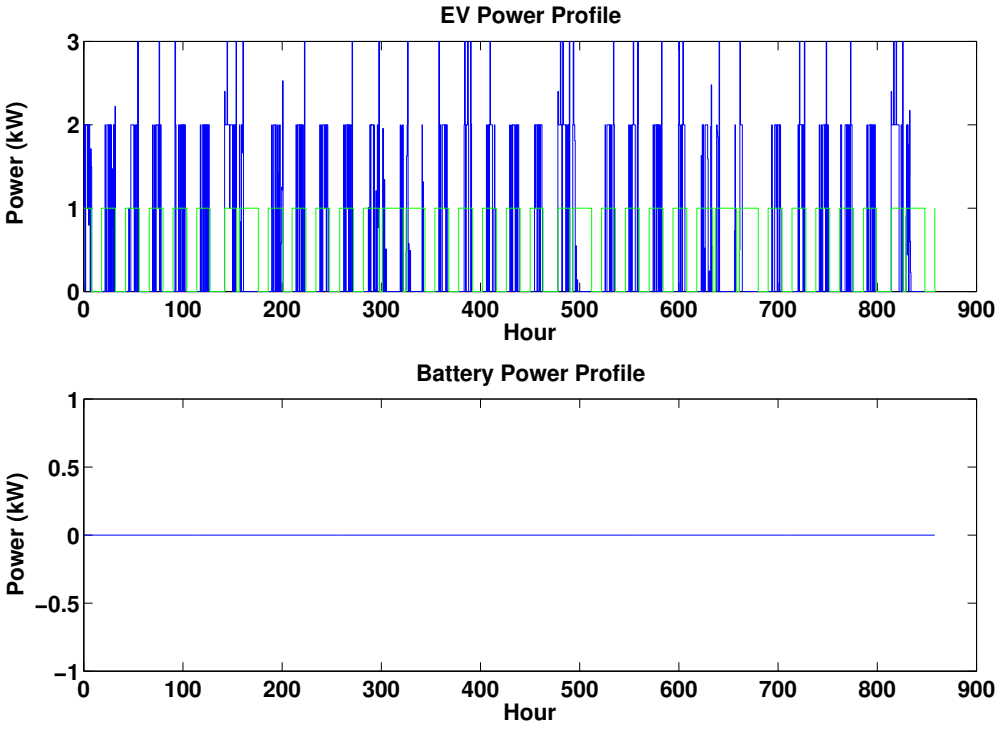

Figure 3.13: Plot of EV and Battery Power Profiles over Simulation Time for Case 2

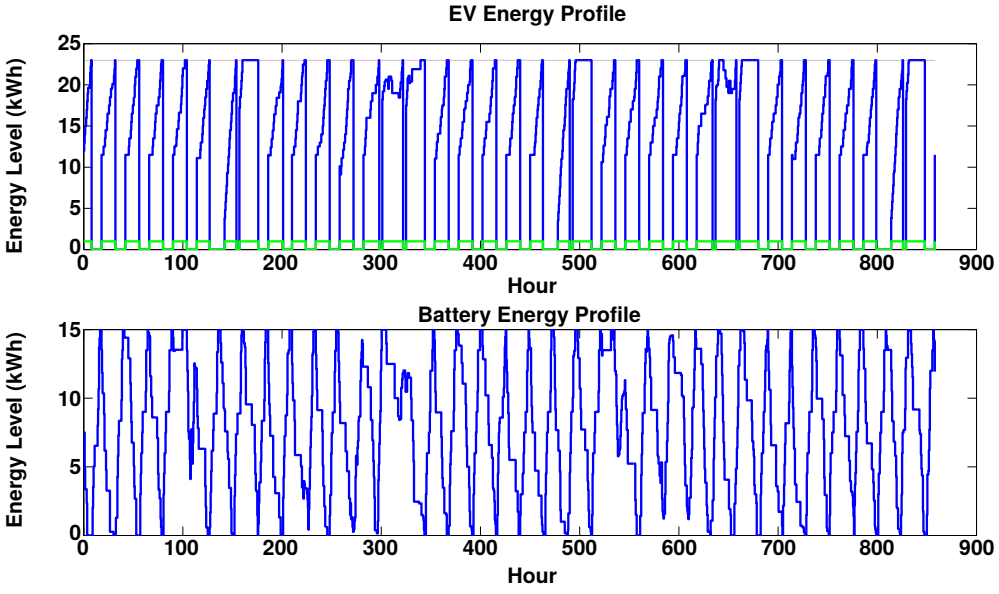

Figure 3.14: Plot of EV and Battery Energy Profiles over Simulation Time for Case 3

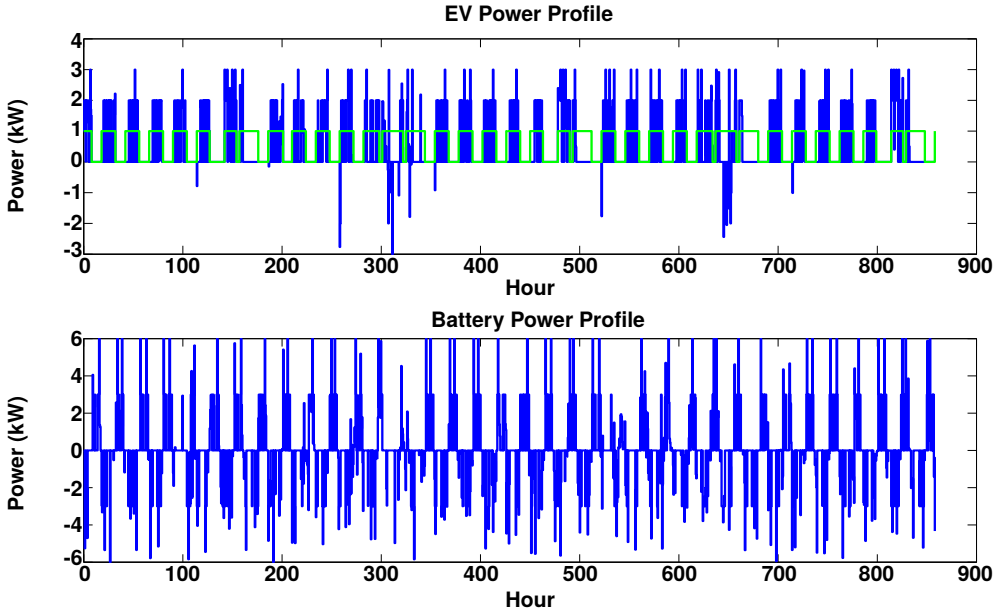

Figure 3.15: Plot of EV and Battery Power Profiles over Simulation Time for Case 3. Negative values indicate discharging; bidirectional charging is considered.

to ensure that the grid signal, seen by the utility grid is relatively flat. However, in Case 2, this is not the case, and in the presence of a battery usage cost $c_{bat} = 0.1$, the optimizer chooses not to utilize the battery at all.

Now, let us compare Cases 2 and 3. The differences between these two cases are the values of the EV and battery usage costs. Now, observing Figures 3.12, 3.13 and Figures 3.14, 3.15, we see that the reduction in usage costs from Case 2 to Case 3 facilitates the optimizer to make use of the storage capabilities of the battery in order to benefit elsewhere, most likely by selling power to the grid in Case 3.

From these observations and inferences, we can conclude that the values of the control variables discussed above affect the behaviour of the A-EMS significantly. Therefore, it is paramount that while assigning values to these variables, care is taken, such that these values reflect the real world costs of utilizing the optimization variables

associated with them. These can be done either through modelling or through the use of data. For instance, demand charge, grid smoothing and flattening charges $\mathbf{c}_{dem}, \mathbf{c}_{smg}$, and $\mathbf{c}_{flat}$ can be obtained from the electricity retailer or distributor.

Solutions to ensure tracking of the multiple time horizons with different time durations for multiple EVs, while ensuring system uncertainties, lead to optimization formulations which are so complex that mathematical tractability is an issue. In addition, the use of cost terms which are hard to quantify in terms of monetary values, it is best served to find alternate approaches to integrate EVs. In the rest of this chapter different optimization formulations which attempt this are discussed.

3.3 Optimization Formulations

The A-EMS solves an optimization problem at every time step of the RH to calculate optimal power values, given the predictions of net demand, EV connection and disconnection times, and their predicted SOCs at time(s) of connection. At each time step, a vector $\mathbf{h} \in \mathbb{R}^{Nh}_{\geq 0}$ is defined such that each of its elements h_i denotes the length of the corresponding time step in the time horizon in hours, with Nh being the number of such time steps in the time horizon. A list of mathematical notations used in the rest of this chapter is available in Appendix B.

In the case where V2G services are available, bidirectional charging is assumed. In some scenarios power can flow only from the microgrid to the EV (unidirectional). Additionally, the A-EMS might only be able to turn charging 'On' or 'Off'. A further restrictive case is one in which the A-EMS loses control of turning charging 'On' or 'Off' once charging commences. In essence, the A-EMS only has control over the time at which the charging of EV starts. In these scenarios, the optimization formulation

in the A-EMS takes the form of a MILP, since decisions are between two discrete states: 'On' and 'Off'. The A-EMS optimization formulations are described in the following sections.

Following are descriptions of the optimization formulations, i.e. the objective function and constraints for both bidirectional and unidirectional charging scenarios. There are two different formulations—Formulations I and II—presented for each of these scenarios. Formulation I makes use of binary decision variables for making charging and discharging of the on-site battery and EV(s) at each time step; and for making decisions for the MG to 'buy' or 'sell' power from and to the utility grid. Formulation II does not use binary variables for these decisions.

3.3.1 Bidirectional Charging

In a microgrid, the power at the point of connection to the grid is the aggregate of the net demand and the power values of the on-site battery and EV(s). As such, assuming bidirectional power flow, the total power at the point of connection in each time horizon is

$$\mathbf{p}_g = \mathbf{p}_d + \mathbf{p}_{bat} + \sum_k \mathbf{p}_{EV_k}, \quad k = 1, 2, \ldots, K \tag{3.21}$$

where $\mathbf{p}_d \in \mathbb{R}^{Nh}$ is the vector of net predicted demand power values, $\mathbf{p}_{bat} \in \mathbb{R}^{Nh}$ is the vector of battery charging or discharging power values, and $\mathbf{p}_{EV_k} \in \mathbb{R}^{Nh}$ is the vector of charging and discharging power rates of the k^{th} EV; K is the total number of EVs in the system. Here, line losses associated with the system are assumed to be negligible and are therefore not considered in (3.21).

Objective Function: Formulation I

The total cost incurred by the microgrid at the point of connection to the grid is

$$cost = \mathbf{c}^T \Big(\mathbf{p}_d + \mathbf{p}_{bat} + \sum_k \mathbf{p}_{EV_k} \Big) \tag{3.22}$$

where $\mathbf{c}^T \in \mathbb{R}^{Nh}$ is vector of grid electricity prices respectively, in ¢/kWh. The goal is to minimize (3.22). It is to be noted that, in general, the cost of electricity is a function of energy. However, in the context of the formulation presented here, (3.25) still holds true since $\mathbf{p}_d$, $\mathbf{p}_{bat}$, and $\mathbf{p}_{EV_k}$ represent the time-averaged values of power. Additional components of electricity cost such as demand charges have not been considered. Separating the buying and selling portions of (3.25), we arrive at the objective function, which is denoted by $\mathcal{F}_I$.

$$\mathcal{F}_I = \mathbf{c}_b^T \Big(\mathbf{p}_d^b + \mathbf{p}_{bat}^b + \sum_k \mathbf{p}_{EV_k}^b \Big) + \mathbf{c}_s^T \Big(\mathbf{p}_d^s + \mathbf{p}_{bat}^s + \sum_k \mathbf{p}_{EV_k}^s \Big) \tag{3.23}$$

Allowing $f(\mathbf{c}_b, \mathbf{c}_s, \mathbf{p}_d, \mathbf{p}_{bat}, \mathbf{p}_{EV_k})$ to denote the right hand side of (3.26a). Below in the optimization formulation for the bidirectional EV charging scenario:

$$\min_{\mathbf{p}_{bat}, \mathbf{p}_{EV_k}} \; f(\mathbf{c}_b, \mathbf{c}_s, \mathbf{p}_d, \mathbf{p}_{bat}, \mathbf{p}_{EV_k}) \tag{3.24a}$$

$$\text{s.t.} \quad p_g^{min} \cdot (\mathbf{1} - \boldsymbol{\delta}^{bs}) \leq \mathbf{p}_d + \mathbf{p}_{bat} + \sum_k \mathbf{p}_{EV_k} \leq p_g^{max} \cdot \boldsymbol{\delta}^{bs} \tag{3.24b}$$

$$E_{bat,i} = \eta_{bat}^c \sum_{\iota=1}^{i} h_\iota p_{bat,\iota}^c + \frac{1}{\eta_{bat}^d} \sum_{\iota=1}^{i} h_\iota p_{bat,\iota}^d + E_{bat}^o - P_{bat}^{loss} \sum_{\iota=1}^{i} h_\iota \tag{3.24c}$$

$$E_{bat}^{min} \leq E_{bat,i} \leq E_{bat}^{max} \tag{3.24d}$$

$$E_{bat,final} \geq E_{bat}^{desired} \tag{3.24e}$$

$$p_{bat}^{min}\boldsymbol{\delta}^{bs} \leq \mathbf{p}_{bat}^{b} \leq p_{bat}^{max}\boldsymbol{\delta}^{bs} \tag{3.24f}$$

$$p_{bat}^{min} \cdot (\mathbf{1} - \boldsymbol{\delta}^{bs}) \leq \mathbf{p}_{bat}^{s} \leq p_{bat}^{max} \cdot (\mathbf{1} - \boldsymbol{\delta}^{bs}) \tag{3.24g}$$

$$\mathbf{0} \leq \mathbf{p}_{bat}^{c} \leq p_{bat}^{max}\boldsymbol{\delta}_{bat}^{cd} \tag{3.24h}$$

$$p_{bat}^{min} \cdot (\mathbf{1} - \boldsymbol{\delta}_{bat}^{cd}) \leq \mathbf{p}_{bat}^{d} \leq \mathbf{0} \tag{3.24i}$$

$$\mathbf{p}_{bat}^{b} + \mathbf{p}_{bat}^{s} = \mathbf{p}_{bat}^{c} + \mathbf{p}_{bat}^{d} \tag{3.24j}$$

$$E_{EV_k,i} = \eta_{EV_k}^{c} \sum_{\iota=\kappa_{l_k}(1)}^{i} h_\iota p_{EV_k,\iota}^{c} + \frac{1}{\eta_{EV_k}^{d}} \sum_{\iota=\kappa_{l_k}(1)}^{i} h_\iota p_{EV_k,\iota}^{d} + E_{EV_k}^{o,l_k} - P_{EV_k}^{loss} \sum_{\iota=\kappa_{l_k}(1)}^{i} h_\iota \tag{3.24k}$$

$$E_{EV_k}^{min} \leq E_{EV_k,i} \leq E_{EV_k}^{max} \tag{3.24l}$$

$$E_{EV_k,final} \geq E_{EV_k}^{desired,l_k}, \forall l_k, \forall k \tag{3.24m}$$

$$p_{EV_k}^{min} \cdot \delta_i^{bs} \leq p_{EV_k,i}^{b} \leq p_{EV_k}^{max} \cdot \delta_i^{bs} \tag{3.24n}$$

$$p_{EV_k}^{min} \cdot (1 - \delta_i^{bs}) \leq p_{EV_k,i}^{s} \leq p_{EV_k}^{max} \cdot (1 - \delta_i^{bs}) \tag{3.24o}$$

$$0 \leq p_{EV_k,i}^{c} \leq p_{EV_k}^{max}\delta_{EV_k,i}^{cd} \tag{3.24p}$$

$$p_{EV_k}^{min} \cdot (1 - \delta_{EV_k,i}^{cd}) \leq p_{EV_k,i}^{d} \leq 0 \tag{3.24q}$$

$$p_{EV_k,i}^{b} + p_{EV_k,i}^{s} = p_{EV_k,i}^{c} + p_{EV_k,i}^{d} \tag{3.24r}$$

$$\text{and} \;\; p_{EV_k,i} = 0 \;\; \forall\, i \notin \kappa_{l_k} \tag{3.24s}$$

In (3.24a), $\mathbf{c}_b^T \in \mathbb{R}^{Nh}$ and $\mathbf{c}_s^T \in \mathbb{R}^{Nh}$ are the buy and sell electricity prices in ¢/kWh; $\mathbf{p}_d^b \in \mathbb{R}^{Nh}$ and $\mathbf{p}_d^s \in \mathbb{R}^{Nh}$ are the buy and sell components of $\mathbf{p}_d$ such that $\mathbf{p}_d^b = \boldsymbol{\delta}^{bs} \cdot \mathbf{p}_d$, $\mathbf{p}_d^s = (\mathbf{1} - \boldsymbol{\delta}^{bs}) \cdot \mathbf{p}_d$, and $\mathbf{p}_d = \mathbf{p}_d^b + \mathbf{p}_d^s$; $\boldsymbol{\delta}^{bs} \in \{0,1\}^{Nh}$ are buy and sell binary decision variables. At the i$^{\text{th}}$ time step, when $\delta_i^{bs} = 1$ power is bought from the grid i.e., power flows from the utility grid to the microgrid; and power is sold to the grid i.e., power flows from the microgrid to the utility grid when $\delta_i^{bs} = 0$. Further,

it is to be noted that in (3.24a), the power values in the first term on the right hand side takes non-zero values when $\delta_i^{bs} = 1$ and those in the second term takes non-zero values when $\delta_i^{bs} = 0$. $\mathbf{p}_{bat}^b \in \mathbb{R}^{Nh}$, $\mathbf{p}_{bat}^s \in \mathbb{R}^{Nh}$ and $\mathbf{p}_{EV_k}^b \in \mathbb{R}^{Nh}$, $\mathbf{p}_{EV_k}^s \in \mathbb{R}^{Nh}$ are the buy and sell portions of the on-site battery and EV powers respectively. In the rest of the chapter, for convenience, $\mathbf{p}_{bat}$ and $\mathbf{p}_{EV_k}$ will denote the sums of their respective buy and sell portions, i.e. $\mathbf{p}_{bat} = \mathbf{p}_{bat}^b + \mathbf{p}_{bat}^s$ and $\mathbf{p}_{EV_k} = \mathbf{p}_{EV_k}^b + \mathbf{p}_{EV_k}^s$. Likewise, $f(\mathbf{c}_b, \mathbf{c}_s, \mathbf{p}_d, \mathbf{p}_{bat}, \mathbf{p}_{EV_k})$ will denote the right hand side of (3.24a). It is worth noting that the objective function can take negative values.

$\mathbf{p}_{bat}$ and $\mathbf{p}_{EV_k}$ also comprise the charging and discharging portions of the on-site battery and EV powers, i.e. $\mathbf{p}_{bat} = \mathbf{p}_{bat}^c + \mathbf{p}_{bat}^d$ and $\mathbf{p}_{EV_k} = \mathbf{p}_{EV_k}^c + \mathbf{p}_{EV_k}^d$. Among the charging and discharging portions, $\mathbf{p}_{bat/EV_k}^c$ and $\mathbf{p}_{bat/EV_k}^d$, one takes a value 0 while the other is non-zero and vice-versa, in the on-site battery and EVs. From the above discussion, it is clear that the value of the sum $\mathbf{p}_{bat/EV_k}^c + \mathbf{p}_{bat/EV_k}^d$, is equal to that of the sum $\mathbf{p}_{bat/EV_k}^b + \mathbf{p}_{bat/EV_k}^s$ in the on-site battery and EVs.

Objective Function: Formulation II

The total cost incurred by the microgrid at the point of connection to the grid can, alternatively, be expressed as

$$cost = \mathbf{c}^T \mathbf{p}_g \tag{3.25}$$

which is similar to (3.22). The goal is to minimize (3.25). As with Formulation I, additional components of electricity cost such as demand charges have not been considered. Separating the buying and selling portions of (3.25), we arrive at the objective function, which is denoted by $\mathcal{F}_{II}$.

$$\mathcal{F}_{II} = \mathbf{c}_b^T \mathbf{p}_g^b + \mathbf{c}_s^T \mathbf{p}_g^s \tag{3.26a}$$

$$\text{and } \mathbf{p}_g = \mathbf{p}_g^b + \mathbf{p}_g^s \tag{3.26b}$$

Given (3.26b), (3.26a) becomes

$$\mathcal{F}_{II} = (c_b^T - c_s^T)\mathbf{p}_g^b + \mathbf{c}_s^T \mathbf{p}_g \tag{3.27}$$

The optimization formulation for the bidirectional EV charging scenario is presented below:

$$\min_{\mathbf{p}_g^b, \mathbf{p}_g} \mathcal{F}_{II} + \varsigma\big(\mathbf{p}_{bat}^c + \sum_k \mathbf{p}_{EV,i}^c\big) \tag{3.28a}$$

$$\text{s.t. } p_g^{min}\mathbf{1} \leq \mathbf{p}_d + \mathbf{p}_{bat} + \sum_k \mathbf{p}_{EV_k} \leq p_g^{max}\mathbf{1} \tag{3.28b}$$

$$\mathbf{p}_g = \mathbf{p}_d + \mathbf{p}_{bat} + \sum_k \mathbf{p}_{EV_k} \tag{3.28c}$$

$$\mathbf{p}_g^b \geq \mathbf{p}_g \tag{3.28d}$$

$$\mathbf{0} \leq \mathbf{p}_g^b \leq p_g^{max}\mathbf{1} \tag{3.28e}$$

$$E_{bat,i} = E_{bat}^o + \left(\eta_{c,bat} - \frac{1}{\eta_{d,bat}}\right) \sum_{\iota=1}^{i} h_\iota p_{bat,\iota}^c + \frac{1}{\eta_{d,bat}} \sum_{\iota=1}^{i} h_\iota p_{bat,\iota} - P_{bat}^{loss} \sum_{\iota=1}^{i} h_\iota \tag{3.28f}$$

$$E_{bat}^{min} \leq E_{bat,i} \leq E_{bat}^{max} \tag{3.28g}$$

$$E_{bat,final} \geq E_{bat}^{desired} \tag{3.28h}$$

$$p_{bat}^{min}\mathbf{1} \leq \mathbf{p}_{bat} \leq p_{bat}^{max}\mathbf{1} \tag{3.28i}$$

$$\mathbf{0} \leq \mathbf{p}_{bat}^c \leq p_{bat}^{max}\mathbf{1} \tag{3.28j}$$

$$\mathbf{p}^c_{bat} \geq \mathbf{p}_{bat} \tag{3.28k}$$

$$E_{EV_k,i} = E^{o,l_k}_{EV_k} + \left(\eta_{c,EV_k} - \frac{1}{\eta_{d,EV_k}}\right)\sum_{\iota=1}^{i} h_\iota p^c_{EV_k,\iota} + \frac{1}{\eta_{d,EV_k}}\sum_{\iota=1}^{i} h_\iota p_{EV_k,\iota} - P^{loss}_{EV_k}\sum_{\iota=1}^{i} h_\iota, \quad \forall l_k, \forall k \tag{3.28l}$$

$$E^{min}_{EV_k} \leq E_{EV_k,i} \leq E^{max}_{EV_k} \tag{3.28m}$$

$$E_{EV_k,final} \geq E^{desired,l_k}_{EV_k} \tag{3.28n}$$

$$p^{min}_{EV_k} \leq p_{EV_k,i} \leq p^{max}_{EV_k} \tag{3.28o}$$

$$0 \leq p^c_{EV_k,i} \leq p^{max}_{EV_k} \tag{3.28p}$$

$$p^c_{EV_k,i} \geq p_{EV_k,i} \tag{3.28q}$$

$$\text{and } \; p_{EV_k,i} = 0 \;\; \forall\, i \notin \kappa_{l_k} \tag{3.28r}$$

The set of equations (3.28a)-(3.28r) represent the A-EMS optimization formulation for the bidirectional EV charging scenario. In (3.28a), $\mathbf{c}_b \in \mathbb{R}^{Nh}$ and $\mathbf{c}_s \in \mathbb{R}^{Nh}$ are the buy and sell electricity prices in ¢/kWh; $\mathbf{c}_b \geq \mathbf{c}_s$. $\bar{\mathbf{p}}^b_g \in \mathbb{R}^{Nh}$ is the buy (positive) component of $\bar{\mathbf{p}}_g$, which can take both positive and negative values. It is worth noting that the objective function (3.28a) can take negative values. Further, variables $\mathbf{p}^b_{bat}, \mathbf{p}^s_{bat}, \mathbf{p}^b_{EV_k}, \mathbf{p}^s_{EV_k}, \mathbf{p}^d_{bat}, \mathbf{p}^d_{EV_k}, \boldsymbol{\delta}^{cd}_{bat}, \boldsymbol{\delta}^{cd}_{EV_k}$, and $\boldsymbol{\delta}^{bs}$, which were present in Formulation I, do not play a role in Formulation II.

$\mathbf{p}^c_{bat}$ and $\mathbf{p}^c_{EV_k}$ are the charging (positive) portions of the on-site battery and EV powers. The small positive coefficient ς in (3.28a) ensures that the optimizer minimizes the value of $\mathbf{p}^c_{bat}$, while the constraint (3.28k) ensures that the minimum value attained by $\mathbf{p}^c_{bat}$ is $\mathbf{p}_{bat}$; therefore $\mathbf{p}^c_{bat} = \max(\mathbf{0}, \mathbf{p}_{bat})$. Similarly ς and (3.28q) ensure that $\mathbf{p}^c_{EV_k} = \max(\mathbf{0}, \mathbf{p}_{EV_k})$. It is to be noted that $\mathbf{p}_{bat}$ and $\mathbf{p}_{EV_k}$ can take both positive

and negative values. Similarly, it is ensured that $\mathbf{p}_g^b = \max(\mathbf{0}, \mathbf{p}_g)$ by a combination of the constraint (3.28d) and the fact that the coefficient of $\mathbf{p}_g^b$ in (3.27), $(\mathbf{c}_b - \mathbf{c}_s) \geq \mathbf{0}$. The constraint (3.28c) serves to define the grid power $\mathbf{p}_g$.

3.3.2 Grid Power Constraints

Grid power of the microgrid is aggregate power measured at the point of connection to the utility grid, given by (3.21). $p_g^{min} \in \mathbb{R}$ and $p_g^{max} \in \mathbb{R}$ are user-defined minimum and maximum grid power limits , where p_g^{min} is a negative number.

Formulation I

In order to ensure that the values of buy and sell power values remain within their limits, constraints defined by (3.24b) are introduced at each time step.

Formulation II

In order to ensure that the values of buy and sell power values remain within their limits, constraints defined by (3.28b) are introduced at each time step.

3.3.3 On-Site Battery Energy & Power Constraints

Formulation I

(3.24c) defines the battery energy $E_{bat,i}$ at each time step i in Formulation I. Constraints shown in (3.24d) are imposed to ensure that the energy level of the on-site battery is maintained within its bounds at all time steps $i = 1, \ldots, Nh$. In (3.24d) , $E_{bat}^{min} \in \mathbb{R}_{\geq 0}$ and $E_{bat}^{max} \in \mathbb{R}_{\geq 0}$ are the minimum and maximum energy bounds for

the on-site battery. Here, η^c_{bat}, η^d_{bat} and P^{loss}_{bat} are the on-site battery charging and discharging efficiencies, and self-discharge loss respectively. In addition, the minimum energy level of the battery at the end of the time horizon can be specified using the constraint (3.24e). In this constraint, $E^{desired}_{bat} \in \mathbb{R}_{\geq 0}$ is the desired minimum battery energy level at the end of the time horizon, $E^o_{bat} \in \mathbb{R}_{\geq 0}$ is the energy level at the beginning of the time horizon, and $\mathbf{1}$ is a unit vector of length Nh.

The battery charging and discharging power values are bounded by the values $p^{min}_{bat} \in \mathbb{R}$ and $p^{max}_{bat} \in \mathbb{R}$, where p^{min}_{bat} is a negative number.Moreover, only one component of $\mathbf{p}_{bat}$, i.e. $\mathbf{p}^b_{bat}$ or $\mathbf{p}^s_{bat}$ can non-zero at any given time. Therefore, constraints defined by (3.24f)-(3.24j) are needed. In this set of constraints, $\boldsymbol{\delta}^{cd}_{bat}$ is the vector of binary charging/discharging decision variables for the on-site battery.

Formulation II

In Formulation II, the maximum energy and power limits, $E^{min}_{bat}, E^{max}_{bat}, p^{min}_{bat}$ and p^{max}_{bat} are defined and used in the same way as in Formulation I. The constraint (3.28f) defines $E_{bat,i}$, while constraints (3.28g) are imposed to ensure that $E_{bat,i}$ is maintained within its bounds. $E_{bat,final}$ can be specified using the constraint (3.28h). Constraints (3.28i) and (3.28j) define the battery power bounds; and $\mathbf{p}^c_{bat} \geq \mathbf{0}$.

3.3.4 Electric Vehicle Energy & Power Constraints

A given EV may be connected to the microgrid over different time periods within a time horizon. For example, the k^{th} EV, EV_k may be connected to the microgrid from hours 1-5, and then from hours 15-20, in a 24 hour time horizon. Thus, EV_k has two time periods in the time horizon, henceforth referred to as *connection periods*,

over which it is connected to the microgrid. A set κ_{l_k} is defined. It contains the indices of consecutive time steps in the time horizon $\mathbf{h}$, which correspond to the ${l_k}^{\text{th}}$ connection period corresponding to the k^{th} EV; $l_k = 1, \ldots, L_k$, where L_k is the number of connection periods in the time horizon for the k^{th} EV. In the above example, for the 1^{st} EV ($k = 1$), $L_1 = 2$, $\kappa_{l_1=1} = \{1, 2, 3, 4, 5\}$, and $\kappa_{l_1=2} = \{15, 16, 17, 18, 19, 20\}$.

Formulation I

EV energy and power constraints are defined differently to (3.24e), & (3.24f)-(3.24j) in Formulation I. The EV energy bounds can be imposed through the constraint (3.24l), where $i \in \kappa_{l_k}, \forall l_k, \forall k$; $E_{EV_k}^{o,l_k} \in \mathbb{R}_{\geq 0}$ is the initial EV energy level of the k^{th} EV in the ${l_k}^{\text{th}}$ connection period; $E_{EV_k}^{min} \in \mathbb{R}_{\geq 0}$ and $E_{EV_k}^{min} \in \mathbb{R}_{\geq 0}$ are the minimum and maximum energy bounds for the k^{th} EV. $\kappa_{l_k}(1)$ represents the first element (index of the earliest time step) of the set κ_{l_k}. (3.24l) mimics the working of the on-site battery constraint (3.24d), which is defined over the entire time horizon.

The constraint (3.24m) ensures that the energy level of EV_k reaches the desired value by the end of connection period l_k. In this constraint, $E_{EV_k}^{desired,l_k} \in \mathbb{R}_{\geq 0}$ denotes the desired minimum final EV energy level of the k^{th} EV in the ${l_k}^{\text{th}}$ connection period. This constraint mimics the operation of the on-site battery constraint (3.24e)

When $i \in \kappa_{l_k}$, the EV power limit constraints are given by (3.24n)-(3.24s), where $p_{EV_k}^{min} \in \mathbb{R}$ and $p_{EV_k}^{max} \in \mathbb{R}$ are the minimum and maximum power bounds; $p_{EV_k}^{min}$ is a negative number; and $\delta_{EV_k,i}^{cd}$ is the binary charging/discharging decision variable at the i^{th} time step for the k^{th} EV. These constraint mimic the operation of the on-site battery constraints (3.24f)-(3.24j).

Formulation II

In a similar fashion to Formulation I, EV energy and power constraints are defined differently to (3.28f)-(3.28k). $p^{min}_{EV_k}, p^{max}_{EV_k}, E^{min}_{EV_k}, E^{max}_{EV_k}, E^{o,l_k}_{EV_k}$, and $E^{desired,l_k}_{EV_k}$ are defined in the same way as in Formulation I. The energy level of the k^{th} EV at time step i, $E_{EV_k,1}$ is defined in (3.28l); EV energy bounds are imposed through (3.28m), where $i \in \kappa_{l_k}, \forall l_k, \forall k$; (3.28m) mimics the working of the on-site battery constraint (3.28g).

The constraint (3.28n) ensures that the energy level of EV_k, $E_{EV_k,final}$ reaches the desired value by the end of connection period l_k. This constraint mimics the operation of the on-site battery constraint (3.28h). When $i \in \kappa_{l_k}$, the EV power limit constraints are given by (3.28o)-(3.28r); $p^c_{EV_k,i} \geq 0$. These constraints mimic the operation of the on-site battery constraints (3.28i)-(3.28k).

3.3.5 Unidirectional Charging: On/Off Control

So far, the optimization formulation has been developed assuming bidirectional charging for EVs. However this might not be true at all times. In addition, it has also been assumed that $p_{EV_k,i}$ can take any value between its upper and lower bounds. This assumption implies that a mechanism to control the value of this time-averaged power over a time step h_i is available. When this is not true, one ought to work with an On/Off type of control, wherein the optimizer decides to either charge (On) an EV or not (Off), at a fixed power level.

Considering the above scenarios, for a given EV, EV_k, the vector $\boldsymbol{\delta}_{EV_k} \in \{0,1\}^{Nh}$, is defined to denote the On and Off decisions in the unidirectional charging case. $\delta_{EV_k,i} = 0$ denotes a decision not to charge (Off), and $\delta_{EV_k,i} = 1$ denotes a decision to charge (On) at a fixed rate, say $p^{max}_{EV_k}$. Here, $\mathbf{p}_{EV_k} = p^{max}_{EV_k}\boldsymbol{\delta}_{EV_k}$ and therefore the

value $p^{max}_{EV_k}\boldsymbol{\delta}_{EV_k}$ can replace $\mathbf{p}_{EV_k}$ in the optimization formulation for the bidirectional charging scenario to derive the On/Off control optimization formulation.

Formulation I

In formulation I, as with the bidirectional charging scenario, $\mathbf{p}_{EV_k} = \mathbf{p}^b_{EV_k} + \mathbf{p}^s_{EV_k}$. Thus, $\mathbf{p}^b_{EV_k} + \mathbf{p}^s_{EV_k} = p^{max}_{EV_k}\boldsymbol{\delta}_{EV_k}$. Taking the formulation in (3.24) as the base, the optimization formulation for On/Off control can be expressed as follows.

$$\min_{\mathbf{p}_{bat},\boldsymbol{\delta}_{EV_k}} f(\mathbf{c}_b, \mathbf{c}_s, \mathbf{p}_d, \mathbf{p}_{bat}, p^{max}_{EV_k}\boldsymbol{\delta}_{EV_k}) \tag{3.29a}$$

$$\text{s.t. } p^{min}_g \cdot (\mathbf{1} - \boldsymbol{\delta}^{bs}) \leq \mathbf{p}_d + \mathbf{p}_{bat} + \sum_k p^{max}_{EV_k}\boldsymbol{\delta}_{EV_k} \leq p^{max}_g \cdot \boldsymbol{\delta}^{bs} \tag{3.29b}$$

$$E_{EV_k,i} = \eta^c_{EV_k} p^{max}_{EV_k} \sum_{\iota=\kappa_{l_k}(1)}^{i} h_\iota \delta_{EV_k,\iota} + E^{o,l_k}_{EV_k} - P^{loss}_{EV_k} \sum_{\iota=\kappa_{l_k}(1)}^{i} h_\iota, i \in \kappa_{l_k}, \forall l_k, \forall k \tag{3.29c}$$

For $i \in \kappa_{l_k}$,

$$0 \leq p^{max}_{EV_k}\delta_{EV_k,i} \leq p^{max}_{EV_k} \cdot \delta^{bs}_i \tag{3.29d}$$

$$0 \leq p^{max}_{EV_k}\delta_{EV_k,i} \leq p^{max}_{EV_k} \cdot (1 - \delta^{bs}_i) \tag{3.29e}$$

$$\mathbf{p}^b_{EV_k,i} + \mathbf{p}^s_{EV_k,i} = p^{max}_{EV_k}\boldsymbol{\delta}_{EV_k} \tag{3.29f}$$

$$\text{and } \delta_{EV_k,i} = 0 \ \ \forall\, i \notin \kappa_{l_k} \tag{3.29g}$$

Here, (3.24a) and (3.24b) are replaced by (3.29a) and (3.29b); while (3.29c) replaces (3.24k); (3.29d)-(3.29g) are equivalent to (3.24n), (3.24o), (3.24r), and (3.24s) respectively. The rest of the constraints in the optimization problem defined by the set of equations (3.24) are carried over, with the exception of (3.24p) and (3.24q), which do not apply to the On/Off control optimization formulation.

Formulation II

Taking the formulation in (3.28) as the base, the optimization formulation for On/Off control can be stated as

$$\min_{\mathbf{p}_g^b, \mathbf{p}_g} \mathcal{F}_{II} + \varsigma \mathbf{p}_{bat}^c \tag{3.30a}$$

$$\text{s.t. } p_g^{min}\mathbf{1} \leq \mathbf{p}_d + \mathbf{p}_{bat} + \sum_k p_{EV_k}^{max} \boldsymbol{\delta}_{EV_k} \leq p_g^{max}\mathbf{1} \tag{3.30b}$$

$$\mathbf{p}_g = \mathbf{p}_d + \mathbf{p}_{bat} + \sum_k p_{EV_k}^{max} \boldsymbol{\delta}_{EV_k} \tag{3.30c}$$

$$E_{EV_k,i} = E_{EV_k}^{o,l_k} + \eta_{c,EV_k} \sum_{\iota=1}^{i} h_\iota p_{EV_k}^{max} \boldsymbol{\delta}_{EV_k,\iota} - P_{EV_k}^{loss} \sum_{\iota=1}^{i} h_\iota$$

$$i \in \kappa_{l_k}, \forall l_k, \forall k \tag{3.30d}$$

$$\delta_{EV_k,i} = 0 \;\; \forall\, i \notin \kappa_{l_k} \tag{3.30e}$$

Here, (3.28a) and (3.28b) are replaced by (3.30a) and (3.30b); while (3.30c), (3.30d), and (3.30e) replace (3.28c), (3.28l), and (3.28r) respectively. The rest of the constraints in the optimization problem defined by the set of equations (3.28) are carried over, with the exception of (3.28o) - (3.28q), which do not apply to the On/Off control optimization formulation.

3.3.6 One Block Charging Constraints

In the case where the optimizer does not have the ability to switch EV charging On and Off more than once in an EV's connection period, the only controllable aspect

of the EV is the time at which the charging of the EV commences. And once charging commences, it cannot be turned off until it reaches its desired final energy level $E_{EV_k}^{final,l_k}$, or disconnected by the user. This problem is termed the 'One Block Charging' problem since the EV is charged at a constant rate for one block of time within a connection period. It can be solved by using the optimization formulation described in both formulations in 3.3.5 for On/Off control with the additional constraints

$$-\delta_{OB,\iota} \leq \delta_{EV_k,\iota} - \delta_{EV_k,\iota-1} \leq \delta_{OB,\iota} \tag{3.31a}$$

$$\delta_{OB,\iota} \in \{0,1\} \tag{3.31b}$$

$$\sum_{\iota \in \kappa_{l_k}} \delta_{OB,\iota} \leq 2,\ \iota \in \kappa_{l_k}, \forall l_k, \forall k \tag{3.31c}$$

where $\delta_{OB,\iota}$ is the binary One Block variable which is used to control the number of transitions between 'On' and 'Off' states of EV charging. The combination of the constraints (3.31a)-(3.31c) solve the One Block charging problem by restricting the number of transitions between 'On' to 'Off' states of EV charging within a connection period κ_{l_k} to a maximum of 2.

3.4 Summary

A MG system containing PV panels, on-site battery, and integrated EVs were considered, with the aim of developing a control framework to function as the EMS. Rolling horizon optimal control frameworks called the A-EMS were presented. Initial attempts tried to expand an earlier version of A-EMS to accommodate EVs primarily by modifying the time horizon used in the optimization. Due to difficulties in keeping track of multiple time horizons for multiple EVs while designing for system

uncertainties, alternative approaches were sought.

Two alternate formulations were presented for integrating EVs under uncertainties. Formulation I made use of binary decision variables to decide between charging and discharging energy storage elements, and between buying and selling electricity from and to the utility grid. Alternatively, Formulation II forwent the use of binary variables in order to decide between charging and discharging; and buying and selling. In these formulations, MILP optimizers are used by the controllers to maximize economic benefits to the owner, while ensuring EVs connected to the microgrid attain specific energy levels at specific times, in different charging scenarios: bidirectional charging, On/Off control, and One Block Charging.

In the next chapter, Stochastic versions of the controller, which make use of scenario based methods to solve chance constraints based optimization are derived. In order to make the comparison easier, results of simulations which compare the performances of the formulations I and II, and those of the stochastic and non-stochastic versions are also discussed in the next chapter.

Chapter 4

A-EMS: Stochastic Formulation & Simulation Results

4.1 Introduction

In the last chapter, A-EMS optimization formulations for optimal control over a rolling time horizon in microgrids was presented. Two different formulations which use different strategies to make charging/discharging, and buying/selling decisions were presented.

One of the most important features of the A-EMS control framework is the ability to integrate EVs. In the system described in Section 3.1, uncertainties may arise in the predicted values of the load demand, power generated by PV panels, times of connections and disconnections of EV(s) connected to the MG, and the energy level of the EV(s) at the time(s) of connection. These are due to the unpredictability of user behaviour, intermittent nature of solar power generation, and the mobility of EVs.

A crucial challenge is to ensure that EV(s) attain specific energy levels, when connected to the system under study, at particular time instances. This is required in order to ensure that user(s) can place confidence in the EV(s) to contain enough energy to complete the trips; i.e., to avoid *range anxiety*. A control technique using chance constraints is proposed in this chapter, which draws samples or "particles" from the uncertainty space of the above parameters to ensure that the probability of failure, i.e. not reaching the desired EV charge level at time of disconnection, is at most a value specified by the user. This technique can work with uncertainties arising from any source distribution. The problem is *stochastic* by virtue of the use of chance constraints in the optimization formulation. The method used to solve the optimization problem falls under the category of *scenario or particle based techniques*. Simulation experiments and comparison of the performance of these formulations are also discussed.

4.2 Stochastic Optimization Formulations

In the discussion thus far, predicted values of net demand, EV connection and disconnection times, and initial energy level of EV at time of connection, were all assumed to be accurate, i.e. the prediction is certain. In reality, the predicted values are seldom accurate and are subject to errors, which can lead to violation of important constraints such as EV charge level at time of disconnection from microgrid. In this chapter, a *chance constraints* based stochastic optimization technique [114] is employed to improve performance when handling such uncertainties. In this method, the stochastic optimization problem is approximated by sampling the distribution of uncertain system parameters to generate "particles". The threshold for probability

of failure can be set by specifying the number of such particles which are allowed to cause infeasibility of the optimization problem.

Consider a discrete-time dynamic system whose current state depends on the previous state and control inputs, The state is denoted by vector $\mathbf{x} \in \mathbb{R}^{Nx}$ and control inputs are denoted by $\mathbf{u} \in \mathbb{R}^{Nu}$. Let $\mathbf{x}_t$ denote the state vector $\mathbf{x}$ at time t and $x_{1:T}$ denotes the state sequence $\langle \mathbf{x}_1, \ldots, \mathbf{x}_T \rangle$. A control problem with chance constraints is described below

$$\begin{aligned} \min \quad & E[h(\mathbf{u}_{0:T-1}, \mathbf{x}_{1:T})] && \text{(4.1a)} \\ \text{s.t.} \quad & p(\mathbf{x}_{1:T} \notin F) \leq \epsilon && \text{(4.1b)} \\ & E[\mathbf{x}_{1:T}] \in G && \text{(4.1c)} \\ & \mathbf{u}_{0:T-1} \in U && \text{(4.1d)} \end{aligned}$$

where $h(\cdot, \cdot)$ is the cost function, F, G, and U are the feasible regions for the state trajectory, expected state trajectory, and control inputs respectively. The problem is to find optimal control inputs $\mathbf{u}_{0:T-1}$ under uncertainty such that the probability that the state trajectory breaches the feasible region F is at most ϵ.

To enable A-EMS handle uncertainties better, the optimization framework discussed earlier ought to be reformulated as a control problem with chance constraints. In other words, (3.28)-(3.31) need to be re-written in a form similar to (4.1a)-(4.1d). Comparing the two sets of equations, at time step h_i, the state vector of the A-EMS optimization framework comprises $E_{bat,i}$ and $E_{EV_k,i}, \forall k$ and the control inputs are $p_{bat,i}$ and $p_{EV_k,i}$. The state dynamics are governed by (3.1).

The parameters which cause uncertainties are the net demand $\mathbf{p}_d$; the times of

connection and disconnection of EVs i.e. the connection periods defined by $\kappa_{l_k}, \forall k$; and the energy level of the EVs at the time(s) of connection $E_{EV_k}^{o,l_k}, \forall l, \forall k$. In Formulation I, since the power constraints (3.24f)-(3.24j), (3.24n)-(3.24s), and (3.31); and energy constraints (3.24c), (3.24d), and (3.24e) not affected by uncertainties, they can be retained as such and are equivalent to (4.1d). In Formulation II, the power constraints (3.28i)-(3.28k), (3.28o)-(3.28r), (3.30e), and (3.31) are not affected by uncertainties, and they can be retained as such and are equivalent to (4.1d). Energy constraints (3.28f) and (3.28h) also remain unaffected and are retained. In regards to (4.1c), the expected trajectory of the state variables $E_{bat,i}$ and $E_{EV_k,i}, \forall k$ is not of interest in the A-EMS framework. In fact, it is desired not to restrict the trajectory of the state in any other way than to maintain it within the feasible region (energy bounds).

Approximate Probability & Cost Functions

To reformulate the A-EMS framework, (3.24b), (3.24k)-(3.24m), (3.29b)-(3.29c) in Formulation I; and (3.28b), (3.28l)-(3.28n), (3.30b), and (3.30d) of Formulation II need to be rewritten in the form of (4.1b), given uncertain system parameters. To achieve this, the probability function in (4.1b) needs to be approximated by sampling from random variables (RVs). Considering the state vector $\mathbf{x}$ in (4.1) as an RV, let $p(\mathbf{x})$ and $q(\mathbf{x})$ be two probability distributions; the former is referred to as the target distribution, and the latter is called the proposal distribution. The probability of an event, $f(\mathbf{x}) \in A$ occurring is given by

$$P_A = \int_{f(\mathbf{x}) \in A} p(\mathbf{x}) d\mathbf{x} \tag{4.2}$$

which can be written in the form of an expectation as follows

$$P_A = E_X[g(\mathbf{x})] = \int g(\mathbf{x})p(\mathbf{x})d\mathbf{x} \tag{4.3a}$$

$$\text{where,} \quad g(\mathbf{x}) = \begin{cases} 0, & f(\mathbf{x}) \in A \\ 1, & f(\mathbf{x}) \notin A \end{cases} \tag{4.3b}$$

However, it is usually not possible to evaluate the integrals in (4.2) and (4.3a) in closed form. It can, instead, be approximated by drawing N independent identically distributed (i.i.d.) samples $\mathbf{x}^{(1)}, \ldots, \mathbf{x}^{(N)}$ from the distribution $q(\mathbf{x})$. The approximate probability of event A occurring, obtained using samples is given by

$$\hat{P_A} = \frac{1}{N}\sum_{n=1}^{N} w_n g(\mathbf{x}^{(n)}), \quad w_n = \frac{p(\mathbf{x}^{(n)})}{q(\mathbf{x}^{(n)})} \tag{4.4}$$

where w_n is called the *importance weight*. And when $p(\mathbf{x}) = q(\mathbf{x})$, i.e. when samples are drawn directly from the target distribution, $w_n = 1$; this case is known as fair sampling. Further details on sampling and chance constraints based control are found in [114]. Using the result from (4.4) in (4.1b), the approximate chance constraint, given by

$$\frac{1}{N}\sum_{n=1}^{N} w_n g(\mathbf{x}_{1:T}^{(n)}) \leq \epsilon \tag{4.5}$$

Similarly, the approximation of the cost function (4.1a), is given by

$$\frac{1}{N}\sum_{n=1}^{N} w_n h(\mathbf{u}_{0:T-1}, \mathbf{x}_{1:T}^{(n)}) \tag{4.6}$$

The choice of the proposal distribution $q(\mathbf{x})$ influences the accuracy of the approximation. The topic of choice of proposal distributions and various methods of sampling are discussed in dedicated texts such as [181]. Given an appropriate proposal distribution, in [114], it is shown that the accuracy of these approximations increase with the number of samples drawn from $q(\mathbf{x})$ and that $\hat{P}_A \longrightarrow P_A$ as $N \longrightarrow \infty$.

Approximate Chance Constraint in Linear Systems with Convex Feasible Regions

To enforce the constraint (4.5), the weighted fraction of particles that fall outside the feasible region need to be constrained. A set of binary variables z_i to $z_N, z_n \in \{0, 1\}$ are defined, such that when $z_n = 0$, particle n is inside the feasible region. Now, the weighted sum of the binary variables are constrained as shown below,

$$\frac{1}{N}\sum_{n=1}^{N} w_n z_n \leq \epsilon \tag{4.7}$$

Now constraints should be described such that

$$z_n = 0 \Longrightarrow \mathbf{x}_{1:T}^{(n)} \in F \tag{4.8}$$

where F is the feasible region of $\mathbf{x}_{1:T}$.

When the feasible region F of the sequence $\mathbf{x}_{1:T}$ is convex, it is a conjunction of convex polygonal feasible regions F_t at each time step t, i.e.

$$\mathbf{x}_{1:T} \in F \Longleftrightarrow \bigwedge_{t=1,\ldots,T} \mathbf{x}_t \in F_t \tag{4.9}$$

Each polygonal feasible region F_t is in turn a conjunction of linear constraints $\mathbf{a}_{st}^T \mathbf{x}_t \leq b_{ts}$ for $s = 1, \ldots, N_t$, where $\mathbf{a}_{ts}$ points outward from the feasible region F_t. Given this definition, $\mathbf{x}_t$ lies in F_t only when all constraints defined above are satisfied [114], such that

$$\mathbf{x}_t \in F_t \iff \bigwedge_{s=1,\ldots,N_t} \mathbf{a}_{st}^T \mathbf{x}_t \leq b_{ts} \tag{4.10}$$

Now that the feasibility of $\mathbf{x}_{1:T}$ has been defined in terms of linear inequality constraints, "Big M" techniques can be applied such that (4.8) is satisfied. The following constraints are defined

$$\mathbf{a}_{ts}^T \mathbf{x}_t^{(n)} - b_{ts} \leq M z_n \quad \forall t \forall s \tag{4.11}$$

where M is a large positive constant. In the above equation, $z_n = 0$ implies that all constraints are satisfied at all time steps for particle n; and for a large enough M, $z_n = 1$ implies particle n is unconstrained. In practice, M is chosen such that, its value is several orders of magnitude larger than the values of relevant coefficients and variables $\mathbf{a}_{ts}$, $\mathbf{x}_t$, and b_{ts}.

A-EMS with Chance Constraints

In the A-EMS system, uncertainties arise in $\mathbf{p}_d$, κ_{l_k}, and $\mathbf{E}_{EV_k}^{o,l_k}$. Let $\boldsymbol{\gamma}_c$ and $\boldsymbol{\gamma}_d$ denote the vectors of connection and disconnection times respectively. It is assumed that $\mathbf{p}_d$, $\boldsymbol{\gamma}_c$, and $\boldsymbol{\gamma}_d$ are uniformly distributed; and $\mathbf{E}_{EV_k}^{o,l_k}$ is normally distributed i.e., $\mathbf{X}_{\mathbf{p}_d} \sim \mathcal{U}(\bar{p_d}^{min}, \bar{p_d}^{max})$, $\mathbf{X}_{\boldsymbol{\gamma}_c} \sim \mathcal{U}(\bar{\gamma_c}^{min}, \bar{\gamma_c}^{max})$, $\mathbf{X}_{\boldsymbol{\gamma}_d} \sim \mathcal{U}(\bar{\gamma_d}^{min}, \bar{\gamma_d}^{max})$, and $\mathbf{X}_{\mathbf{E}_{EV_k}^{o,l_k}} \sim \mathcal{N}(\bar{\mathbf{E}_{EV_k}^{o,l_k}}, \boldsymbol{\sigma}^2_{\mathbf{E}_{EV_k}^{o,l_k}})$

Here $\mathbf{X}_{\mathbf{p}_d}$, $\mathbf{X}_{\boldsymbol{\gamma}_c}$, $\mathbf{X}_{\boldsymbol{\gamma}_d}$, and $\mathbf{X}_{\mathbf{E}_{EV_k}^{o,l_k}}$ are random variables; $\bar{p_d}^{min}$, $\bar{\gamma_c}^{min}$, $\bar{\gamma_d}^{min}$ and

$\bar{p_d}^{min}$, $\bar{\gamma_c}^{min}$, $\bar{\gamma_d}^{min}$ are the lower and upper limits of $\mathbf{p}_d$, $\boldsymbol{\gamma}_c$, and $\boldsymbol{\gamma}_d$ respectively; and $\boldsymbol{\sigma}^2_{\mathbf{E}^{o,l_k}_{EV_k}}$ is the covariance corresponding to $\mathbf{E}^{o,l_k}_{EV_k}$.

Samples are drawn from a joint distribution of $\mathbf{p}_d$, $\boldsymbol{\gamma}_c$, $\boldsymbol{\gamma}_d$, and $\mathbf{E}^{o,l_k}_{EV_k}$. Since uncertainties in each of these parameters are considered to be independent of each other, it suffices to draw samples simultaneously from the individual distributions to form a composite sample $\boldsymbol{\varrho}^{(n)}$, shown below

$$\boldsymbol{\varrho}^{(n)} = \begin{bmatrix} \mathbf{p}_d^{(n)} & \boldsymbol{\gamma}_c^{(n)} & \boldsymbol{\gamma}_d^{(n)} & \mathbf{E}^{o,l_k\ (n)}_{EV_k} \end{bmatrix}^T \tag{4.12}$$

where the superscript (n) refers to the n^{th} sample.

In order to use the drawn sample in A-EMS, $\boldsymbol{\gamma}_c^{(n)}$ and $\boldsymbol{\gamma}_d^{(n)}$ are converted to their corresponding $\kappa_{l_k}^{(n)}, \forall l_k \forall k$ to obtain

$$\boldsymbol{\rho}^{(n)} = \begin{bmatrix} \mathbf{p}_d^{(n)} & \kappa_{l_k}^{(n)} & \mathbf{E}^{o,l_k\ (n)}_{EV_k} \end{bmatrix}^T,\ \forall l_k \forall k \tag{4.13}$$

The expectation of the uncertain power demand is defined as $\bar{\mathbf{p}}_d = E[\mathbf{p}_d] = \frac{1}{N}\sum_n \mathbf{p}_d^{(n)}$. The objective functions (3.28a) and (3.30a) depend on the the uncertain power demand, through the definition of $\mathcal{F}$ in (3.27) and the constraints (3.28c) and (3.30c). Given the definition of $\bar{\mathbf{p}}_d$, the constraints (3.28c) and (3.30c), in the context of the stochastic formulation, can be written as follows

$$\bar{\mathbf{p}}_g = \bar{\mathbf{p}}_d + \mathbf{p}_{bat} + \sum_k \mathbf{p}_{EV_k} \tag{4.14a}$$

$$\bar{\mathbf{p}}_g = \bar{\mathbf{p}}_d + \mathbf{p}_{bat} + \sum_k \mathbf{p}^{max}_{EV_k} \boldsymbol{\delta}_{EV_k} \tag{4.14b}$$

for the bidirectional and On/Off charging cases respectively. The constraint (3.28d)

becomes

$$\bar{\mathbf{p}}_g^b \geq \bar{\mathbf{p}}_g \tag{4.15}$$

where $\bar{\mathbf{p}}_g^b$ is the buying (positive) portion of $\bar{\mathbf{p}}_g$. Now, $\mathcal{F}$ is redefined as

$$\bar{\mathcal{F}}_{II} = (c_b^T - c_s^T)\bar{\mathbf{p}}_g^b + \mathbf{c}_s^T \bar{\mathbf{p}}_g \tag{4.16}$$

Using the definition of $\bar{\mathcal{F}}_{II}$ from (4.16), (3.28a) and (3.30a) can be written in the form of (4.1a).

Given N samples of the form (4.13), z_1 to z_N being N binary variables, and M being a large positive number, the versions of the bidirectional and On/Off control optimization formulations can be derived easily.

Bidirectional Charging: Formulation I The optimization problem using chance constraints with bidirectional EV charging is obtained by substituting (3.24a), (3.24b), (3.24k),(3.24l), and (3.24m) with:

$$\min_{\mathbf{p}_{bat}, \mathbf{p}_{EV_k}} f(\mathbf{c}_b, \mathbf{c}_s, \bar{\mathbf{p}_d}, \mathbf{p}_{bat}, \mathbf{p}_{EV_k}) \tag{4.17a}$$

$$\text{s.t.} \quad \mathbf{p}_d^{(n)} + \mathbf{p}_{bat} + \sum_k \mathbf{p}_{EV_k} \leq M z_n \mathbf{1} + p_g^{max} \cdot \boldsymbol{\delta}^{bs} \tag{4.17b}$$

$$-\mathbf{p}_d^{(n)} - \mathbf{p}_{bat} - \sum_k \mathbf{p}_{EV_k} \leq M z_n \mathbf{1} - p_g^{min} \cdot (\mathbf{1} - \boldsymbol{\delta}^{bs}) \tag{4.17c}$$

$$E_{EV_k,i}{}^{(n)} = \eta^c_{EV_k} \sum_{\iota=\kappa_{l_k}{}^{(n)}(1)}^{i} h_\iota p^c_{EV_k,\iota} + \frac{1}{\eta^d_{EV_k}} \sum_{\iota=\kappa_{l_k}{}^{(n)}(1)}^{i} h_\iota p^d_{EV_k,\iota}$$
$$+E^{o,l_k}_{EV_k}{}^{(n)} - P^{loss}_{EV_k} \sum_{\iota=\kappa_{l_k}{}^{(n)}(1)}^{i} h_\iota \tag{4.17d}$$

$$E_{EV_k,i}{}^{(n)} \leq M z_n + E^{max}_{EV_k} \tag{4.17e}$$

$$-E_{EV_k,i}{}^{(n)} \leq M z_n - E^{min}_{EV_k} \tag{4.17f}$$

$$i \in \kappa_{l_k}{}^{(n)}, \forall l_k, \forall k, \forall n$$

$$-E_{EV_k,final}{}^{(n)} \leq M z_n - E^{desired,l_k}_{EV_k} \tag{4.17g}$$

Bidirectional Charging: Formulation II The optimization problem using chance constraints with bidirectional EV charging is obtained by retaining (4.17e)-(4.17g); and substituting (3.28c) and (3.28d) with (4.14a) and (4.15); and (3.28a)-(3.28b) and (3.28l)-(3.28n) with:

$$\min_{\bar{\mathbf{p}}^b_g, \bar{\mathbf{p}}_g} \bar{\mathcal{F}}_{II} + \varsigma\big(\mathbf{p}^c_{bat} + \sum_k \mathbf{p}^c_{EV,i}\big) \tag{4.18a}$$

$$\mathbf{p}^{(n)}_d + \mathbf{p}_{bat} + \sum_k \mathbf{p}_{EV_k} \leq M z_n \mathbf{1} + p^{max}_g \mathbf{1} \tag{4.18b}$$

$$-\mathbf{p}^{(n)}_d - \mathbf{p}_{bat} - \sum_k \mathbf{p}_{EV_k} \leq M z_n \mathbf{1} - p^{min}_g \mathbf{1} \tag{4.18c}$$

$$E_{EV_k,i}{}^{(n)} = E^{o,l_k}_{EV_k}{}^{(n)} + \left(\eta^c_{EV_k} - \frac{1}{\eta^d_{EV_k}}\right) \sum_{\iota=1}^{i} h_\iota p^c_{EV_k,\iota} + \frac{1}{\eta^d_{EV_k}} \sum_{\iota=1}^{i} h_\iota p_{EV_k,\iota} - P^{loss}_{EV_k} \sum_{\iota=1}^{i} h_\iota \tag{4.18d}$$

$$i \in \kappa_{l_k}{}^{(n)}, \forall l_k, \forall k, \forall n$$

Unidirectional On/Off Control: Formulation I The optimization problem using chance constraints with unidirectional EV charging and On/Off control is obtained by substituting (3.29a)-(3.29c) with:

$$\min_{\mathbf{p}_{bat},\boldsymbol{\delta}_{EV_k}} f(\mathbf{c}_b, \mathbf{c}_s, \bar{\mathbf{p}}_d, \mathbf{p}_{bat}, p_{EV_k}^{max}\boldsymbol{\delta}_{EV_k}) \tag{4.19a}$$

$$\text{s.t.} \quad \mathbf{p}_d^{(n)} + \mathbf{p}_{bat} + \sum_k p_{EV_k}^{max}\boldsymbol{\delta}_{EV_k} \leq M z_n \mathbf{1} + p_g^{max} \cdot \boldsymbol{\delta}^{bs} \tag{4.19b}$$

$$-\mathbf{p}_d^{(n)} - \mathbf{p}_{bat} - \sum_k p_{EV_k}^{max}\boldsymbol{\delta}_{EV_k} \leq M z_n \mathbf{1} - p_g^{min} \cdot (\mathbf{1} - \boldsymbol{\delta}^{bs}) \tag{4.19c}$$

$$E_{EV_k,i}{}^{(n)} = \eta_{EV_k}^c p_{EV_k}^{max} \sum_{\iota=\kappa_{l_k}{}^{(n)}(1)}^{i} h_\iota \boldsymbol{\delta}_{EV_k,\iota} + E_{EV_k}^{o,l_k}{}^{(n)} - P_{EV_k}^{loss} \sum_{\iota=\kappa_{l_k}{}^{(n)}(1)}^{i} h_\iota \tag{4.19d}$$

$$E_{EV_k,i}{}^{(n)} \leq M z_n + E_{EV_k}^{max} \tag{4.19e}$$

$$-E_{EV_k,i}{}^{(n)} \leq M z_n - E_{EV_k}^{min} \tag{4.19f}$$

$$i \in \kappa_{l_k}{}^{(n)}, \forall l_k, \forall k, \forall n$$

$$-E_{EV_k,final}{}^{(n)} \leq M z_n - E_{EV_k}^{desired,l_k} \tag{4.19g}$$

Unidirectional On/Off Control: Formulation II Similarly, the optimization problem using chance constraints with unidirectional EV charging and On/Off control is obtained by retaining equations (4.19d)-(4.19g); replacing (3.30c) and (3.28d) with

(4.14b) and (4.15); and substituting (3.30a)-(3.30d) with:

$$\min_{\bar{\mathbf{p}}_g^b, \bar{\mathbf{p}}_g} \bar{\mathcal{F}}_{II} + \varsigma \mathbf{p}_{bat}^c \tag{4.20a}$$

$$\mathbf{p}_d^{(n)} + \mathbf{p}_{bat} + \sum_k p_{EV_k}^{max} \boldsymbol{\delta}_{EV_k} \leq M z_n \mathbf{1} + p_g^{max} \mathbf{1} \tag{4.20b}$$

$$-\mathbf{p}_d^{(n)} - \mathbf{p}_{bat} - \sum_k p_{EV_k}^{max} \boldsymbol{\delta}_{EV_k} \leq M z_n \mathbf{1} - p_g^{min} \mathbf{1} \tag{4.20c}$$

$$E_{EV_k,i}{}^{(n)} = E_{EV_k}^{o,l_k}{}^{(n)} + \eta_{EV_k}^c \sum_{\iota=1}^{i} h_\iota p_{EV_k}^{max} \boldsymbol{\delta}_{EV_k,\iota} - P_{EV_k}^{loss} \sum_{\iota=1}^{i} h_\iota \tag{4.20d}$$

The probability distributions described earlier are considered to be the target distributions. Therefore, in Equation (4.7), $w_n = 1$. Thus we have

$$\frac{1}{N} \sum_{n=1}^{N} z_n \leq \epsilon \tag{4.21}$$

Equations (4.17a)-(4.17g) along with (3.24c)-(3.24j), (3.24n)-(3.24s), and (3.29d)-(3.29g) constitute Formulation I of the stochastic, chance constraints based A-EMS optimization framework.

Equations (4.18a)-(4.21) along with (4.14)-(4.15), (3.28e), (3.28i)-(3.28k), (3.28o)-(3.28r), (3.30e), and (3.31) constitute Formulation II of the stochastic, chance constraints based A-EMS optimization framework.

4.3 Simulation Results

Simulations were carried out to compare the performances of the optimization formulation presented in Sections 3.3 and 4.2. For all the results presented, the number of samples, N was chosen to be 100. The length of each rolling horizon window was

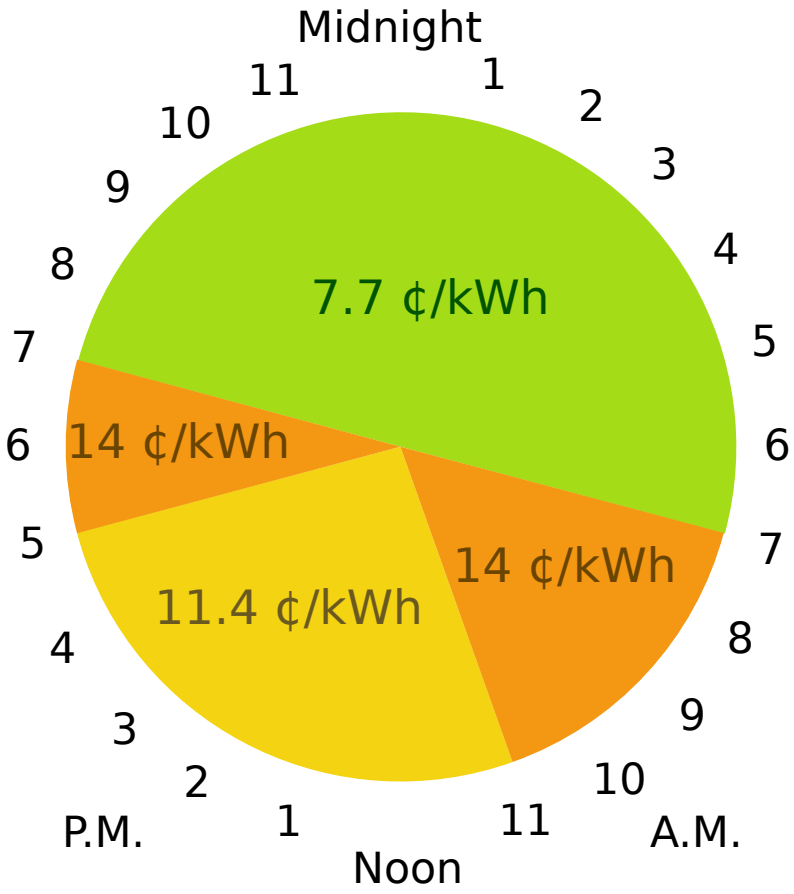

Figure 4.1: Illustration of TOU Electricity Prices used in A-EMS simulations

12 hours with 15 minute time steps.

The winter TOU prices for residential/commercial customers (Ontario) was used as both the buy and sell objective function cost coefficients. The rates are 14 ¢/kWh between 7-11 A.M and 5-7 P.M., 11.4 ¢/kWh between 11 A.M to 5 P.M., and 7.7 ¢/kWh from 7 P.M to 7 A.M. [182]; this pricing scheme is illustrated in 4.1.

In real-life scenarios, the fast-acting power electronics controllers responsible for charging/discharging the storage devices may not execute the charge/discharge actions requested by the optimal controller precisely. Therefore, at each RH time step, small errors, ε were introduced to control decisions, $\mathbf{p}_{bat}$ and $\mathbf{p}_{EV_k}$, so as to simulate

Table 4.1: Default Parameter Values used in Simulations. Values in parentheses are defaults for On/Off control and One Block Charging cases.

Parameter	Default	Parameter	Default
Horizon	12 hrs	Nh	48
N	100	ς	0.001
$E_{EV_k}^{max}$	23kW h	$p_{EV_k}^{min/max}$	$\pm$1.6kW(0/1.6kW)
ϵ	0.05, i.e. 5%	$E_{EV_k}^{desired}$ (SOC)	$70-100\%(70-85\%)$

Table 4.2: Parameter Values for different cases used in simulations to compare execution times.

Parameter	Case C1	Case C2	Case C3
K	3	15	30
E_{bat}^{max}	50kW h	250kW h	500kW h
$p_{bat}^{min/max}$	$\pm$5kW	$\pm$25kW	$\pm$50kW
$p_g^{min/max}$	$\pm$20kW	$\pm$100kW	$\pm$200kW
M	100	500	1000

the imprecise nature of these controllers. These errors were generated such that the mean of these errors is equal to the optimal control decisions and their errors are at most $\pm 10\%$ of p_{bat/EV_k}^{max}; i.e. (3.1) becomes

$$E_{i+1} = E_i + h_i\big(\eta^c p_i^c + \frac{1}{\eta^d} p_i^d - P^{loss}\big) + \varepsilon \tag{4.22}$$

for Formulation I and for Formulation II it becomes

$$E_{i+1} = E_i + h_i\big(\eta^c p_i^c + \frac{1}{\eta_d}(p_i - p_i^c) - P^{loss}\big) + \varepsilon \tag{4.23}$$

for both the on-site storage and EV batteries.

Default values of system parameters used in simulations are shown in Table 4.1. In order to compare the performance of the optimization formulation for systems of various sizes, simulations were carried out using parameters presented under cases C1, C2, and C3 in Table 4.2. All simulations were carried out in Matlab in a 64 bit Microsoft Windows environment with IBM ILOG CPLEX MILP solver, on a 3.4 GHz Intel Core i7-3770 machine with 32 GB RAM. The relative Mixed Integer Problem (MIP) gap value used was CPLEX's default value of 0.01%.

For generating particles, mean values of $\mathbf{p}_d$, $\boldsymbol{\gamma}_c$, and $\boldsymbol{\gamma}_d$ were used and samples drawn from a uniform distribution, the bounds of which are equal on either side of the mean, were added to them. For $\mathbf{E}_{EV_k}^{o,l_k}$, samples were drawn from a normal distribution. For case C1, the mean for the $\mathbf{p}_d$ used were an aggregate of hourly usage data from a Residential/Commercial load with peak usage less than 50kW, and hourly generation data from a PV solar generation station with peak generation of 30kW—scaled down to 5kW—provided by Burlington Hydro Inc. (Burlington, Ontario, Canada). For cases C2 and C3, the aggregate values used for generating the mean of $\mathbf{p}_d$ in C1 were scaled by factors of 5 and 10 respectively. In the simulations presented here, the means for $\mathbf{E}_{EV_k}^{o,l_k}$, $\boldsymbol{\gamma}_c$, and $\boldsymbol{\gamma}_d$, for each EV, were generated such that, the duration of connection to microgrid lasts between 9-13 hours while time durations when the EV is not connected lasts between 6-13 hours; whereas the SOC at the time of connection is between 20-35%. The bounds of the uncertainties in $\mathbf{p}_d$ are $0.15\mathbf{p}_d$ on either side of its mean and the values have temporal correlation from the value at one time step to the next. The bounds are 2 hours on either side of the means of $\boldsymbol{\gamma}_c$, and $\boldsymbol{\gamma}_d$. The value of the standard deviation $\boldsymbol{\sigma}_{\mathbf{E}_{EV_k}^{o,l_k}}$ used was 4%. The statistical parameters

Table 4.3: Mean execution times of the Stochastic and Non-Stochastic A-EMS optimizations, in Formulation I, for each time step with different number of EVs, calculated over 624 time steps for cases C1, C2, and C3 from Table 4.2, for bidirectional charging, On/Off Control, and One Block charging scenarios. The times taken for setting up the optimization problem and execution of the solver are shown separately.

		Execution Time (seconds): Formulation I							
		Bidirectional Charging		On/Off Control			One Block Charging		
		C1	C2	C1	C2	C3	C1	C2	C3
Stochastic	Set-up	0.3105	20.3798	0.3481	4.9266	22.1666	0.572	8.8025	40.4467
	Solver	0.8825	98.6087	0.1206	0.3351	0.5969	0.088	0.6375	1.3718
	Total	1.193	118.9885	0.4687	5.2617	22.7635	0.66	9.44	41.8185
Non-Stochastic	Set-up	0.0035	0.1652	0.0029	0.0329	0.1293	0.0064	0.067	0.2739
	Solver	0.0071	0.0639	0.0079	0.0088	0.01	0.0269	0.1098	0.19
	Total	0.0106	0.2291	0.0108	0.0417	0.1393	0.0333	0.1768	0.4639

Table 4.4: Mean execution times (rounded off) of the Stochastic and Non-Stochastic A-EMS optimizations, in Formulation II, for each time step with different number of EVs, calculated over 624 time steps for cases C1, C2, and C3 from Table 4.2, for bidirectional charging, On/Off Control, and One Block charging scenarios. The times taken for setting up the optimization problem and execution of the solver are shown separately.

		Execution Time (seconds): Formulation II								
		Bidirectional Charging			On/Off Control			One Block Charging		
		C1	C2	C3	C1	C2	C3	C1	C2	C3
Stochastic	Set-up	0.58	11.1	46.9	0.29	3.58	13.68	0.39	6.21	23.04
	Solver	0.46	10.17	9.98	0.05	0.21	0.42	0.16	1.02	2.67
	Total	1.04	21.27	56.87	0.35	3.8	14.11	0.55	7.23	25.72
Non-Stochastic	Set-up	0.009	0.113	0.537	0.004	0.029	0.11	0.006	0.072	0.27
	Solver	0.005	0.014	0.026	0.004	0.007	0.011	0.021	0.10	0.20
	Total	0.014	0.127	0.563	0.008	0.037	0.12	0.027	0.17	0.47

Table 4.5: Number of variables and constraints for one time step of the Stochastic and Non-Stochastic A-EMS optimizations, in Formulation I, with different number of EVs, calculated over 624 time steps for cases C1 and C2 from Table 4.2, for bidirectional charging. For values which vary from one time step to another, values of mean and standard deviation rounded off to the nearest integers are presented.

Bidirectional Charging: Formulation I			
		C1	C2
Stochastic	Constraints(mean)	54441	254886
	Constraints(S D)	5402	16110
	Variables(cont)	384	1536
	Variables(Binary)	292	868
Non-Stochastic	Constraints(mean)	1021	6025
	Constraints(S D)	56	64
	Variables(cont)	384	1536
	Variables(Binary)	192	768

described above—means and uncertainty bounds for uniform distributions and mean and standard deviation for the normal distribution—were used as the predicted values for the RH controller.

The number of samples $N = 100$ used to make decisions at each time step, would adequately represent range of uncertainties, for the bounds chosen above. Further, the values of M are chosen in a way that they are small enough not to cause numerical issues, but large enough to ensure that the chance constraints formulation using the "Big M" methods are valid.

4.3.1 Effect of System Size

The size of the microgrid changes when the number of EVs connected to it changes. In Tables 4.3 and 4.4, the execution times of one time step of the stochastic and non-stochastic optimization formulations are presented for the system parameters shown

Table 4.6: Number of variables and constraints for one time step of the Stochastic and Non-Stochastic A-EMS optimizations, in Formulation II, with different number of EVs, calculated over 624 time steps for cases C1, C2, and C3 from Table 4.2, for bidirectional charging. For values which vary from one time step to another, values of mean and standard deviation rounded off to the nearest integers are presented.

Bidirectional Charging: Formulation II				
		C1	C2	C3
Stochastic	Constraints(mean)	54686	235999	461507
	Constraints(S D)	2868	6972	10870
	Variables(cont)	384	1536	2976
	Variables(Binary)	100	100	100
Non-Stochastic	Constraints(mean)	1213	4736	9129
	Constraints(S D)	30	72	112
	Variables(cont)	384	1536	2976

Table 4.7: Number of variables and constraints for one time step of the Stochastic and Non-Stochastic A-EMS optimizations, in Formulation I, with different number of EVs, calculated over 624 time steps for cases C1, C2 and C3 from Table 4.2, for On/Off Control. For values which vary from one time step to another, values of mean and standard deviation rounded off to the nearest integers are presented.

On/Off Control: Formulation I				
		C1	C2	C3
Stochastic	Constraints(mean)	39992	160600	312400
	Constraints(S D)	4223	14729	13472
	Variables(cont)	96	96	96
	Variables(Binary)	292	868	1588
Non-Stochastic	Constraints(mean)	591	1800	3319
	Constraints(S D)	44	153	140
	Variables(cont)	96	96	96
	Variables(Binary)	192	768	1488

Table 4.8: Number of variables and constraints for one time step of the Stochastic and Non-Stochastic A-EMS optimizations, in Formulation II, with different number of EVs, calculated over 624 time steps for cases C1, C2 and C3 from Table 4.2, for On/Off Control. For values which vary from one time step to another, values of mean and standard deviation rounded off to the nearest integers are presented.

On/Off Control: Formulation II				
		C1	C2	C3
Stochastic	Constraints(mean)	39545	159005	309642
	Constraints(S D)	4565	12202	16376
	Variables(cont)	96	96	96
	Variables(Binary)	244	820	1540
Non-Stochastic	Constraints(mean)	635	1829	3338
	Constraints(S D)	47	129	171
	Variables(cont)	96	96	96
	Variables(Binary)	144	720	1440

Table 4.9: Number of variables and constraints for one time step of the Stochastic and Non-Stochastic A-EMS optimizations, in Formulation I, with different number of EVs, calculated over 624 time steps for cases C1, C2 and C3 from Table 4.2, for One Block Charging. For values which vary from one time step to another, values of mean and standard deviation rounded off to the nearest integers are presented.

One Block Charging: Formulation I				
		C1	C2	C3
Stochastic	Constraints(mean)	40457	161080	315030
	Constraints(S D)	5639	8033	9986
	Variables(cont)	96	96	96
	Vars (Binary, mean)	393	1271	12349
	Vars (Binary, S D)	16	89	155
Non-Stochastic	Constraints(mean)	745	2573	4908
	Constraints(S D)	108	164	207
	Variables(cont)	96	96	96
	Vars (Binarymean)	267	1152	2233
	Vars (Binary, S D)	17	83	158

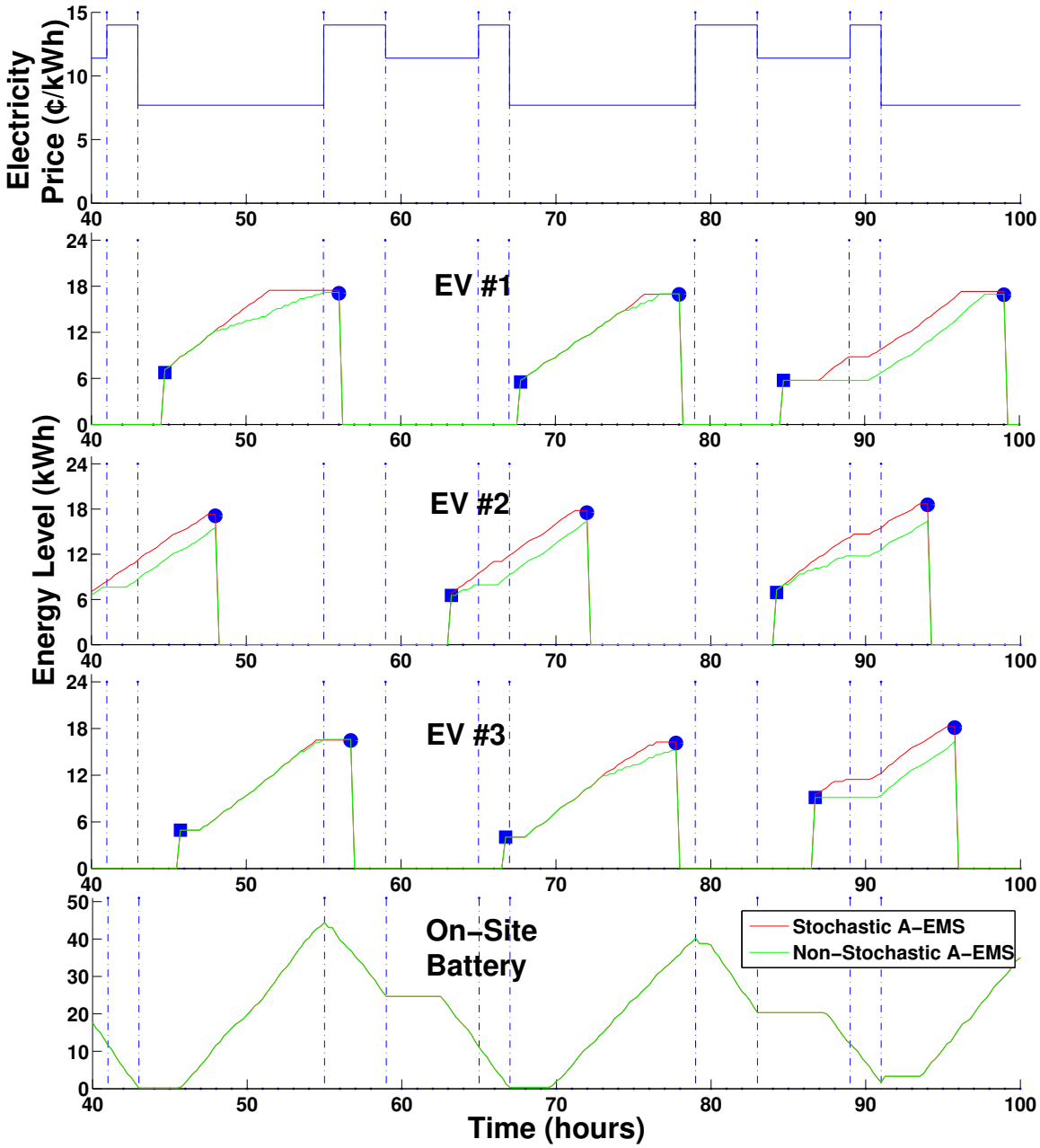

Figure 4.2: An illustrative example showing electricity price, energy levels of 3 EVs, and on-site battery, over a 60 hour simulation period, for a particular Monte Carlo scenario, using bidirectional charging. The red line shows the energy levels using (4.23), based on the optimal EV and battery power values obtained using stochastic A-EMS, while the green line shows those obtained using non-stochastic A-EMS. The blue squares indicate the EV energy levels at the beginning of each connection period; the blue dots denote the desired final energy levels $E_{EV_k}^{desired}$ for each EV.

Table 4.10: Number of variables and constraints for one time step of the Stochastic and Non-Stochastic A-EMS optimizations, in Formulation II, with different number of EVs, calculated over 624 time steps for cases C1, C2 and C3 from Table 4.2, for One Block Charging. For values which vary from one time step to another, values of mean and standard deviation rounded off to the nearest integers are presented.

One Block Charging: Formulation II				
		C1	C2	C3
Stochastic	Constraints(mean)	39706	162699	312427
	Constraints(S D)	4878	6552	14620
	Variables(cont)	96	96	96
	Vars (Binary, mean)	342	1334	2542
	Vars (Binary, S D)	23	30	70
Non-Stochastic	Constraints(mean)	779	2628	4829
	Constraints(S D)	98	139	278
	Variables(cont)	96	96	96
	Vars (Binarymean)	215	1098	2168
	Vars (Binary, S D)	25	40	69

in Table 4.1 and cases shown in Table 4.2, for Formulations I and II respectively. In Tables 4.5, 4.7, and 4.9, the number of variables and constraints—and where appropriate, their means and standard deviations rounded off to the nearest integers—are shown for Formulation I. Similarly Tables 4.6, 4.8, and 4.10 show the number of variables and constraints for Formulation II.

Analyzing the execution times and the number of variables and constraints together, it is noted that for all three charging cases in Formulations I and II, both the stochastic and non-stochastic versions of the A-EMS take a small amount of the time relative to the length of each time step (15 minutes) to calculate the optimal power values.

It can also be observed that the number of constraints in the stochastic formulation is roughly $N = 100$ times that of those in the non-stochastic problem in Formulation

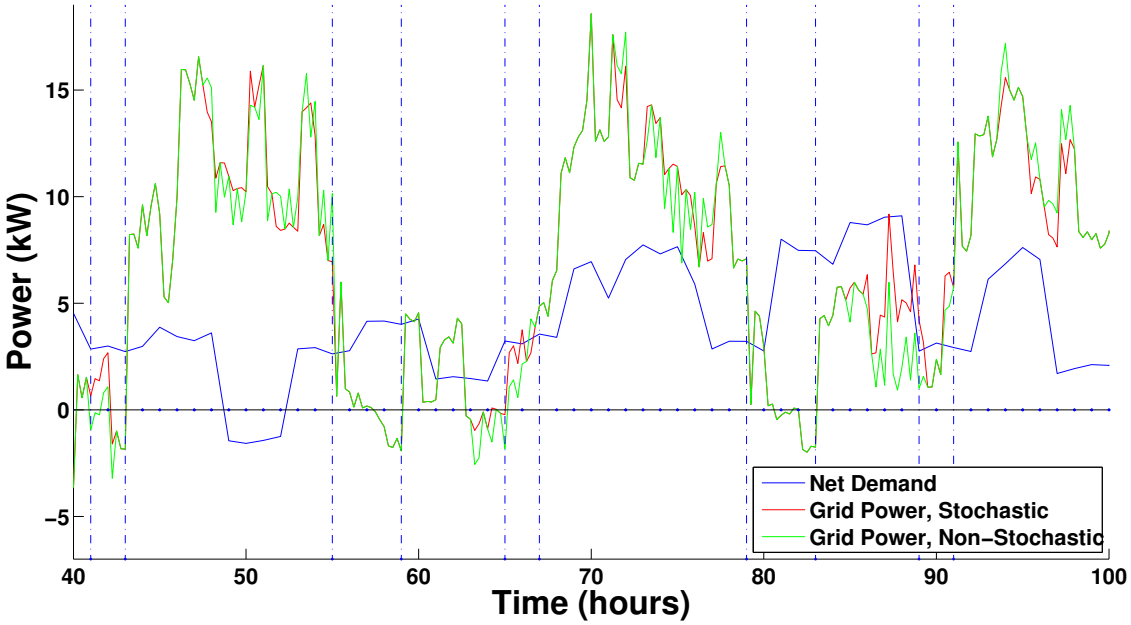

Figure 4.3: An illustrative example showing net demand and grid power values for stochastic and non-stochastic A-EMS, over a 60 hour simulation period, for a particular Monte Carlo scenario, using bidirectional charging.

I and roughly 2 orders of magnitude, proportional to $N = 100$, in Formulation II. The number of binary variables also increase by the same value from the non-stochastic to the stochastic problem. The number of variables and constraints also increase proportionally with the number of EVs connected to the system. The number of time steps Nh would also affect the number of variables and constraints, since each variable vector has length Nh and most constraints are defined for each time step.

4.3.2 Economic Benefits Due to A-EMS

The objective function of the A-EMS controller is designed to maximize the economic benefits for the user. Simulations were carried out to compare the effectiveness of the controller in reducing costs. All simulations were carried out for case C1 for

156 simulation hours. In order to assess the optimizers in a variety of scenarios with different values of uncertain system parameters, Monte Carlo simulations were performed for 100 different scenarios using stochastic and non-stochastic versions of the optimizer for each of the cases, i.e. bidirectional charging, On/Off Control, and One Block charging.

Since Formulations I and II effectively solve the same optimization problems, the results presented in the rest of this section are the same for both formulations[1]. Therefore in discussions on economic benefits and robustness that follow, no distinction is made between Formulations I and II.

The effect of this can be seen clearly in Table 4.11 which compares the mean and S.D. of electricity costs incurred in systems with and without the Stochastic and non-Stochastic A-EMS systems. In all 3 charging cases, the Non-Stochastic A-EMS results in the least cost, followed by the stochastic A-EMS and the system without any controller. It should be pointed out that the non-stochastic controller has lower cost than stochastic controller mostly because it fails to charge the EV(s) to the desired final levels in many cases due to uncertainty, as will be seen shortly.

4.3.3 Effect Of Stochastic Formulation

Equations (3.24m) and (3.28n) were designed such that an EV battery, attains a user specified energy level $E_{EV_k}^{desired}$ at the end of each connection period. These conditions are sometimes violated, as illustrated in Fig. 4.2: these are instances when the red or green line(s) do not reach a level equal to or above the blue dots in the energy plots at

[1]For the same inputs (system parameters), in a given time step, solving the optimization problem using Formulations I and II will result in the same optimal objective function value, but not necessarily in the same values of decision variables.

Table 4.11: Comparison of mean and standard deviation (S.D.) of electricity costs in $, incurred for case C3, during 156 simulation hours, for 100 Monte Carlo scenarios, while using stochastic and Non-stochastic A-EMS vs No A-EMS, for different charging cases

-	Cost ($)					
	Stochastic		Non-Stochastic		No A-EMS	
	Mean	S.D.	Mean	S.D.	Mean	S.D.
Bidirectional Charging	95.38	1.31	94.13	1.25	102.27	1.36
On/Off Control	90.5	1	88.95	0.99	96.36	0.93
One Block Charging	93.17	1.39	92.8	1.39	98.05	1.04

the time instances when the dots appear on the figure. From simulations, it was noted that this is primarily due to uncertainties in $\boldsymbol{\gamma}_c$ and $\boldsymbol{\gamma}_d$, which affect the optimizer's ability to charge an EV to the appropriate energy level before disconnection.

Figs. 4.2 and 4.3 show that the on-site battery and EVs try to charge when the cost of electricity is lower and discharge when the cost of electricity is high in both the stochastic and non-stochastic optimization formulations. The optimizers work in such a way that energy is stored in the available storage devices so that the grid power levels shown in Fig. 4.3 are equal to or lower than the net demand during periods of high prices and vice versa. Further it can also be noted that both formulations try to accommodate the $E_{EV_k}^{desired}$ constraints, and charge the EVs even during periods of high prices, and try to offset this by discharging the on-site battery.

Table 4.12 shows the number of such violations in each of the charging scenarios for both stochastic and non-stochastic A-EMS formulations, compared to the total possible violations in Monte Carlo Simulations. There are cases in which, even while charging at the maximum rated power values throughout the connection period, the desired $E_{EV_k}^{desired}$ value cannot be attained. Therefore, a fair comparison should exclude

Table 4.12: Number of instances when desired $E_{EV_k}^{desired}$ value is not reached for the different charging scenarios, with 3 EVs, during 156 simulation hours, for 100 Monte Carlo Scenarios.

-	$E_{EV_k}^{desired}$ Violations, Stochastic	$E_{EV_k}^{desired}$ Violations, Non-Stochastic	Total Possible Violations
Bidirectional Charging	208	545	1900
On/Off Control	35	219	2000
One Block Charging	69	190	2000

these physically infeasible cases.

Attaining $E_{EV_k}^{desired}$ values is directly relate-able to the user's confidence in being able to complete trips and may contribute to range anxiety. It can be seen that in all 3 scenarios the stochastic formulation fares significantly better than the non-stochastic version in this respect. This can be attributed to the fact that the stochastic formulations consider the effect of uncertainties in connection and disconnection times.

4.3.4 Effect of Rolling Horizon Controller

The RH controller updates parameter values at each time step, enabling it to adapt to changes. This characteristic inherently enables the controller to mitigate the effect of uncertainties to an extent. For example, even though $\boldsymbol{\gamma}_c$ and $\mathbf{E}_{EV_k}^{o,l_k}$ are uncertain parameters, once an EV connects to the microgrid, uncertainties in their values are removed once the RH controller updates their values.

The other constraints related to EVs which were susceptible to violations due to uncertain system parameters were those enforcing EV energy bounds. However, no violations of these constraints was observed in the simulations due to the effectiveness

of RH controller in handling uncertainties.

4.3.5 Interpretation of Results: Robustness

The results shown in Table 4.12 were obtained from simulations where the parameters were exactly the same for both the stochastic and non-stochastic optimization formulations. As shown, the stochastic formulation results in significantly less number of violations for constraints related to attaining $E_{EV_k}^{desired}$ values. The uncertain parameters, which affect the constraints in question are $\boldsymbol{\gamma}_c$ and $\boldsymbol{\gamma}_d$, with uncertainties in time (time of occurrence an event: connection or disconnection) and $\mathbf{E}_{EV_k}^{o,l_k}$, with uncertainties in magnitude (EV energy level at the time of connection).

Cases in which both the stochastic and non- stochastic controllers resulted in the violations of this constraint were examined. When the stochastic controller generates particles for solving the optimization problem, each particle is a different realization of the uncertain parameter. Given a large enough number N, the optimizer is equipped with enough particles to adequately account for the entire range of the uncertainty sets of the uncertain parameters, including $\boldsymbol{\gamma}_c$ and $\boldsymbol{\gamma}_d$. On the contrary, the non-stochastic optimizer computes a solution using only one value, which in the cases presented in the chapter, are the means of the uncertain parameters.

Further, once the uncertainty in connection times and the EV energy level at the time of connection are resolved (i.e. once the EV connection to the microgrid occurs), the stochastic controller, in most cases, appears to be better prepared for the uncertainty in disconnection times by scheduling the charging and discharging of EV(s), in order to ensure that $E_{EV_k}^{desired}$ is reached. This is reflected in the fewer constraint violations observed in the Monte Carlo Simulations. The stochastic controller

appears to be more robust for the uncertain system parameters, the system model, and scenarios considered, than the non-stochastic controller.

Both the stochastic and non-stochastic controllers employ a rolling horizon model predictive controller. In order to demonstrate that the stochastic controller, which also employs chance constraints in addition, is more robust to uncertainties than the non-stochastic controller, the following *hypothesis test(s)* were performed, on the results for $E_{EV_k}^{desired}$ shown in Table 4.12.

The results from the use of non-stochastic controller were taken as the reference (null hypothesis) for the test. Given the nature of the results shown—$E_{EV_k}^{desired}$ being reached or not—the Binomial distribution is a good fit. For the bidirectional charging case, the probability that $E_{EV_k}^{desired}$ is not reached, $p = \frac{545}{1900}$ with a sample size $n = 1900$. So the reference distribution for the bidirectional charging case is $B(n, p)$, i.e., $B(1900, \frac{545}{1900})$. Now the following hypotheses are considered:

H_0: Stochastic Controller is not more robust than Non-Stochastic Controller

H_1:Stochastic Controller is more robust than Non-Stochastic Controller

This hypothesis test is performed using the *critical value approach*. A significance level $\alpha = 1\%$ is chosen. In the above test, the critical value is the maximum number $E_{EV_k}^{desired}$ violations observed, for which the probability of occurrence given the null hypothesis (original distribution), is at most 0.01. If the observed number of $E_{EV_k}^{desired}$ violations is less than this value, H_0 is rejected and H_1 is accepted.

For the bidirectional scenario with $B(1900, \frac{545}{1900})$ and $\alpha = 0.01$, the critical value is 499. For the On/Off control scenario with $B(2000, \frac{219}{2000})$ and $\alpha = 0.01$, the critical

value is 177. For the One Block charging scenario with $B(2000, \frac{190}{2000})$ and $\alpha = 0.01$, the critical value is 152. From Table 4.12 it is clear that for all three charging scenarios, the observed $E_{EV_k}^{desired}$ violations with the use of the stochastic controller are way below the respective critical values. Therefore, H_0 is rejected and the hypothesis H_1 which claims that the stochastic controller is more robust than the non-stochastic controller is accepted.

4.3.6 Interpretation of Results: Computational Complexity

From Tables 4.3 and 4.4, it can be inferred that for all cases C1, C2, and C3 for across all charging scenarios, in both formulations, the non-stochastic formulation is orders of magnitude faster than the corresponding stochastic formulation. The term 'set-up time' refers to the time it takes to set up the matrices which define the objective function, lower and upper bounds of variables, and the equality and inequality constraints of each optimization problem. This makes up a large portion of the total execution time, especially in the One Block and On/Off charging scenarios.

As explained earlier in section 4.3.1, this is due to the fact that the number of constraints in the stochastic formulation is approximately N times the number of constraints in the non-stochastic formulation. In addition, there are also N additional binary variables in each of the stochastic formulations. The number of time steps Nh and the number of EVs K also affect the computational complexity. Although for small system sizes and $N = 100$, such as in case C1, the optimization formulations were shown to execute very quickly, the controllers can become highly complex with increase in value of one or more of K, Nh, and N. For example, in Formulation I (4.3), for case C3, for the bidirectional charging scenario, the execution was halted

since the large number of constraints and variables resulted in the system not being able to accommodate all of them in the available memory. However this was not the case in the case of Formulation II. Further, observing the computational times for the simulations presented in this work, it can be seen that the execution times of the largest problems solved are well within the duration of the time steps.

From subsections 4.3.2, 4.3.3, and 4.3.5, it is clear that although the non-stochastic formulation of the A-EMS gives more economic benefits, the stochastic version ensures that $E_{EV_k}^{desired}$ values of EVs are reached at most times. It deals with uncertainties in a significantly better fashion and makes their presence almost transparent to the user.

4.3.7 Interpretation of Results: Formulation I vs. Formulation II

Comparing Tables 4.5, 4.7, and 4.9 with Tables 4.5, 4.7, and 4.9, it is evident that across different charging scenarios, Formulation II results in significantly fewer variables and constraints, and thus smaller optimization problems. Further, comparing Tables 4.3 and 4.3, it can be seen that the average total time taken to execute both stochastic and non-stochastic versions of the A-EMS is way lower when using Formulation II than when using Formulation I. It was also seen that case C3 in the bidirectional charging scenario were too complex (computationally infeasible) and simulations were halted as a result. It is inferred that using Formulation II in the A-EMS results in superior computational performance, without any loss in cost savings or robustness.

4.4 Summary

In this chapter, the results of simulations designed to compare the performance of the AEMS formulations I and II, and those of the stochastic and non-stochastic versions were presented. The system parameter values used in the simulations were discussed. It was shown that Formulation II resulted in significant improvements in computational performance over Formulation I.

The performance of the stochastic versions is significantly improved with respect to uncertainties in system parameters. Monte Carlo simulation results were shown to demonstrate the economic benefits of the controllers in various scenarios. It was shown that the stochastic version of the controller performs significantly better in ensuring that desired energy levels are reached in EVs at user specified times. It was inferred that when there are uncertainties in the time of occurrence of an event in the system, a rolling horizon controller may benefit from the use of chance constraints.

Chapter 5

Distributed Energy Management System

5.1 Introduction

In the previous chapter, the system under consideration was a single microgrid connected to the utility grid, while integrating EVs into the system. The discussion centred around the development of optimization problems which made use of MILP formulations in a RH control framework. Uncertainties were dealt with through the use of stochastic optimization techniques.

In this chapter, a network of microgrids forming a local energy trading market is the centre of focus. MGs in such a network are assumed to contain renewable energy sources, and on-site battery storage. Starting with a centralized RH control framework using a multi-objective method called the *utopia point* method, a distributed control framework is developed. *Alternating Direction Method of Multipliers*

(ADMM) is the technique utilized to arrive at the distributed optimization formulation. The resulting Distributed Energy Management System accommodates data privacy concerns, is scalable, and offers significant performance improvements over the central formulation, without compromising accuracy and cost benefits.

5.2 The Energy Management System

The system under consideration is a network of grid-connected MGs participating in a power exchange market. Each MG contains a distributed power source, an energy storage system, and local loads. In the system under study the distributed source is a PV generator and the energy storage system is a battery. A conceptual illustration of the network is presented in Fig. 5.1. The MGs considered could be residential, commercial, or industrial loads in one or a group of distribution feeders.

The aim is to develop an EMS which enables the network of MGs to utilize the resources they contain to meet the network's load demands as best as possible, thus reducing their reliance on the utility grid. This will enable economic benefits to participating MGs, while reducing the burden on the electric power system. The premise of this work is that, while each MG trades power with the distribution network, during accounting, the kW h value bought or sold by the i^{th} MG is broken down into the virtual components: $\mathbf{p}_{g_i}$ the component traded with the grid and $\mathbf{p}_{l_i}$ the component traded with the local MGs in the network. $\mathbf{p}^b_{g_i}$ and $\mathbf{p}^b_{l_i}$ are their corresponding buying portions. An electricity pricing scheme is assumed such that $\mathbf{c}^b_g > \mathbf{c}^b_l > \mathbf{c}^s_l > \mathbf{c}^s_g$; where $\mathbf{c}^b_g$, $\mathbf{c}^b_l$, $\mathbf{c}^s_l$, and $\mathbf{c}^s_g$ are the grid buy, local buy, local sell, and grid sell prices respectively. This ensures that there is an economic incentive for MGs to control their assets (mainly batteries) in such a way that network's demands are met using

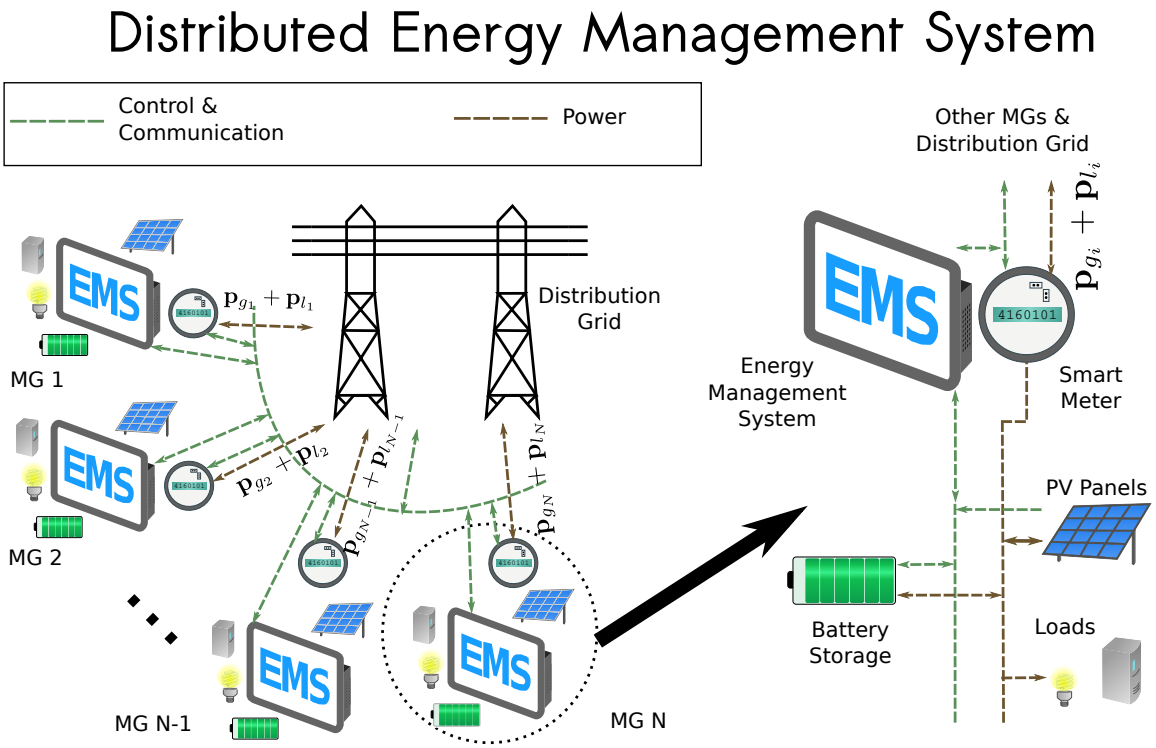

Figure 5.1: Illustration of Network of Microgrids System (Distributed EMS configuration)

local power first. Further, the difference in values of $\mathbf{c}_l^b$ and $\mathbf{c}_l^s$ can be chosen to cover the cost of operation of the network of MGs.

5.2.1 Optimization Formulation

A central optimization problem, originally developed in the research group, is described in [183]. It requires data from all MGs to be collected over a communication network. A Rolling Horizon control framework is considered, where, at each time step, given predicted net demand $\mathbf{p}_{dem_i}$ for the i^{th} MG, an optimization problem is solved over a future time horizon. $\mathbf{p}_{dem_i}$ comprises the predicted value of load demand as well as local solar power generation, generated by a prediction software block, the

scope of which is beyond this work. The future time horizon is represented by the vector $\mathbf{h}$; each element h_k denotes the duration of the k^{th} time step. The number of elements in $\mathbf{h}$ is Nh which is the number of time steps in the time horizon. All power values discussed in this chapter denote the *time-averaged* value of power in a given time step.

To define the objective, a method which enables a measurement of closeness to the best possible outcome for each microgrid is sought. The *utopia point* method method is an approach to solve optimization problems with multiple objective functions, which defines a known best possible outcome for each of the objectives, called the utopia point. Essentially, the utopia point $\mathcal{U}$ is a vector each element of which is a known best possible outcome for the corresponding objective function. While these values can almost never be obtained in practice, a compromise solution is reached such that the value of each of the objective functions is the closest to the corresponding utopia point in some way.

For the network in question, the utopia point $\mathcal{U} = [u_1, \cdots, u_N]^T$, can be calculated by solving optimization problems individually for the microgrids to obtain optimal storage activities over the control horizon, assuming preferred local buy/sell electricity rates. In other words in an ideal situation, all power transactions would occur locally. The cost of electricity in a given time horizon for an individual microgrid is,

$$f_i = (\mathbf{c}^b_{l_i} - \mathbf{c}^s_{l_i})^T \mathbf{p}^b_{l_i} + \mathbf{c}^{s\,T}_{l_i} \mathbf{p}_{l_i} + (\mathbf{c}^b_{g_i} - \mathbf{c}^s_{g_i})^T \mathbf{p}^b_{g_i} + \mathbf{c}^{s\,T}_{g_i} \mathbf{p}_{g_i} \tag{5.1}$$

Here, the subscript i denotes the i^{th} MG in the network. $\mathbf{c}^b_{g_i} \in \mathbb{R}^{Nh}$ and $\mathbf{c}^s_{g_i} \in \mathbb{R}^{Nh}$ are the electricity rates for the microgrid to buy from and sell to the utility grid, respectively. $\mathbf{c}^b_{l_i} \in \mathbb{R}^{Nh}$ and $\mathbf{c}^s_{l_i} \in \mathbb{R}^{Nh}$ are the electricity rates for the microgrid

to buy from and sell to the MGs in the local network. And $\mathbf{c}^b_{g_i} > \mathbf{c}^b_{l_i} > \mathbf{c}^s_{l_i} > \mathbf{c}^s_{g_i}$. $\mathbf{p}_{g_i} \in \mathbb{R}^{Nh}$ are the values of power bought from or sold to the utility grid. $\mathbf{p}^b_{g_i} \in \mathbb{R}^{Nh}$ is the buying (positive) component of $\mathbf{p}_{g_i}$. Similarly, $\mathbf{p}_{l_i} \in \mathbb{R}^{Nh}$ are the values of power bought from or sold to the MGs in the network. $\mathbf{p}^b_{l_i} \in \mathbb{R}^{Nh}$ is the buying (positive) component of $\mathbf{p}_{l_i}$.

Using 1-norm distance $\mathcal{D} = \|F - \mathcal{U}\|_1; F = [f_1, \ldots, f_N]^T$ to measure closeness to $\mathcal{U}$, the multi-objective optimization, as described in [183], is formulated as follows.

$$\min \sum_{i=1}^{N} t_i + \epsilon(\mathbf{p}_{l_i}^b + \mathbf{p}_{g_i}^b + p_{bat_i}^c) \tag{5.2a}$$

$$\text{s.t.,} \ \forall i, \ f_i - u_i \leq t_i \tag{5.2b}$$

$$\text{s.t.,} \ p_g^{min}\mathbf{1} \leq \mathbf{p}_{l_i} \leq p_g^{max}\mathbf{1} \tag{5.2c}$$

$$\mathbf{0} \leq \mathbf{p}_{l_i}^b \leq p_g^{max}\mathbf{1} \tag{5.2d}$$

$$\mathbf{p}_{l_i}^b \geq \mathbf{p}_{l_i} \tag{5.2e}$$

$$p_g^{min}\mathbf{1} \leq \mathbf{p}_{g_i} \leq p_g^{max}\mathbf{1} \tag{5.2f}$$

$$\mathbf{0} \leq \mathbf{p}_{g_i}^b \leq p_g^{max}\mathbf{1} \tag{5.2g}$$

$$\mathbf{p}_{g_i}^b \geq \mathbf{p}_{g_i} \tag{5.2h}$$

$$p_g^{min}\mathbf{1} \leq \mathbf{p}_{g_i} + \mathbf{p}_{g_i} \leq p_g^{max}\mathbf{1} \tag{5.2i}$$

$$p_{bat}^{min}\mathbf{1} \leq \mathbf{p}_{bat_i} \leq p_{bat}^{max}\mathbf{1} \tag{5.2j}$$

$$\mathbf{0} \leq \mathbf{p}_{bat_i}^c \leq p_{bat}^{max}\mathbf{1} \tag{5.2k}$$

$$\mathbf{p}_{bat_i}^c \geq \mathbf{p}_{bat_i} \tag{5.2l}$$

$$\mathbf{p}_{g_i} + \mathbf{p}_{l_i} = \mathbf{p}_{bat_i} + \mathbf{p}_{dem} \tag{5.2m}$$

$$E_{bat_i,k} = \sum_{\gamma=1}^{k} h_\gamma \cdot \left(\eta_{bat_i}^c p_{bat_i,\gamma}^c + \frac{1}{\eta_{bat_i}^d}(p_{bat_i,\gamma} - p_{bat_i,\gamma}^c)\right) + E_{bat_i}^o - P_{bat_i}^{loss}\sum_{\gamma=1}^{k} h_\gamma, \ \forall k \tag{5.2n}$$

$$E_{bat_i}^{min} \leq E_{bat_i,k} \leq E_{bat_i}^{max} \tag{5.2o}$$

$$E_{bat_i,final} \geq E_{bat_i}^{desired} \tag{5.2p}$$

$$\sum_i \mathbf{p}_{l_i} = \mathbf{0} \tag{5.2q}$$

In this formulation, $\mathbf{p}_{bat_i} \in \mathbb{R}^{Nh}$ are the charge and discharge power rates of the battery, whereas $\mathbf{p}^c_{bat_i} \in \mathbb{R}^{Nh}$ is the charging (positive) component of $\mathbf{p}_{bat}$. $E_{bat_i,k}$ is the battery energy level at the k^{th} time step. $\eta^c_{bat_i} \in [0,1]$ and $\eta^d_{bat_i} \in [0,1]$ are the charging and discharging efficiencies of the battery, respectively. p^{max}_g is the maximum power limit at the point of connection to the utility grid and p^{max}_{bat} is the maximum charging power limit of the battery; both are positive values. p^{min}_g is the minimum power limit at the point of connection to the utility grid and p^{min}_{bat} is the maximum discharging power limit of the battery; both are negative values.

In (5.1), $\mathbf{p}_{g_i}$, $\mathbf{p}^b_{g_i}$, $\mathbf{p}_{bat_i}$, and $\mathbf{p}^c_{bat_i}$ are the decision variables. These values are computed at every time step as the horizon rolls over, by solving the above optimization problem, which is in the form of a linear program (LP). In the second term in (5.2a), ϵ is a very small positive number. It ensures that the optimizer tries to minimize the value of $\mathbf{p}^b_{g_i}$, $\mathbf{p}^b_{l_i}$, and $\mathbf{p}^c_{bat_i}$. The combination of this and the constraint (5.2l) ensure that $\mathbf{p}^c_{bat_i}$ is the positive component of $\mathbf{p}_{bat_i}$. Similarly, the combinations of (5.2e) and (5.2h) along with ϵ guarantee that $\mathbf{p}^b_{l_i}$ and $\mathbf{p}^b_{g_i}$ are the positive components of $\mathbf{p}_{l_i}$ and $\mathbf{p}_{g_i}$ respectively. The constraints in (5.2c), (5.2d), (5.2f), (5.2g), (5.2j), and (5.2k) limit the decision variables within their respective bounds. (5.2i) ensures that the the sum value of power at the point of connection to the grid does not exceed set limits. The equality constraint (5.2m) ensures that the sum of local and grid powers is equal to the sum of the net demand and battery power values. (5.2) defines the battery energy level at k^{th} time step; here $E^o_{bat_i} \in \mathbb{R}$ is the battery energy level at the beginning of the time horizon and $P^{loss}_{bat_i}$ is the self-discharge power loss value, a characteristic of the battery. (5.2o) defines the energy bounds of the battery, whereas

(5.2p) ensures that the battery attains a predefined desired energy level $E_{bat_i}^{desired}$ at the end of the time horizon. Since, $\mathcal{U}$ is the vector of least possible values for each f_i, the combination of constraint (5.2b) and the first term in the objective function (5.2a) ensure that, at the optimal solution, for each microgrid i the value of f_i is at the least possible distance away from u_i in the 1-norm sense. The problem described above shall be referred to as the *central utopia problem* or the *central problem* in the rest of this text. It is in the form of a LP and can be solved using efficient solvers.

The equality (5.2q) requires that the vector sum of local power values exchanged between all microgrids in the network be $\mathbf{0}$. Solving (5.2) is equivalent to minimizing the cost incurred by the entire network exchanging power with the utility grid, within a given time horizon. At the same time, this formulation ensures that the cost incurred by each individual MG is at the closest possible value to its least possible cost, in the 1-norm sense. A more detailed discussion on deriving the central utopia formulation can be found in [183].

5.3 Distributed Energy Management

The utopia-point formulation of the optimization problem in (5.2) can be solved to find optimal solutions for networks of microgrids of varying sizes. However for very large networks, the size of optimization problem may grow to the extent that a single centralized computer may not have sufficient computational power and memory resources to find the solution in real time. Moreover at each time step, the centralized computer would require to communicate the individual MG's predicted net demand, battery charge level, and battery charge/discharge commands over a network. Such centralized computing architecture may pose security and privacy concerns. The

entire network would also be vulnerable to disruptions in the communications with the central controller or its failure.

In this chapter, a novel distributed method, for solving the optimization problem is introduced, largely addressing the above-noted issues. The idea is to breakdown the computations to smaller parts that can be executed locally in parallel across the MGs, significantly reducing the amount of centralized computations. The solutions to local distributed optimizations would yield optimal values for the decisions variables of the corresponding MG.

5.3.1 ADMM

Alternating Direction Method of Multipliers (ADMM) is an effective iterative technique to solve optimization algorithms, with a certain degree of decomposability, in parallel. It solves problem in the form

$$\min f(\mathbf{x}) + g(\mathbf{x}') \tag{5.3a}$$

$$s.t., \;\; \mathbf{A}\mathbf{x} + \mathbf{B}\mathbf{x}' = \mathbf{c} \tag{5.3b}$$

where the objective function is separable across the two sets of variables $\mathbf{x} \in \mathbb{R}^n$ and $\mathbf{x}' \in \mathbb{R}^m$; $\mathbf{A} \in \mathbb{R}^{p \times n}$, $\mathbf{B} \in \mathbb{R}^{p \times m}$, and $\mathbf{c} \in \mathbb{R}^p$. An augmented Lagrangian function is formed as follows

$$\mathcal{L}_\rho = f(\mathbf{x}) + g(\mathbf{x}') + \mathbf{y}^T(\mathbf{A}\mathbf{x} + \mathbf{B}\mathbf{x}' - \mathbf{c}) + \frac{\rho}{2}\|\mathbf{A}\mathbf{x} + \mathbf{B}\mathbf{x}' - \mathbf{c}\|_2^2 \tag{5.4}$$

where $\mathbf{y}$ is the dual variable or the Lagrange multiplier and $\rho > 0$ is the penalty parameter. ADMM solution consists of the following iterations until specified stopping

criteria are met,

$$\mathbf{x}^{j+1} := \arg\min_{\mathbf{x}} \mathcal{L}_\rho(\mathbf{x}, \mathbf{x}'^j, \mathbf{y}^j) \tag{5.5a}$$

$$\mathbf{x}'^{j+1} := \arg\min_{\mathbf{x}'} \mathcal{L}_\rho(\mathbf{x}^{j+1}, \mathbf{x}', \mathbf{y}^j) \tag{5.5b}$$

$$\mathbf{y}^{j+1} := \mathbf{y}^j + \rho(\mathbf{A}\mathbf{x}^{j+1} + \mathbf{B}\mathbf{x}'^{j+1} - \mathbf{c}) \tag{5.5c}$$

The use of ADMM for different classes of problems is discussed in detail in [184]. For the problem considered here, objective function (5.2a), and constraints (5.2b)-(5.2p) are separable into N components corresponding to each microgrid in the network. The only constraint shared among microgrids is (5.2q). This problem resembles the *optimal exchange* problem described in [184], where the following problem is solved,

$$\min \sum_{i=1}^{N} f_i(\mathbf{x}_i) \tag{5.6a}$$

$$s.t., \ \sum_{i=1}^{N} \mathbf{x}_i = \mathbf{0} \tag{5.6b}$$

The solution to this problem is achieved by iterating through the following steps

$$\mathbf{x}_i^{j+1} := \arg\min_{\mathbf{x}_i} \ \left(f_i(\mathbf{x}_i) + \frac{\rho}{2} \|\mathbf{x}_i - \mathbf{x}_i^j + \bar{\mathbf{x}}^j + \mathbf{v}^j\|_2^2 \right) \tag{5.7a}$$

$$\mathbf{v}^{j+1} := \mathbf{v}^j + \rho \bar{\mathbf{x}}^{j+1} \tag{5.7b}$$

where $\bar{\mathbf{x}}^j$ is the mean of $\mathbf{x}_i, \forall i$ from iteration j, i.e. $\bar{\mathbf{x}}^j = \sum_{i=1}^{N} \mathbf{x}_i^j$; $\mathbf{v}^j$ is the *scaled* dual variable at iteration j and $\mathbf{v}^j = \frac{1}{\rho}\mathbf{y}^j$. It is worth noting that the first step is

carried out in parallel across all i microgrids.

5.3.2 The Distributed Problem

The 2-step iterative ADMM solution described by (5.7) can be adapted to the central problem, resulting in a *distributed utopia problem*. First, the utopia point $\mathcal{U}$ is calculated, as before, solving a problem similar to (5.2) for each MG by removing the grid power decision variables and constraints removed. Then, several iterations of ADMM solution steps are carried out until the stopping criterion, discussed below, is met. The first step of each iteration is solving N optimization problems in parallel to obtain the solutions for iteration $j+1$, with (5.2b)-(5.2p) as constraints, and (5.8) as the objective function.

$$\min \ \frac{\rho^j}{2}\|\mathbf{p}_{l_i} - \mathbf{p}^j_{l_i} + \bar{\mathbf{p}}^j_{l_i} + \mathbf{v}^j\|_2^2 + t_i + \epsilon(\mathbf{p}^b_{l_i} + \mathbf{p}^b_{g_i} + p^c_{bat_i}) \tag{5.8}$$

Here $\mathbf{v}^j$ is the scaled dual variable at the j^{th} iteration. Each optimization yields optimal values of $\mathbf{p}^b_{l_i}$, $\mathbf{p}^b_{g_i}$, $\mathbf{p}^c_{bat_i}$, $\mathbf{p}_{l_i}$, $\mathbf{p}_{g_i}$, and $\mathbf{p}_{bat_i}$, for iteration $j+1$ denoted by $\{\mathbf{p}^{j+1}_i\}$. The next step in the iteration is to compute the mean $\bar{\mathbf{p}}^{j+1}_{l_i}$ using (5.9). Subsequently, the scaled dual for iteration $j+1$ is calculated using (5.7b), substituting $\bar{\mathbf{p}}^{j+1}_{l_i}$ for $\bar{\mathbf{x}}^{j+1}$.

$$\bar{\mathbf{p}}^{j+1}_{l_i} = \sum_{i=1}^{N} \mathbf{p}^{j+1}_{l_i} \tag{5.9}$$

The final step in the iteration is to check if the *stopping criterion* is met. The difference between the central and distributed problems is that the global constraint (5.2q) is brought into the objective function (5.8) of the distributed problem. At each

Algorithm 1 Pseudocode to execute the ADMM-based Distributed Energy Management

1: Calculate $\mathcal{U}$ as described in subsection 5.3.2
2: **repeat**
3: **for all** microgrids $i = 1, \cdots, N$ **do**
4: $\{\mathbf{p}_i^{j+1}\} \leftarrow$ Solve (5.8) & (5.2b)-(5.2p)
5: **end for**
6: Find ρ^{j+1} according to (5.10)
7: $\bar{\mathbf{p}_{l_i}}^{j+1} \leftarrow \sum_{i=1}^{N} \mathbf{p}_{l_i}^{j+1}$
8: $\mathbf{v}^{j+1} \leftarrow \mathbf{v}^{j} + \rho \bar{\mathbf{p}_{l_i}}^{j+1}$
9: **until** $\| \sum_{i=1}^{N} \mathbf{p}_{l_i}^{j+1} \|_2 \leq \alpha$

iteration, this constraint gets closer to being satisfied. Therefore, the two norm of the sum of powers exchanged among microgrids $\| \sum_{i=1}^{N} \mathbf{p}_{l_i}^{j+1} \|_2$, in iteration $j+1$ is chosen as the measure of interest. The procedure is terminated when this value falls below a small positive value α.

In order to ensure fast convergence, at each iteration, the value of ρ is modified based on the relationship between the value of the measure of convergence, $\| \sum_{i=1}^{N} \mathbf{p}_{l_i}^{j} \|_2$ from the previous iteration to that of the current iteration $\| \sum_{i=1}^{N} \mathbf{p}_{l_i}^{j+1} \|_2$, such that,

$$\rho^{j+1} = \begin{cases} \rho^j \times \tau & \text{if } \| \sum_{i=1}^{N} \mathbf{p}_{l_i}^{j+1} \|_2 > \mu \| \sum_{i=1}^{N} \mathbf{p}_{l_i}^{j} \|_2 \\ \frac{\rho^j}{\tau} & \text{if } \| \sum_{i=1}^{N} \mathbf{p}_{l_i}^{j+1} \|_2 < \mu \| \sum_{i=1}^{N} \mathbf{p}_{l_i}^{j} \|_2 \\ \rho^j & \text{otherwise} \end{cases} \tag{5.10}$$

where μ and τ are constants. The pseudocode to perform the distributed energy management is summarized in Algorithm 1. Here, step 4 can be solved using efficient Quadratic Program (QP) solvers which are available.

5.3.3 Computation & Communication Requirements

In the central problem, all of the inputs to the LP solver and subsequently, the control decisions for all the MGs in the network ought to be communicated to and from the machine, on which the central problem is solved. Since critical information and decisions regarding the resources and operations of individual MGs are transported across the network, data security and privacy concerns are an issue. Further, if one or more of the communication links between individual MGs and the central computing unit fail, or if the central computing unit is out of commission, significant economic losses could occur either to the affected MG or the entire network.

In the distributed problem, each MG is expected to have some computing capability, typically low-cost and low-power hardware, in order to perform step 4 in Algorithm 1 iteratively. Steps 7, 8, and 9 need to be calculated centrally. The computation requirements to perform these calculations are not very demanding and any of the MGs, given the available computing capability could execute these steps.

At each iteration, $\mathbf{p}_{l_i}^{j+1}$ values from each MG has to be sent to the central computing unit of the distributed problem, and the $\bar{\mathbf{p}_{l_i}}^{j+1}$ and $\mathbf{v}_{l_i}^{j+1}$ values are returned. Communication between one or more of the MGs and the central computing unit could break down. In such scenarios, the nature of the calculations in steps 7, 8, and 9—means and norms—facilitate the smooth operation of the rest of the MGs, while the affected MG could fall back to using the local EMS to make control decisions to trade energy solely with the utility grid.

Strategies for sharing of the resources and responsibilities for central computations are out of the scope of this work. However, simple strategies like using more than one MG, or a small percentage of MGs in the network, say $5-10\%$, to perform these

tasks could enhance the network's *resiliency* in case of failures in communications.

In addition, in the distributed problem, only the values of the power over the time horizon, exchanged with MGs in the network are communicated to the central computing unit, in each iteration. Since this information is readily available to anyone who can measure the power at the point of connection of the MG to the grid, this method does not pose any significant additional threat to data security or privacy.

5.4 Evaluation: Simulation Experiments

Simulation experiments were designed and carried out to prove the cost benefits of using an EMs in a network of MGs; and to demonstrate the superiority in computational efficiency, speed, and scalability of the distributed problem.

5.4.1 Setup

All simulations were carried out in Matlab running in a Mac OSX environment, on an Intel Core i5 2.5GHz machine with 8GiB DDR3 RAM. Gurobi Optimization's LP and QP solvers were used to solve the central and distributed problems.

Ontario Weekday Time-of-Use rates for Winter 2016 were used for $\mathbf{c}^b_{g_i}$ to calculate electricity prices: 17.5 ¢/kWh between 7-11 A.M and 5-7 P.M.; 12.8 ¢/kWh between 11 A.M to 5 P.M.; and 8.3 ¢/kWh from 7 P.M to 7 A.M; this pricing scheme is illustrated in Fig. 5.2. Values of the other cost coefficients were chosen as follows: $\mathbf{c}^s_{g_i} = 0.07 \cdot \mathbf{c}^b_{g_i}$, $\mathbf{c}^b_{l_i} = 0.47 \cdot \mathbf{c}^b_{g_i}$, and $\mathbf{c}^s_{l_i} = 0.45 \cdot \mathbf{c}^b_{g_i}$.

Real-world hourly demand values for a commercial building (peak demand under 50kW and hourly generation values for a solar generator (peak generation values

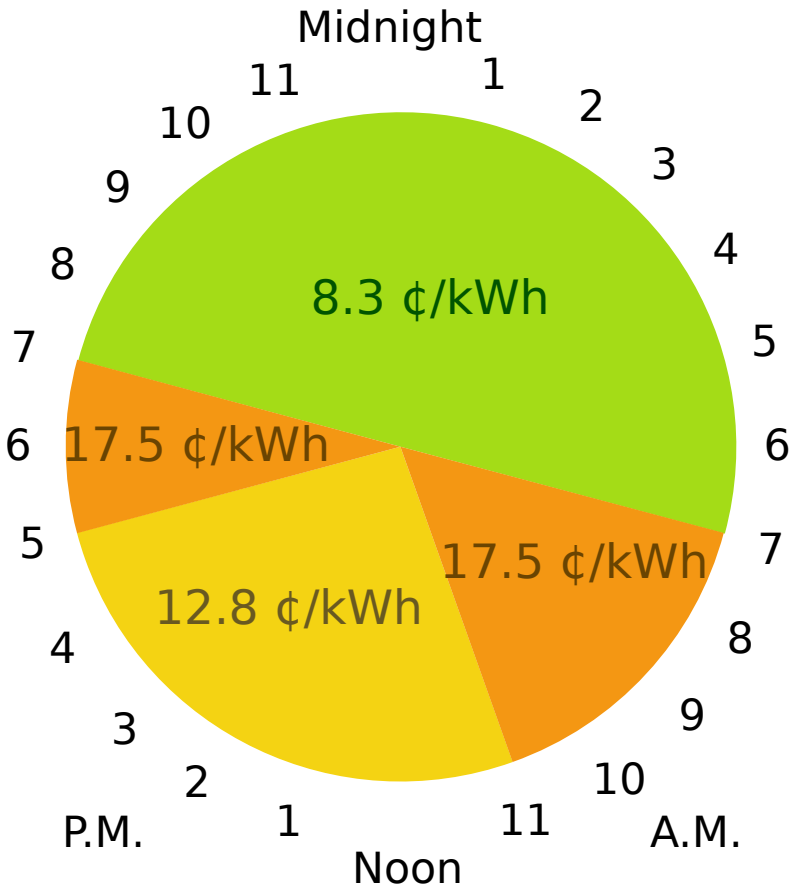

Figure 5.2: Illustration of TOU Grid Electricity Buy Prices used in network of microgrids simulations

between 45kW and 50kW) were obtained from Burlington Hydro Inc. (Burlington, Canada) and used to generate $\mathbf{p}_{dem}$.

The RH controller utilized makes decisions on a 24 hour future time horizon with 15 minute time steps. At each time step the time horizon vector $\mathbf{h} = [0.25, 0.25, 0.5, 0.5, 0.5, 1, 1, 2, 2, 4, 4, 8]^T$, where each element represents the duration of the time step in hours. It can be observed that the most immediate future time step is of the shortest duration, while the one farthest in the future is the longest. This ensures that the decisions made for the immediate future is more accurate in shorter time-resolutions

compared to those in the future, while also serving to reduce the size of the problem solved.

Parameters whose values throughout all simulations were the same are: $\epsilon = 10^{-4}$, $\mu = 10$, $\tau = 2$, $Nh = 12$, $\eta^c_{bat_i} = \eta^d_{bat_i} = 0.95$, and $E^{min}_{bat_i} = 0$. At each time step, $E^{desired}_{bat_i}$ was set equal to the energy level at beginning of the time horizon $E^o_{bat_i}$. This ensures that the optimizer does not choose to drain the battery by the end of the time horizon in order to achieve economic benefits. The value of ρ^1 at the first iteration is 0.005 and its value at any iteration j is capped at $\rho^j = 1$.

5.4.2 Network of Microgrids: Cost Savings

Scenarios with varying numbers of MGs were considered, where at least 80% had PV generators and at least 25% had on-site batteries with $E^{max}_{bat_i}$ values between 80kWh and 90kWh; $p^{max}_{bat_i} = -p^{min}_{bat_i} = 25$kW; and $p^{max}_g = -p^{min}_g = 45$kW.

A case where these MGs had individual EMS-s trading energy directly with the utility grid; this case shall be referred to as the *isolated MG* case. Another case considered was that of the central problem, i.e. a centralized EMS with energy traded among MGs and between MGs and the utility grid. The sum cost of electricity incurred by the MGs in two cases, over a period of 30 simulation days, were compared against a case where there was no EMS, i.e. no battery is present and no control is performed. The results are tabulated in Table 5.1.

It can be observed that while the use of EMS, in the isolated MG case, brings about some cost reduction, the improvement enabled by the Central Utopia problem over the isolated MG case is significant in network of MGs of varying sizes. It can be inferred that a network multiple MGs which allow for energy trade among each other

Table 5.1: Comparison of costs over 30 simulation days by varying number of MGs in 3 cases: No EMS, Isolated MG, & Central Utopia problem. Column 4 shows the improvement by the Isolated MG case over No EMS; Column 6 shows improvement over the Isolated MG case by the Central problem.

No. of MGs	No EMS Cost ($)	Isolated MG Cost ($)	Improvement over No EMS (%)	Central Utopia Cost ($)	Improvement over Isolated MG (%)
5	872.56	734.14	15.86	344.05	53.14
10	4039.72	3664.21	9.3	1663.04	54.61
25	11651.59	9958.43	14.53	5059.23	49.2
50	21363.08	18154.07	15.02	8550.87	52.9
100	44245.27	38844.71	12.21	18648.32	51.99
200	91995.1	81209.56	11.72	39660.33	51.16
250	117790.35	105061.36	10.81	52939.22	49.61

reap significant economic benefits.

5.4.3 Central vs. Distributed Problem

96 single time step simulations—equivalent to the duration of one simulation day—were carried out to assess, compare, and contrast the computational performances, accuracies, effectiveness of the central problem and three different flavours of the distributed problem—with α values equal to 10^{-3}, 10^{-2}, 10^{-1}—for networks with varying numbers of MGs. In each of these simulations, the system parameter inputs were exactly the same for the central problem as well as the three flavours of the distributed problem. All MGs were assumed to contain PV generators and batteries; with $E_{bat_i}^{max} = 60\text{kWh}$, $p_{bat_i}^{max} = -p_{bat_i}^{min} = 5\text{kW}$; and $p_g^{max} = -p_g^{min} = 25\text{kW}$.

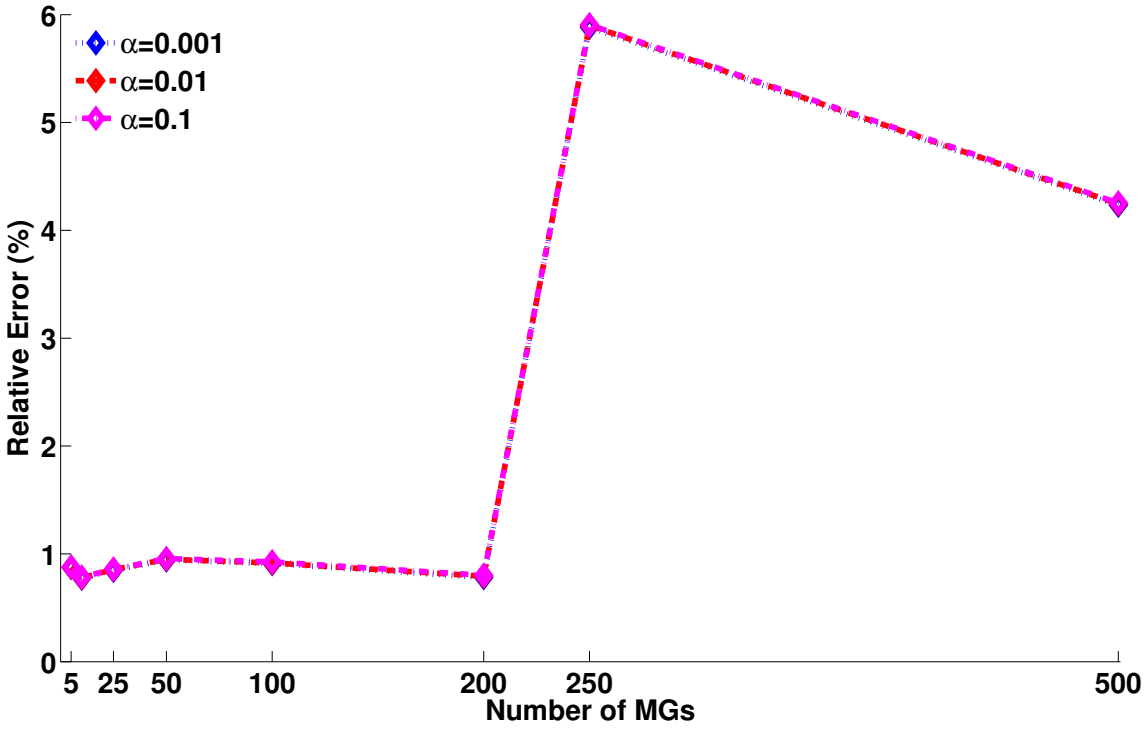

Figure 5.3: Average values of $\mathcal{E}_{d001}$, $\mathcal{E}_{d01}$, and $\mathcal{E}_{d1}$ in percentages, over 96 simulations, for networks of MGs of varying sizes. It is noted that the accuracy of the distributed problem does not depend on the choice between the tested values of α.

Accuracy

The 1-norm distance to the utopia point $\mathcal{D}_c$ of the central problem was chosen to be the benchmark to compare the accuracy of the solutions of the distributed problems. The 1-norm distances of distributed problems corresponding to α values equal to 10^{-3}, 10^{-2}, and 10^{-1}, are denoted by $\mathcal{D}_{d001}$, $\mathcal{D}_{d01}$, and $\mathcal{D}_{d1}$ respectively. The relative error between $\mathcal{D}_c$ and each of the corresponding 1-norm distances between the three distributed problems was used as a measure of accuracy of the solutions of the distributed problems. The relative error $\mathcal{E}_{d001}$ between $\mathcal{D}_c$ and $\mathcal{D}_{d001}$ is defined as $\mathcal{E}_{d001} = \frac{|\mathcal{D}_{d001} - \mathcal{D}_c|}{|\mathcal{D}_c|}$; $\mathcal{E}_{d01}$ and $\mathcal{E}_{d1}$ are defined similarly.

Plots of the average percent values of $\mathcal{E}_{d001}$, $\mathcal{E}_{d01}$, and $\mathcal{E}_{d1}$ over 96 simulations are

displayed in Fig. 5.3 for networks of varying sizes. It was noted that the values $\mathcal{D}_{d001}$, $\mathcal{D}_{d01}$, and $\mathcal{D}_{d1}$ were larger than $\mathcal{D}_c$ in all cases. However, the deviances of the solutions of the distributed problems from those of the central problem—their average relative errors—are very small, in the range of $0.77 - 5.88\%$. It is inferred that the solutions to the distributed problems are fairly accurate.

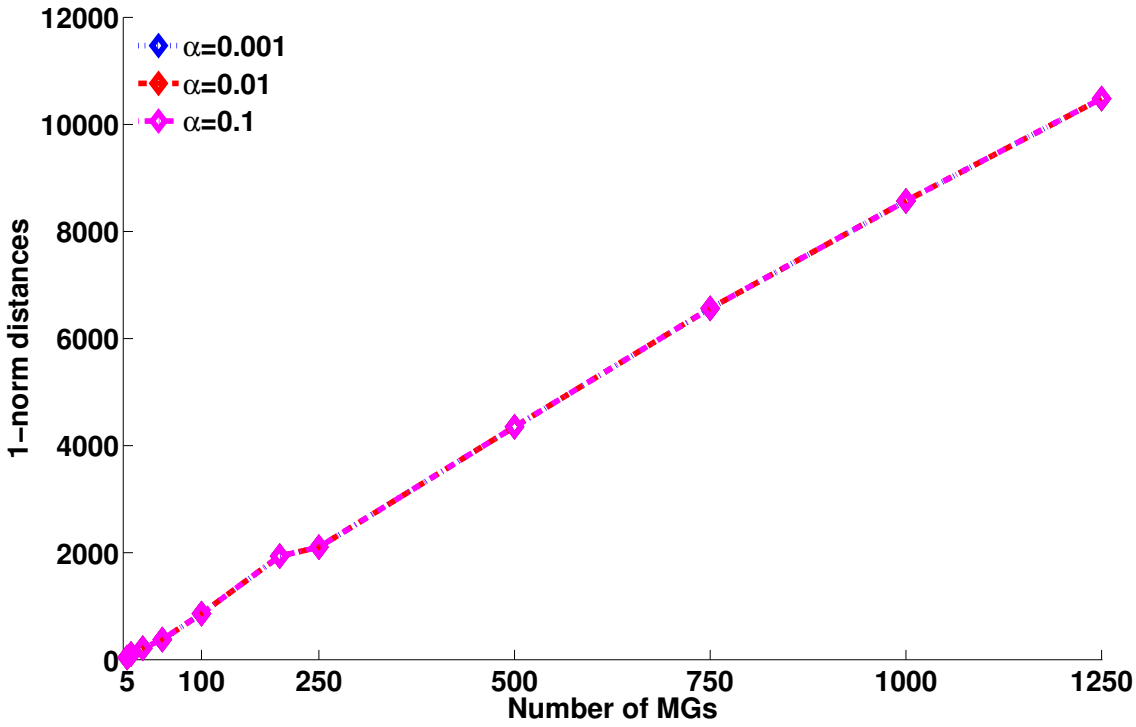

Figure 5.4: Average values of $\mathcal{D}_{d001}$, $\mathcal{D}_{d01}$, and $\mathcal{D}_{d1}$, over 96 simulations, for networks of MGs of varying sizes.

It is observed that the values of α that were utilized, on average, do not result in solutions which deviate significantly differently, from those of the central problem. In other words, the accuracy of the distributed problem does not depend on the choice between the tested values α. This inference is further emphasized by the plot of the average values of $\mathcal{D}_{d001}$, $\mathcal{D}_{d01}$, and $\mathcal{D}_{d1}$ for different network sizes shown in Fig. 5.4. It

can be seen that the average values of the 1-norm distances are virtually the same in all of the distributed problems. Fig. 5.4 shows results from a wider range of network sizes. The reasons will be explained later in the text.

Power and Energy Signals

Above, it was demonstrated that the values of 1-norm distance between the Central and Distributed problems do not vary significantly. However, the decisions made by the Central and Distributed problems, in order to achieve these values, may differ from each other. In order to illustrate this, Figures 5.5 and 5.6 show the buy and sell values of local and grid powers in the Central and Distributed problems respectively. A network of 200 MGs and a value of $\alpha = 10^{-3}$ for the distributed problem were chosen for the purpose of illustration.

Each curve in the plot represents the corresponding power value of an individual MG. It is observed that more MGs in the Central Problem buy power in the local market and that their peak values are higher, compared to those in the Distributed problem. This can be attributed to the fact that, in the distributed problem the use of $\| \sum \mathbf{p}_{l_i} \|_2$ in the stopping criterion and in the quadratic objective function, has the effect of smoothening the local power values. This is further illustrated in Fig. 5.7 where it can be observed that the magnitudes of the local powers span a significantly larger range of values in the Central problem than in the Distributed problem.

Additionally, it is observed that both in the Central and Distributed solutions to the problem there is a significantly higher amount of local buy or sell activity between hours 7-11 and 17-19. These represent the time periods during which the cost to buy electricity from the grid is highest. It is evident that both approaches

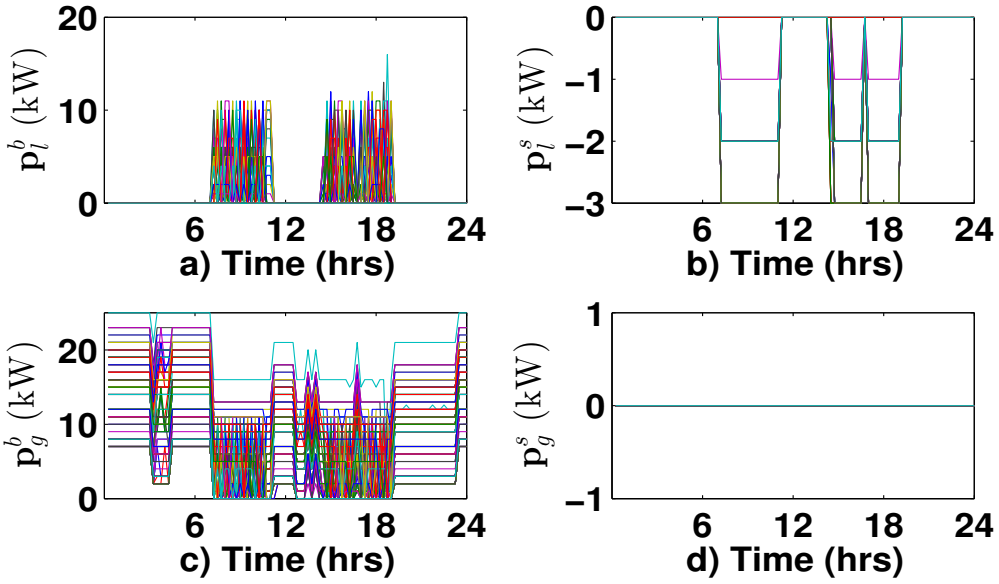

Figure 5.5: Plot of a) local buy b) local sell c) grid buy and d) grid sell power values over a 24 hour horizon, obtained using the Central Problem for a network of 200 MGs

attempt to reduce electricity costs by ensuring that a higher proportion of electricity is exchanged locally within the network than with the grid during these time intervals.

Figures 5.8 and 5.9 show plots of the battery power and energy values, the net power at each MG, and the total net power exchanged between the entire network and the grid. Observing the two figures it is clear that, the battery charging and discharging activities follow a similar pattern in both the Central and Distributed problem. Similarly, beyond minor differences in the shapes of the signals the grid power values in both the Central and Distributed problems appear similar to each other.

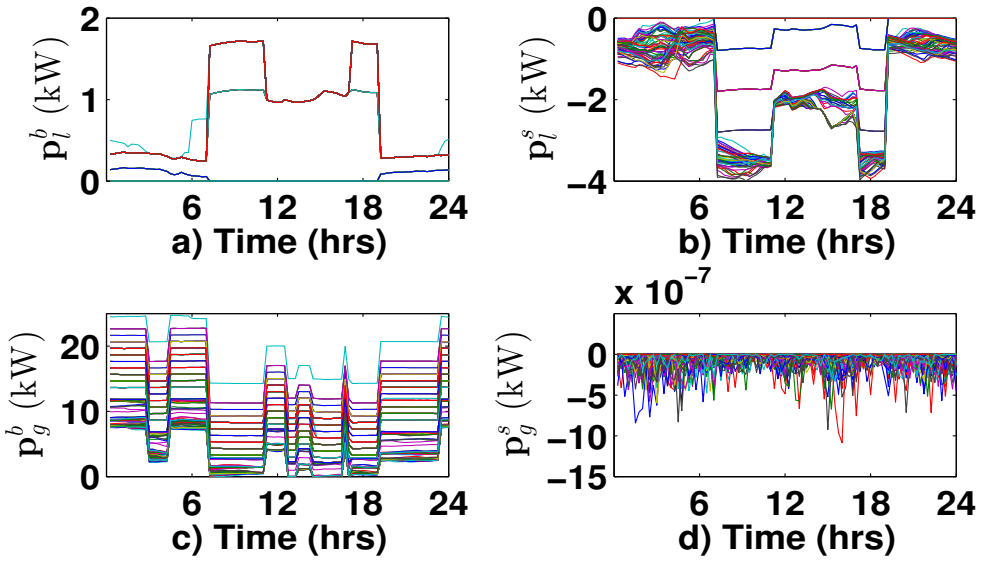

Figure 5.6: Plot of a) local buy b) local sell c) grid buy and d) grid sell power values over a 24 hour horizon, obtained using the Distributed Problem ($\alpha = 10^{-3}$) for a network of 200 MGs

Computational Performance

The amount of time it takes to perform computations was the chosen metric to compare the central and distributed problems. In both problems, the value of $\mathcal{U}$ is calculated in the same way; and was therefore ignored in the comparison. In the central problem, the value used is the time taken to solve problem (5.2); whereas, in the case of the distributed problems it is the sum, over all iterations, of the execution times of steps 7, 8, 9, and the maximum time taken by step 4 over all MGs, in Algorithm 1, until the stopping criterion is met.

Fig. 5.10 shows the semi-log plot of average execution times, over 96 simulations, of the central and distributed problems, for networks of MGs of varying sizes. It can be seen that for a given value of α, the execution times remain in the same order of

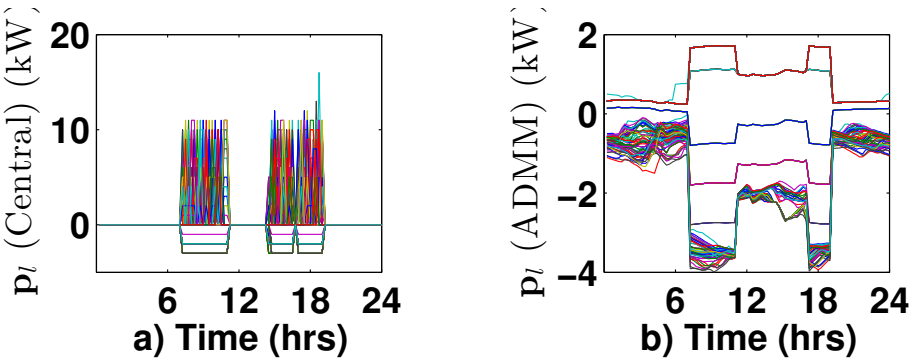

Figure 5.7: Comparison of the local power values between the Central and Distributed Problems over a 24 hour horizon, for a network of 200 MGs

magnitude with minimal variations over the different size of the networks that were simulated.

In the case of the central problem, it was observed that, although the performance was marginally better than the distributed problems for small network sizes, the computation times steadily increased as the network size increased until at $N = 500$, the average computation time for each time step was higher than the duration of the first time step (15 minutes).

Further, it is observed in Fig. 5.10 that the average computation time for the central problem jumps several orders of magnitude between $N = 250$ and $N = 500$. It was found out that this was the result of the size of the problem, i.e. the space occupied by the inputs to the optimization solver, being larger than the primary memory of the machine used, at $N = 500$. This resulted in a large amount of data paged in from the virtual memory to the main memory, a process which can take a considerable amount of time depending on hardware specifications. Sizes of the input in GiB to the optimization solver, for the central problem, for different network sizes are tabulated in Table 5.2.

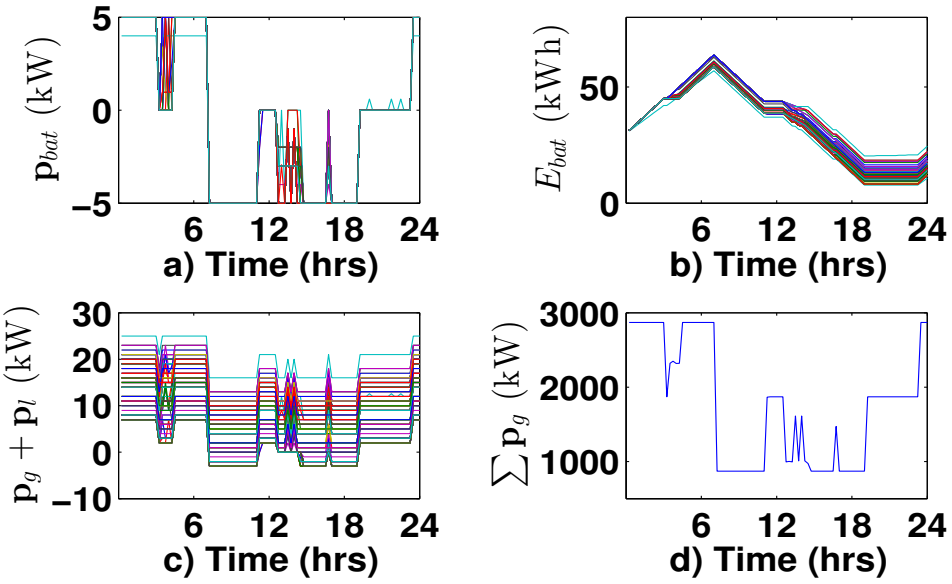

Figure 5.8: Plot of a) battery power b) battery energy c) net power at individual MG and d) total grid power values over a 24 hour horizon, obtained using the Central Problem for a network of 200 MGs

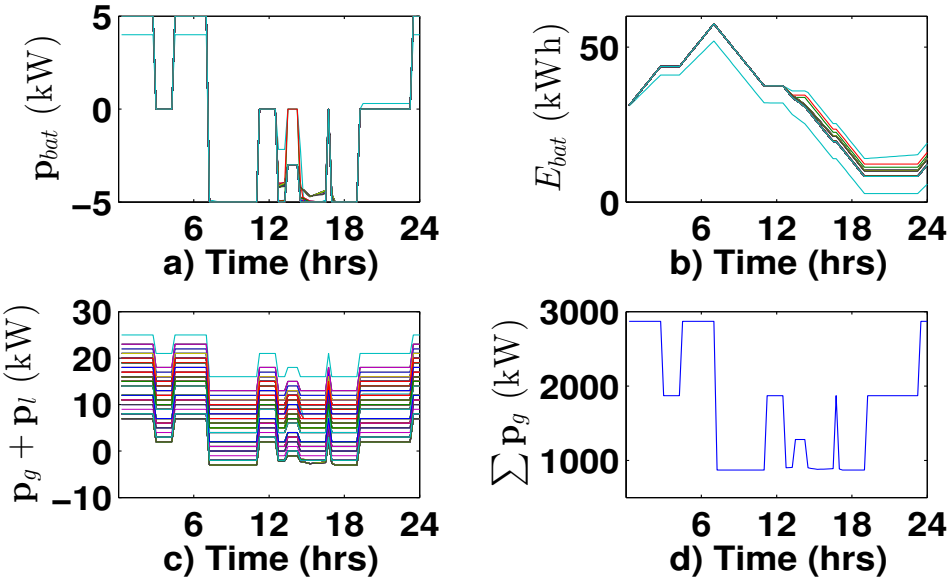

Figure 5.9: Plot of a) battery power b) battery energy c) net power at individual MG and d) total grid power values over a 24 hour horizon, obtained using the Distributed Problem ($\alpha = 10^{-3}$) for a network of 200 MGs

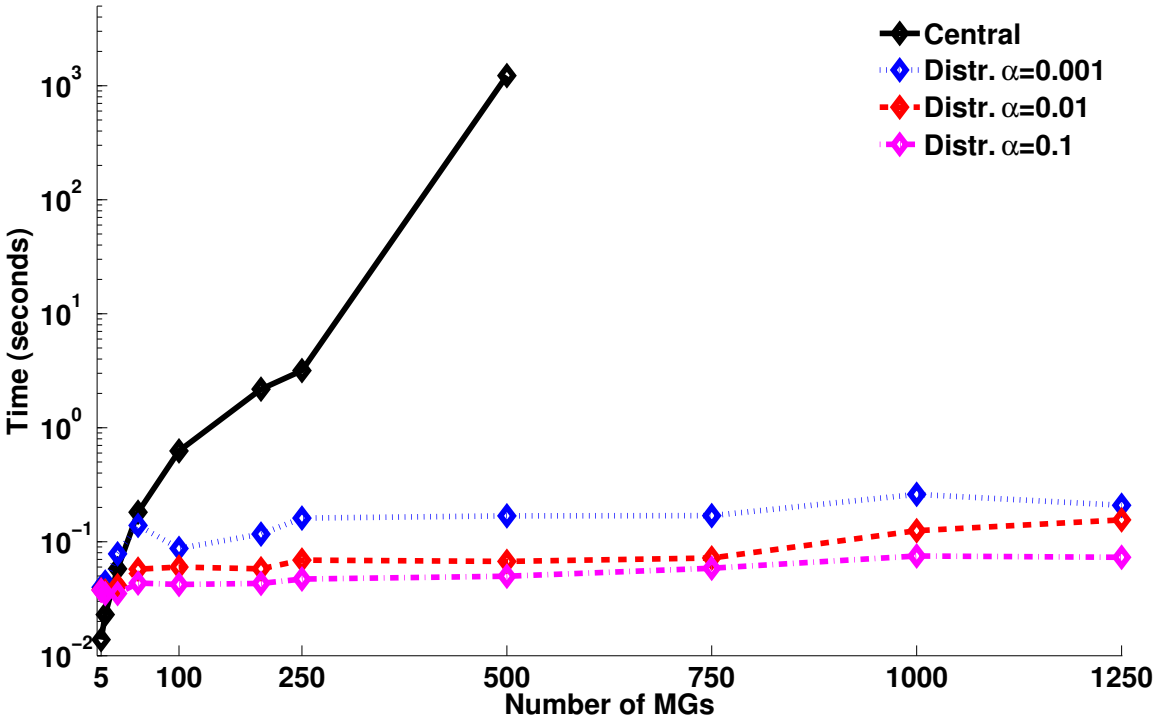

Figure 5.10: Average computation times of the central and distributed problems. At $N = 500$ and beyond, the average computation time of the central problem was longer than the duration of each time step.

It is observed that, at $N = 500$ the input size far exceeds the available main memory size of 8GiB in the machine used. Observing the estimated input sizes for problems with $N = 750$, $N = 1000$, and $N = 1250$, it can be seen that for networks with over 1000 MGs, current high performance work stations, which typically have 32GiB of main memory may not be able to deliver a good computational performance, requiring clusters of computing nodes or cloud computing.

In the distributed problem, the input to each QP optimization solver in step 4 of Algorithm 1 is 99.6KiB. Steps 7, 8, and 9 which are required to be computed centrally, have space requirements of $8 \times Nh \times \mathrm{N}$ bytes. For $Nh = 12$ and $N = 1250$, the largest network size simulated, the storage requirement for these central computations is

Table 5.2: Optimization solver input sizes for the central problem for different network sizes. Values shown in italics are estimates for network sizes for which the distributed problems were solved.

No. of MGs	Input Size (GiB)	No. of MGs	Input Size (GiB)	No. of MGs	Input Size (GiB)
5	0.001	100	0.53	*750*	29.99
10	0.005	200	2.13	*1000*	53.31
25	0.034	250	3.33	*1250*	83.29
50	0.13	500	13.33	-	-

117.19KiB. Thus, it is evident that both in terms of computation times and memory requirements, the distributed problem is far superior to the central problem for large network sizes, i.e. it is *scalable*.

Note on Communication Times

Developing communication strategies among the MGs and computing units is not within the scope of this work. However, it's worthwhile examining ideas which may reduce communication burden on the overall system. At each time step, in the central problem, each MG sends and receives a few bytes of information and control decisions to and from the machine which solves the optimzation problem. However, as alluded to in subsection 5.3.3, at each iteration of the distributed problem, $\mathbf{p}_{l_i}^{j+1}$, $\bar{\mathbf{p}_{l_i}}^{j+1}$ and $\mathbf{v}_{l_i}^{j+1}$ values exchanged between each MG and the central computing unit.

Fig. 5.11 shows the plot of average number of iterations taken by the distributed problems ranging from those with $\alpha = 10^{-3}$, representing the strictest stopping criterion, to $\alpha = 10^{-1}$, representing the least strict stopping criterion. $\alpha = 10^{-1}$ results in the least number of iterations, by a large margin, across all sizes of the network. This will result in the least amount of communications within the network. It was already shown that the accuracy of results with $\alpha = 10^{-1}$ is almost the same as that

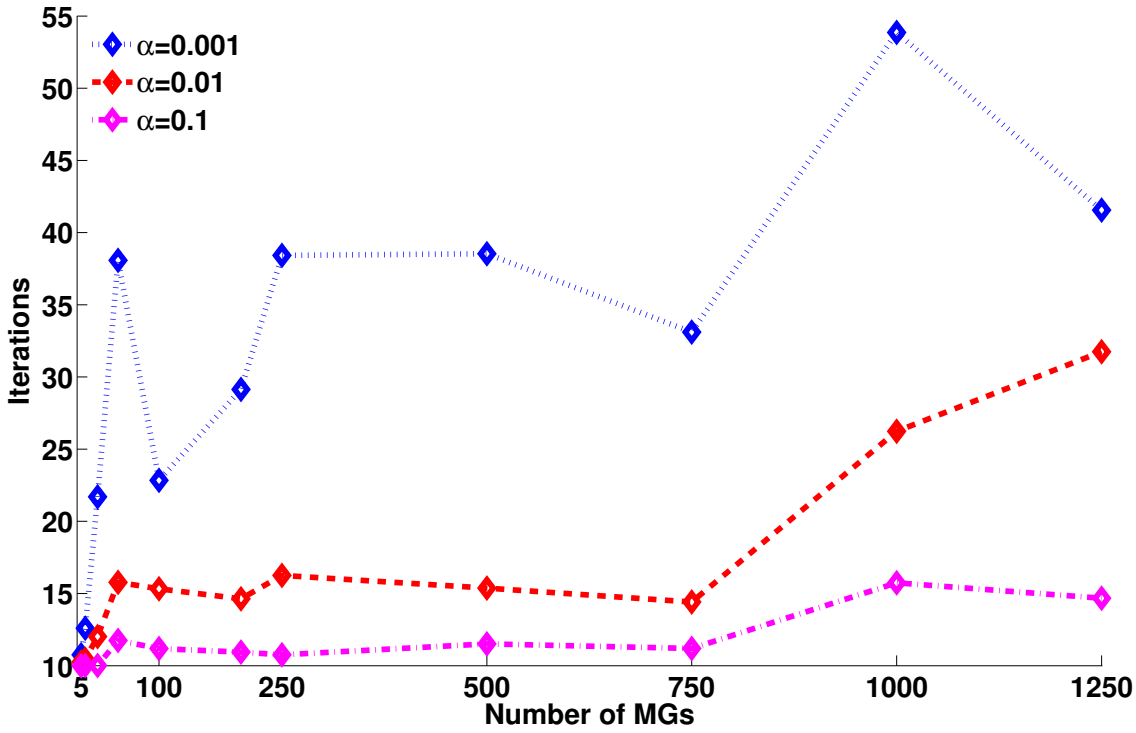

Figure 5.11: Average number of iterations taken by the distributed problems, for each value of α, to satisfy the stopping criterion.

with $\alpha = 10^{-3}$. Therefore, it is recommended that the value $\alpha = 10^{-1}$ be used for the stopping criterion of the distributed problem.

5.5 Summary

A network of MGs containing PV generators and on-site batteries, capable of trading energy among themselves as well as with the utility grid, was considered. A central, utopia point-based, optimization formulation for energy management of this network was developed, in the form of a LP. It was demonstrated, through simulations, that the network, with central energy management, affords significant economic benefits over MGs trading energy only with the utility grid.

A distributed energy management scheme, which is inherently is more data-secure and resilient to communication issues, was developed from the central optimization using ADMM. Using simulations, it was shown that the solutions achieved by this method was scalable, accurate in comparison with the central version, faster to compute, and requires far less powerful hardware. Analyzing the number of iterations it took to converge, a value for the parameter α in the stopping criterion was recommended.

Chapter 6

Conclusion

6.1 Summary

The stress imposed on the environment by climate change and increasing energy needs across the world has spurred interest in green technologies. In response, grid integration of RES, storage, and EVs is a major challenge that is being addressed by scientists, engineers, businesses, policy-makers, and governments. Microgrids are a viable solution to integrate RES, storage, and EVs quickly into the grid, while facilitating economic benefits, grid resiliency, and energy security.

The thesis focussed on developing, describing, and validating optimization-based control frameworks to serve as EMSs for a variety of MG system configurations. Each of the systems under consideration in this thesis were grid-connected microgrids, containing RES and energy storage devices; some of them contain integrated EVs.

6.1.1 Contributions

The Adaptive Energy Management System was discussed in Chapter 3. Attention was largely centred on developing an optimization-based RH controller for MGs with RES, storage, and integrated EVs. An attempt was made to extend earlier work, which described an EMS for MGs with RES and storage, to integrate EVs. This was primarily accomplished by modifying the time horizon used in the optimization based on the EV connection periods. Difficulties arise in keeping track of multiple time horizons for multiple EVs while simultaneously designing the system for uncertainties.

Two optimization formulations, which solve the same problem, using slightly different methods were proposed for the controller. One of them, Formulation I, made use of binary variables to decide between buying and selling from and to the grid; while the other, Formulation II, avoided them. Both formulations accommodated different charging scenarios for EVs: bidirectional charging, unidirectional charging with On/Off control, and One block charging. The stochastic versions of Formulation I and II both use binary variables. However the version using Formulation II had fewer binary variables than that using Formulation II; the difference in the number of binary variables was the highest in the bidirectional charging scenario. It was shown in Section 4.3 that this resulted in some cases, especially in the bidirectional charging scenario using the stochastic version, where use of Formulation II resulted in computational times which were up to 5 times as fast as those using Formulation I.

In Chapter 4, stochastic versions of the controller, which utilize scenario based

methods to solve chance constraints based problem were discussed. Samples or particles were drawn from probability distributions of uncertain parameters. Then stochastic optimization problems were formulated such that for a desired value of probability of failure were, at most a specific fraction of the total number of particles drawn fall outside the feasible region when optimal decisions are obtained. The controllers based on stochastic methods, resulted in significantly fewer instances in which the controller fails to charge EVs to desired final energy levels within the connection period. For the bidirectional charging scenario, the stochastic controller failed $\frac{208}{1900}$ times whereas the non-stochastic version failed $\frac{545}{1900}$ times. The denominator indicates the total possible instances of failure. Similarly for On/Off control, the stochastic controller failed $\frac{35}{2000}$ times and the non-stochastic version failed $\frac{219}{2000}$ times. For One Block Charging, the stochastic controller failed $\frac{69}{2000}$ times and the non-stochastic version failed $\frac{190}{2000}$ times.

Contributions of this work are summarized below:

- A more complete system with renewable power generation, on-site energy storage, and electric vehicles, whose presence in the system is intermittent was considered; along with the use of an online model predictive controller which makes new decisions at every time step while considering uncertain system parameters over a future rolling time horizon.

- The controller accommodated various EV charging scenarios, namely adjustable power bidirectional, single-level unidirectional, and unidirectional block charging.

- Stochastic optimization techniques were employed with rolling horizon control to overcome uncertainties in magnitude of uncertain parameters and uncertainties in time. This was shown to significantly improve robustness of the system

response over conventional rolling horizon control.

In Chapter 5, a network of MGs was considered. Scenarios where MGs within a network trade energy among themselves and with the utility grid were considered. A rolling horizon centralized controller for the network, described in [183], based on a multi-objective optimization technique, the utopia point method, was shown to result in significant economic benefits in comparison to MGs connected to the grid alone.

A distributed version of the multi-objective optimization was derived from the centralized form through the use of Alternating Direction Method of Multipliers. Results of numerical simulations demonstrated that the decisions made by the distributed formulation are very close to those of the central controller. Contributions of this work are summarized below:

- It enables the decisions pertaining to each MG to be made locally, does not require significant computing power, and has the following advantages over the centralized framework:
  - **Scalability:** The algorithm enables its application to networks of MGs of varying sizes since the computational resources needed at each MG is minimal
  - **Computational Efficiency:** Local computational resources are utilized efficiently, by making decisions and storing variables locally
  - **Speed:** Using distributed computational resources enables computations to be performed faster
  - **Data privacy and resilience:** The only variables that are to be communicated externally from each MG is the portion of virtual power that is to

be traded by the MG within the network. This component of power does not provide information regarding the decisions made within the MG. Thus data privacy and security are improved compared to the central formulation, where all decision variables and parameters need to be communicated across the network

6.2 Potential Future Research Areas

In addition to presenting significant contributions beyond the state-of-the-art, this work opens new avenues for future research. The results presented in Section 4.3 are very pertinent to the current and future energy markets. Home and commercial energy storage systems are being marketed and adopted widely. Therefore the need for smart energy management systems is becoming very apparent. The algorithms described in this work can be implemented in any of a variety of devices—smart controllers and thermostat to improve cost savings as well as to ensure user comfort and allay EV user range-anxiety. However, such smart controllers are not as powerful as the system on which the algorithms in the thesis were tested. Therefore, lighter, more efficient implementations of the stochastic optimizer described in the thesis for deployment in commercial systems is a promising area for future work. The work presented in Chapter 3 has potential to be expanded to more scenarios where EVs exchange energy with buildings. For instance, it may be interesting to consider cases where there are uncertainties in the possibility of EV connection, number of connections, and number of EVs. These uncertainties may arise in certain real-life scenarios such as big music concerts and sports events.

In subsection 4.3.6 the complexity of the optimization formulations of the controller was discussed. One of the possible areas of future work is to look at ways to reduce the set-up time involved, by perhaps reusing, in a smart way, some of the matrices generated for the optimization problem in more than one time step. Another area to consider would be coming up with optimization formulations which reduce the problem size—number of variables and constraints—when the number of samples and time steps become high. The research presented in this thesis relies heavily on availability of reliable predicted values of uncertain system parameters. Several combinations of algorithms available in the literature can be used to obtain these values. However, if these are to be executed in the same local controllers as those on which the optimization algorithms are executed, they must be computationally efficient. Work on the development of smart and efficient prediction algorithms for power demand, renewable generation, and EV mobility is another potential future research direction.

Concerning the work presented in Chapter 5, the development of a network communication scheme among MGs could help improve the overall time it takes for the distributed optimization to arrive at a solution. Strategies for sharing responsibility and resources for central computations required could also be explored. Another area for innovation is to expand the distributed problem to handle uncertainties in the predicted demand and PV power generation. Research on how to integrate electric vehicles (EVs) into the control framework and exploring how fleets of EVs and the network of MGs could be leveraged to provide transportation and energy while using resources most efficiently are all promising fields for future work. An extension of problem to networks of microgrids (buildings or communities) with EVs travelling

among the microgrids is another possible direction for future research. Interesting ramifications of this may be scenarios where EVs travel among microgrids and choose one which provides energy at the lowest price. This might lead to regarding EVs as mobile energy storage devices which can be used in microgrids (communities) in need of energy, in case of floods, natural disasters, etc.

The potential to save costs further by controlling the magnitude and timing of the load in the system is very attractive. With the share of smart appliances and HVAC systems in the market, which have varying degrees of control and communication integrated in them, demand side management is another key area for potential research. Further, with the growing amount of components at all levels of the electricity infrastructures being connected to the internet, there is potential to leverage the vast amounts of data that would inevitably be generated. Analysis of this data can be used to plan smarter and more efficient infrastructure development and operation in the future. Thus data analysis in the energy infrastructure field is full of potential for research.

Appendix A

A-EMS: Earlier Formulation

In this appendix, discussion on the theory, implementation, and performance of an earlier version of the A-EMS is presented. This work was published in [96].

Glossary of Terms and Nomenclature

Constants

$N_h \in \mathbb{N}$	number of time steps in horizon
$\mathbf{h} \in \mathbb{R}^{N_h}$	vector of time step lengths in hours
$E_{bat}^{min} \in \mathbb{R}$	minimum battery energy level
$E_{bat}^{max} \in \mathbb{R}$	maximum battery energy level
$P_{bat}^{loss} \in \mathbb{R}$	battery hourly self-discharge power loss
$\eta_c \in \mathbb{R}$	battery charging efficiency
$\eta_d \in \mathbb{R}$	battery discharging efficiency
$p_{bat}^{gc,max} \in \mathbb{R}$	max battery green zone charging rate
$p_{bat}^{rc,max} \in \mathbb{R}$	max red zone incremental charging rate
$p_{bat}^{gd,max} \in \mathbb{R}$	max battery green zone discharging rate
$p_{bat}^{rd,max} \in \mathbb{R}$	max red zone incremental discharging rate
$\Delta p_{bat} \in \mathbb{R}$	max change in battery power rate
$T^{maxon} \in \mathbb{R}$	red zone maximum on-time in hours
$T^{minoff} \in \mathbb{R}$	red zone minimum off-time in hours
$\Gamma \in \mathbb{R}$	polyhedral set size robustness parameter

Rolling Horizon Control Variables

$\mathbf{c}_{buy} \in \mathbb{R}^{N_h}$	electricity usage buying cost
$\mathbf{c}_{sell} \in \mathbb{R}^{N_h}$	electricity selling price
$c_{peak} \in \mathbb{R}$	peak electricity demand usage cost
$\mathbf{c}_{bat} \in \mathbb{R}^{N_h}$	battery usage cost
$\mathbf{c}_{smb} \in \mathbb{R}^{N_h}$	battery signal smoothing penalty
$\mathbf{c}_{smg} \in \mathbb{R}^{N_h}$	grid signal smoothing penalty
$c_{flat} \in \mathbb{R}$	grid signal flattening penalty
$E^{o}_{bat} \in \mathbb{R}$	actual battery energy at start of horizon
$E^{final}_{bat} \in \mathbb{R}$	desired battery energy at end of horizon
$p^{base}_{g} \in \mathbb{R}$	baseline for demand charges in horizon
$\bar{\mathbf{p}}_d \in \mathbb{R}^{N_h}$	estimate of predicted net demand
$\Delta\bar{\mathbf{p}}_d \in \mathbb{R}^{N_h}$	error estimate of predicted net demand
$\mathbf{P}^{d_b max}_{s} \in \mathbb{R}^{N_h x N_h}$	diagonal matrix of upper bounds
$\mathbf{P}^{d_u max}_{s} \in \mathbb{R}^{N_h x N_h}$	diagonal matrix of upper bounds
$\mathbf{P}^{c_s max}_{s} \in \mathbb{R}^{N_h x N_h}$	diagonal matrix of upper bounds
$\mathbf{P}^{c_u max}_{s} \in \mathbb{R}^{N_h x N_h}$	diagonal matrix of upper bounds

Optimization Variables

$\mathbf{p}_s^{c_s} \in \mathbb{R}^{N_h}$	storage charging rate (offset selling portion)
$\mathbf{p}_s^{c_u} \in \mathbb{R}^{N_h}$	storage charging rate (uncertain portion)
$\mathbf{p}_s^{c_b} \in \mathbb{R}^{N_h}$	storage charging rate (grid buying portion)
$\mathbf{p}_s^{d_b} \in \mathbb{R}^{N_h}$	storage discharging rate (offset buying portion)
$\mathbf{p}_s^{d_u} \in \mathbb{R}^{N_h}$	storage discharging rate (uncertain portion)
$\mathbf{p}_s^{d_s} \in \mathbb{R}^{N_h}$	storage discharging rate (grid selling portion)
$\mathbf{p}_{bat}^{gc} \in \mathbb{R}^{N_h}$	green zone battery charging power rate
$\mathbf{p}_{bat}^{rc} \in \mathbb{R}^{N_h}$	incremental red zone battery charging power rate
$\mathbf{p}_{bat}^{gd} \in \mathbb{R}^{N_h}$	green zone battery discharging power rate
$\mathbf{p}_{bat}^{rd} \in \mathbb{R}^{N_h}$	incremental red zone battery discharging rate
$\mathbf{u}_g \in \mathbb{R}^{N_h}$	auxiliary vector for grid signal smoothing
$\mathbf{u}_b \in \mathbb{R}^{N_h}$	auxiliary vector for battery signal smoothing
$p_g^{ob} \in \mathbb{R}$	maximum net power demand over some baseline
$p_g^{max} \in \mathbb{R}$	maximum net power demand
$p_g^{min} \in \mathbb{R}$	minimum net power demand
$\boldsymbol{\delta}_{bs1} \in \mathbb{Z}^{N_h}$	binary vector for buying/uncertain/selling states
$\boldsymbol{\delta}_{bs2} \in \mathbb{Z}^{N_h}$	binary vector for buying/uncertain/selling states
$\boldsymbol{\delta}_{cd} \in \mathbb{Z}^{N_h}$	binary vector for battery charging/discharging
$\boldsymbol{\delta}_r \in \mathbb{Z}^{N_h}$	binary vector for battery red-zone rate usage
$t \in \mathbb{R}$	auxiliary variable used to minimize worst case
$z_c \in \mathbb{R}$	robust counterpart auxiliary variable
$z_d \in \mathbb{R}$	robust counterpart auxiliary variable
$\mathbf{w}_c \in \mathbb{R}^{N_h}$	robust counterpart auxiliary vector
$\mathbf{w}_d \in \mathbb{R}^{N_h}$	robust counterpart auxiliary vector

A.1 A-EMS MILP Formulation

A.1.1 Rolling Horizon Control

The A-EMS control algorithm employs a rolling prediction horizon or window at each time step. It is assumed a prediction algorithm generates an estimated net demand power vector $\bar{\mathbf{p}}_d$ for each future time step in the horizon. Typically such a prediction algorithm would employ past information or a learning window of past data to generate estimates of net demand.

A MILP optimization problem, to be described in detail in the next section, is solved at each time step and the optimized decision variables corresponding to the current time step are used for controlling the battery charge and discharge power rates. The optimized algorithm assumes the following discrete-time battery model

$$E_{i+1} = E_i + \eta_c h_i p^c_{bat_i} - \frac{1}{\eta_d} h_i p^d_{bat_i} - P^{loss}_{bat} h_i \tag{A.1}$$

where E_i is the energy in the battery at time step i typically measured in kW h, h_i is the length of each time step in the prediction horizon measured in hours, P^{loss}_{bat} is a self discharge loss expressed as kW h per hour, $p^c_{bat_i}$ and $p^d_{bat_i}$ battery charging and discharging power rates, η_c and η_d are charging and discharging efficiencies respectively. The frequency at which the Rolling Horizon controller operates is dictated by h_1, i.e. the first element of horizon time step duration vector $\mathbf{h}$. Note that since battery charging/discharging are mutually exclusive events the vector property $(\mathbf{p}^c_{bat})^T \mathbf{p}^d_{bat} = 0$ must hold.

It may be desired to employ a battery usage cost in the optimization to avoid unnecessary battery activity that would otherwise reduce battery life; this usage cost

can be expressed in units of ¢/kW h. A simple way to estimate this cost can be done by assuming half-life behaviour such that the capacity of the battery drops by some multiplicative factor after each charging cycle. Let this be denoted as Capacity Factor Per Discharge ($CFPD$) where $CFPD < 1$. The total number of charging cycles can then be estimated via the sum of geometric series formula $CFPD/(1-CFPD)$. Consider a battery rated for approximately 2700 charging cycles before capacity drops to 80% of its initial value, therefore $CFPD = 0.99991735$ and maximum number of cycles becomes 12099. Assuming an upfront battery cost of $300 per kW h translates to a usage cost of 2.5 $¢/kWh$. More sophisticated approaches to estimate and adjust/update the usage cost over time can also be implemented.

There is some flexibility in choosing the final battery energy level at the end of the rolling horizon window, such choices tend to be based on some heuristic decisions. Not having any condition or constraint as to the end of horizon battery energy level would in many cases result in an optimized profile that would completely drain the battery. The reason is that from the optimization algorithm's point of view any initial stored energy would be considered "free" energy and completely used. A simple choice that may be amenable to steady state conditions is to enforce a condition that the battery energy levels at the start and end of the rolling horizon be equal, i.e. $E_{bat}^{final} = E_{bat}^{o}$. Alternatively an initial optimization can be first performed to determine E_{bat}^{final}. The goal of this optimized E_{bat}^{final} approach is that it would in the long run move the battery energy level to fluctuate around some optimal level.

A significant portion of electricity costs for large commercial and industrial consumers result from peak usage demand costs during a billing cycle, for example the peak average power measured over any 15 minute interval during a month. It would

be desirable to minimize these costs over the time frame of the billing cycle. However since the rolling horizon window would typically be chosen in the range of hours to a few days, constantly minimizing as much as possible, the peak usage over all these windows may be unnecessary and may potentially degrade performance. Instead it is better to keep track of a running peak usage, i.e. p_g^{base} , and penalize usage above this baseline for subsequent rolling horizons in the same billing cycle. At the start of the billing cycle the baseline is reset to $p_g^{base} = 0$, and this baseline is raised only if necessary.

Although the optimization provides a profile or schedule of battery power activity, only the decisions corresponding to the first time step in the future time horizon is implemented at each iteration of the rolling horizon controller. As a result a significant reduction in optimization computational costs can be gained by relaxing the integer constraints to all but the first (few) time step(s). A reduction in performance would be expected.

A.1.2 Non Robust Optimization Approach

In this section a non robust optimization problem is presented for the case where net demand can be perfectly predicted. Prior to describing the formulation a preliminary linear program and the standard form MILP is first presented. This is followed by the MILP formulation to be used with the Rolling Horizon controller. This section concludes with remarks on an alternative MILP formulation.

Preliminary Linear Program Formulation

A simple linear program can be formulated by considering only time of use usage costs, i.e.

$$\min_{\mathbf{p}_s} \mathbf{c}^T \left(\overbrace{\mathbf{p}_d + \mathbf{p}_s}^{\mathbf{p}_g} \right) \Rightarrow \min_{\mathbf{p}_s} \mathbf{c}^T \mathbf{p}_s \tag{A.2}$$

where $\mathbf{c} = \mathbf{c}_{buy} = \mathbf{c}_{sell}$ is time of use electricity costs, $\mathbf{p}_d$ is the electrical demand usage vector, $\mathbf{p}_s$ is battery power storage activity, and $\mathbf{p}_g$ the net flow with the external grid. Battery charging occurs when $\mathbf{p}_{s_i} > 0$ and discharging when $\mathbf{p}_{s_i} < 0$. To handle different buy/selling prices and different charging/discharging efficiencies a MILP formulation is needed, this is described in the subsections that follow. Finally note the term $\mathbf{c}^T\mathbf{p}_d$ in (A.2) is constant. A counterpart optimization problem that yields an identical optimized battery storage profile $\mathbf{p}_s$ can be obtained by dropping the term $\mathbf{c}^T\mathbf{p}_d$ as seen in (A.2). This same simplification is also used in subsequent MILP formulations.

Mixed Integer Linear Programs

The standard form for a MILP typically used for many solvers is given as

$$\min_{\mathbf{x},\boldsymbol{\delta}} \mathbf{c}_x^T\mathbf{x} + \mathbf{c}_\delta^T\boldsymbol{\delta} \tag{A.3}$$

$$[\mathbf{A}_x \;\; \mathbf{A}_\delta] \left[\mathbf{x}^T \;\; \boldsymbol{\delta}^T\right]^T \leq \mathbf{b} \tag{A.4}$$

$$[\mathbf{E}_x \;\; \mathbf{E}_\delta] \left[\mathbf{x}^T \;\; \boldsymbol{\delta}^T\right]^T = \mathbf{f} \tag{A.5}$$

$$\mathbf{x}_{lb} \leq \mathbf{x} \leq \mathbf{x}_{ub} \tag{A.6}$$

$$\boldsymbol{\delta}_{lb} \leq \boldsymbol{\delta} \leq \boldsymbol{\delta}_{ub} \tag{A.7}$$

where $x \in \Re$ and $\boldsymbol{\delta} \in \mathbb{Z}$. Equality constraints are shown in (A.5), inequality constraints are given in (A.4), (A.6) and (A.7); the latter two represent lower and upper bounds that can also be put into the form (A.4). In many circumstances the integer variables may only need to be binary, in which case $\boldsymbol{\delta}_{lb} = \mathbf{0}$ and $\boldsymbol{\delta}_{ub} = \mathbf{1}$ in (A.7).

MILP Formulation

The MILP formulation is presented in this subsection, the cost function is first presented, followed by the constraints on the optimization variables; these variables were listed in glossary. A multi-objective optimization cost function is formulated as follows

$$\min \Big(\cancel{\mathbf{c}_{bs}^T \mathbf{p}_d} + \mathbf{c}_{sell}^T \mathbf{p}_s^{c_s} + \mathbf{c}_{buy}^T \mathbf{p}_s^{c_b} - \mathbf{c}_{buy}^T \mathbf{p}_s^{d_b} - \mathbf{c}_{sell}^T \mathbf{p}_s^{d_s} \tag{A.8a}$$

$$+ \mathbf{c}_{bat}^T \left(\mathbf{p}_{bat}^{gc} + \mathbf{p}_{bat}^{rc} + \mathbf{p}_{bat}^{gd} + \mathbf{p}_{bat}^{rd} \right) + \mathbf{c}_{smb}^T \mathbf{u}_b \tag{A.8b}$$

$$+ \mathbf{c}_{smg}^T \mathbf{u}_g + c_{peak} p_g^{ob} + c_{flat} \left(p_g^{max} - p_g^{min} \right) \Big) \tag{A.8c}$$

The sum of terms in (A.8a) represent the net electricity usage cost where $\mathbf{p}_s^{c_s}$ is the portion of battery charging power to offset any negative net demand grid selling, $\mathbf{p}_s^{c_b}$ is the portion of battery charging power which is bought from the grid, $\mathbf{p}_s^{d_b}$ is battery discharging power to offset any positive net demand grid buying, and $\mathbf{p}_s^{d_s}$ is the portion of battery discharging power which is sold to the grid. The different possible cases of these storage activity vectors is illustrated in Fig. A.1. The term $\mathbf{c}_{bs}^T \mathbf{p}_d$ is the usage cost assuming zero battery activity such that $\mathbf{c}_{bs_i} = \mathbf{c}_{buy_i}$ when

$\mathbf{p}_{d_i} > 0$ and $\mathbf{c}_{bs_i} = \mathbf{c}_{sell_i}$ when $\mathbf{p}_{d_i} \leq 0$. Since this cost term is not affected by the optimization variables it can be neglected via identical arguments as those in (A.2), therefore the remaining terms in (A.8a) represent electricity usage cost savings. Note that since the vectors are express in units corresponding to power, the elements of the cost vectors $\mathbf{c}_{buy}$ and $\mathbf{c}_{sell}$ have to be consistent with the variable time step length vector $\mathbf{h}$. The same applies to the other cost vectors.

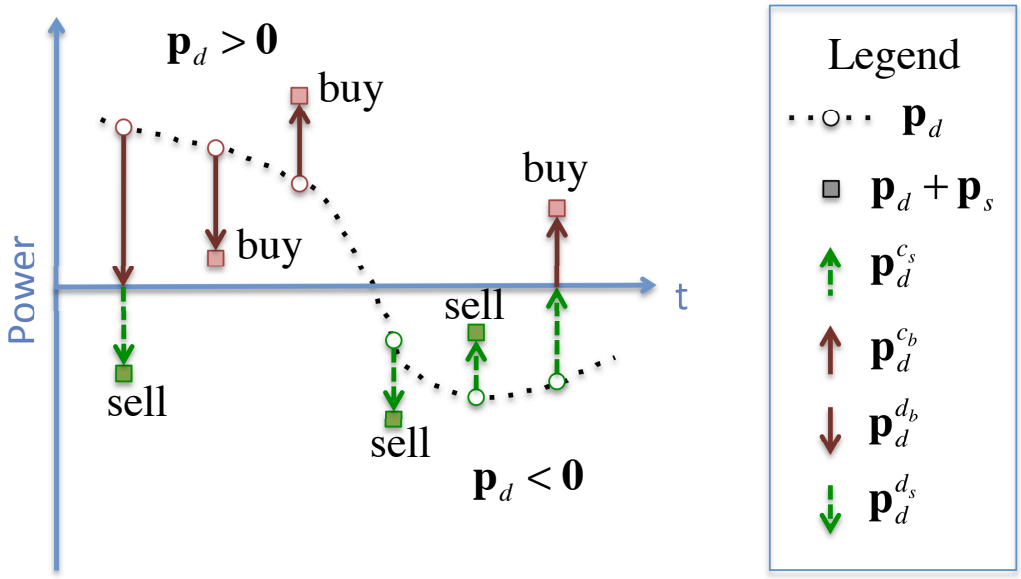

Figure A.1: Possible grid buy/sell outcomes for different storage control actions $\mathbf{p}_s = \mathbf{p}_s^{c_s} + \mathbf{p}_s^{c_b} - \mathbf{p}_s^{d_b} - \mathbf{p}_s^{d_s}$. Up arrows indicate battery charging; down arrows battery discharging.

The terms in (A.8b) represent battery usage costs and a battery signal smoothing term. The battery is modelled such that there exist so called green zone power limits that the battery power rates can always lie between, hence the vectors $\mathbf{p}_{bat}^{gc}$ and $\mathbf{p}_{bat}^{gd}$ represent the *green zone power rates* for charging and discharging, respectively. The battery power rate can be temporarily increased via so called *incremental red zone power rates* denoted by vectors $\mathbf{p}_{bat}^{rc}$ and $\mathbf{p}_{bat}^{rd}$ for charging and discharging, respectively.

These vectors are related to the buying/selling storage power vectors via the equality constraint

$$\mathbf{p}_s^{c_s} + \mathbf{p}_s^{c_b} = \mathbf{p}_{bat}^{gc} + \mathbf{p}_{bat}^{rc} \tag{A.9}$$

$$\mathbf{p}_s^{d_b} + \mathbf{p}_s^{d_s} = \mathbf{p}_{bat}^{gd} + \mathbf{p}_{bat}^{rd} \tag{A.10}$$

The use of the above equality constraints allows the possibility to easily add additional storage components into the system, e.g. flywheels and ultra capacitors, by adding their corresponding power terms to the right hand sides of (A.9) and (A.10). The term $\mathbf{u}_b$ represents the absolute value of the change in successive horizon time step battery power rates, it is used to smooth the battery power profile signal.

In (A.8c) grid signal shaping cost/penalty terms are shown. The term $\mathbf{c}_{smg}^T \mathbf{u}_g$ smoothes the grid signal by minimizing successive differences in the power grid signal $\mathbf{p}_g = \mathbf{p}_s^{c_s} + \mathbf{p}_s^{c_b} - \mathbf{p}_s^{d_b} - \mathbf{p}_s^{d_s} + \mathbf{p}_d$. The middle term $c_{peak} p_g^{ob}$ represents incremental peak usage costs above baseline p_g^{base} to enable peak shaving. The last term in (A.8c) enables flattening or squeezing of the grid signal $\mathbf{p}_g$.

State Decision Constraints The optimization in the rolling horizon controller makes decisions whether to either charge or discharge the battery storage device, to enforce this exclusive behaviour the following constraints are used on the battery power rate variables

$$\mathbf{0} \leq \mathbf{p}_{bat}^{gc} \leq p_{bat}^{gc,max} \boldsymbol{\delta}_{cd} \tag{A.11}$$

$$\mathbf{0} \leq \mathbf{p}_{bat}^{rc} \leq p_{bat}^{rc,max} \boldsymbol{\delta}_{cd} \tag{A.12}$$

$$\mathbf{0} \leq \mathbf{p}_{bat}^{gd} \leq p_{bat}^{gd,max} (\mathbf{1} - \boldsymbol{\delta}_{cd}) \tag{A.13}$$

$$\mathbf{0} \leq \mathbf{p}_{bat}^{rd} \leq p_{bat}^{rd,max} \left(\mathbf{1} - \boldsymbol{\delta}_{cd}\right) \tag{A.14}$$

$$\mathbf{0} \leq \boldsymbol{\delta}_{cd} \leq \mathbf{1} \tag{A.15}$$

where $\boldsymbol{\delta}_{cd}$ is a binary vector such that for the i^{th} element $\delta_{cd_i} = 1$ indicates charging and $\delta_{cd_i} = 0$ indicates charging. The scalar constants $p_{bat}^{gc,max}$, $p_{bat}^{gd,max}$ represent maximum green zone charging/discharging power rates, while $p_{bat}^{rc,max}$ and $p_{bat}^{rd,max}$ represent maximum incremental red zone charging/discharging power rates.

The controller also decides whether the micro grid draws power from the outside grid (buying state), or power flows from the local micro grid to the outside grid (selling state). The following constraints effect the magnitude of battery charging/discharging power rates that relate to buying/selling state decisions

$$\mathbf{P}_s^{d_b max} \left(\mathbf{1} - \boldsymbol{\delta}_{bs2}\right) \leq \mathbf{p}_s^{d_b} \leq \mathbf{P}_s^{d_b max} \mathbf{1}, \tag{A.16}$$

$$\mathbf{0} \leq \mathbf{p}_s^{d_s} \leq \left(p_{bat}^{gd,max} + p_{bat}^{rd,max}\right) \left(\mathbf{1} - \boldsymbol{\delta}_{bs2}\right) \tag{A.17}$$

$$\mathbf{P}_s^{c_s max} \boldsymbol{\delta}_{bs1} \leq \mathbf{p}_s^{c_s} \leq \mathbf{P}_s^{c_s max} \mathbf{1}, \tag{A.18}$$

$$\mathbf{0} \leq \mathbf{p}_s^{c_b} \leq \left(p_{bat}^{gc,max} + p_{bat}^{rc,max}\right) \boldsymbol{\delta}_{bs1} \tag{A.19}$$

where

$$\mathbf{0} \leq \boldsymbol{\delta}_{bsj} \leq \mathbf{1}, \;\; j = 1, 2 \tag{A.20}$$

$$\mathbf{P}_{s_{k,k}}^{d_b max} = \min\Big(\max\left(0, \mathbf{p}_{d_i}\right), p_{bat}^{gd,max} + p_{bat}^{rd,max} \Big) \tag{A.21}$$

$$\mathbf{P}_{s_{k,k}}^{c_s max} = \min\Big(\max\left(0, -\mathbf{p}_{d_i}\right), p_{bat}^{gc,max} + p_{bat}^{rc,max} \Big) \tag{A.22}$$

for $k \in [1, N_h]$. The binary vectors $\boldsymbol{\delta}_{bs1}$ and $\boldsymbol{\delta}_{bs2}$ are used to make buy/sell state

decisions. The truth table in Table A.1 incidates the different possible scenarios. The constraints in (A.16)-(A.19) are designed such that power rates $\mathbf{p}_s^{d_b}$ and $\mathbf{p}_s^{c_s}$ are utilized first for discharging and charging respectively; also note that their maximums, given in (A.21) and (A.22), are depend on net demand $\mathbf{p}_d$.

Table A.1: Grid Flow Decisions - Net Demand Known

$\boldsymbol{\delta}_{cd_i}$	$\boldsymbol{\delta}_{bs1_i}$	$\boldsymbol{\delta}_{bs2_i}$	$\mathbf{p}_{d_i} > 0$	$\mathbf{p}_{d_i} < 0$
0	0	0	sell*	sell
0	0	1	buy	sell$^+$
0	1	0	sell*	*infeasible*
0	1	1	buy	*infeasible*
1	0	0	*infeasible*	sell
1	0	1	buy$^+$	sell
1	1	0	*infeasible*	buy*
1	1	1	buy	buy*

*may not be possible due to storage power limits
$^+$indicates storage power activity is zero

Battery Energy and Power Rate Change Constraints To enforce that at each time step in the horizon battery energy levels remain within certain bounds, given battery model (A.1), one employs

$$E_{bat}^{min} \leq \eta_c \sum_{i=1}^{k} \mathbf{h}_i (\mathbf{p}_{bat_i}^{gc} + \mathbf{p}_{bat_i}^{rc}) - P_{bat}^{loss} \sum_{i=1}^{k} \mathbf{h}_i \tag{A.23}$$
$$-\frac{1}{\eta_d} \sum_{i=1}^{k} \mathbf{h}_i (\mathbf{p}_{bat_i}^{gd} + \mathbf{p}_{bat_i}^{rd}) + E_{bat}^{o} \leq E_{bat}^{max},\ k \in [1, N_h]$$

where E_{bat}^{o} is the energy level at the start of the horizon, and E_{bat}^{min} and E_{bat}^{max} are lower and upper bounds, respectively.

The end of horizon battery energy level can be set via

$$\eta_c \mathbf{h}^T \left(\mathbf{p}_{bat}^{gc} + \mathbf{p}_{bat}^{rc}\right) - \frac{1}{\eta_d}\mathbf{h}^T \left(\mathbf{p}_{bat}^{gd} + \mathbf{p}_{bat}^{rd}\right) - P_{bat}^{loss}\mathbf{h}^T\mathbf{1} = E_{bat}^{final} - E_{bat}^{o} \tag{A.24}$$

where E_{bat}^{final} is the desired end of horizon battery energy level.

Constraints related to battery signal smoothing and power rate change limits are represented by

$$\begin{aligned} -\Delta p_{bat}\mathbf{h} \leq -\mathbf{u}_{b_i} \leq \mathbf{p}_{bat_i}^{gc} + \mathbf{p}_{bat_i}^{rc} - \mathbf{p}_{bat_i}^{gd} - \mathbf{p}_{bat_i}^{rd} \\ -\mathbf{p}_{bat_{i-1}}^{gc} - \mathbf{p}_{bat_{i-1}}^{rc} + \mathbf{p}_{bat_{i-1}}^{gd} + \mathbf{p}_{bat_{i-1}}^{rd} \leq \mathbf{u}_{b_i} \leq \Delta p_{bat}\mathbf{h} \end{aligned} \tag{A.25}$$

for $k \in [1, N_h]$ and $\mathbf{u}_b \geq \mathbf{0}$. The term δp_{bat} represents the maximum allowed battery power rate change typically given in units of $\mathrm{kW\,h^{-1}}$. Note that when $i = 1$ battery activity from the previous iteration of the rolling horizon controller is needed and are treated as constants in the inequality constraints. Also note that this constraint can be rewritten with different variables by using equality constraints (A.9) and (A.10).

Battery Red-zone Power Rate Constraints

The optimization can decide when to enable/disable battery red zone incremental power rates by using the following

$$\mathbf{0} \leq \mathbf{p}_{bat}^{rc} \leq p_{bat}^{rc,max}\boldsymbol{\delta}_r \tag{A.26}$$

$$\mathbf{0} \leq \mathbf{p}_{bat}^{rd} \leq p_{bat}^{rd,max}\boldsymbol{\delta}_r \tag{A.27}$$

$$\mathbf{0} \leq \boldsymbol{\delta}_r \leq \mathbf{1} \tag{A.28}$$

where the elements of binary vector $\boldsymbol{\delta}_r$ indicate when incremental red-zone power rates are active. To ensure green-zone power rates are first used the following constraints are needed

$$p_{bat}^{gc,max}\boldsymbol{\delta}_r - p_{bat}^{gc,max}\left(\mathbf{1} - \boldsymbol{\delta}_{cd}\right) \leq \mathbf{p}_{bat}^{gc} \tag{A.29}$$

$$p_{bat}^{gd,max}\boldsymbol{\delta}_r - p_{bat}^{gd,max}\boldsymbol{\delta}_{cd} \leq \mathbf{p}_{bat}^{gd} \tag{A.30}$$

It is assumed the red-zone power rates can be active for a limited amount of time and thus have a maximum on-time denoted by T^{maxon}. Moreover it is also assumed that a minimum cool down like time period is required before the red-zone power rates can be reactivated, this minimum off-time is denoted by T^{minoff}. The maximum on-time and minimum off-time constraints considering variable time steps in the horizon are formulated as

$$\sum_{k=j}^{j+T_j^{maxon}} h_i\delta_{r_i} \leq T^{maxon}, \forall j \in [j_{min}, j_{max}] \tag{A.31a}$$

$$j_{min} = 2 - \min_{h_1\ell > T^{maxon}} \ell \in \mathbb{Z} \tag{A.31b}$$

$$j_{max} = \max_{\sum_{k=\gamma}^{N_h} h_i > T^{maxon}} \gamma \in \mathbb{Z} \tag{A.31c}$$

$$T_j^{maxon} = \min_{\sum_{k=j}^{j+\tau} h_i > T^{maxon}} \tau \in \mathbb{Z} \tag{A.31d}$$

$$\boldsymbol{\delta}_{r_{j-i-1}} - \boldsymbol{\delta}_{r_{j-i}} \leq 1 - \boldsymbol{\delta}_{r_j}, \forall k \in [1, T_j^{minoff} - 1] \tag{A.32a}$$

$$\forall j \in \left\{ [1, N_h] \middle| T_j^{minoff} \geq 2 \right\} \tag{A.32b}$$

$$T_j^{minoff} = \min_{\sum_{k=j-\tau}^{j-1} \mathbf{h}_i \geq T^{minoff}} \tau \in \mathbb{Z}, \ \tau \geq 1 \tag{A.32c}$$

where the first element $h_i = h_1$ is used when $i \leq 0$. Note that a history of previous red-zone activity is needed, the time length of which is dictated by T^{maxon} and T^{minoff}. These past binary values are treated as constants in the inequality constraints. The maximum on-time constraints are given in (A.31), these constraints function by scanning rolling windows of time length just greater than T^{maxon}. In (A.32) the minimum off-time constraints are shown, they operate by scanning sufficiently back such that the last time red-zone activity was disabled does not occur within the last T^{minoff} hours. The terms in (A.31b)-(A.31d) and (A.32c) are used to find the correct range of integer indicies in the variable time step horizon; they can be precomputed by using only $\mathbf{h}$, T^{maxon} and T^{minoff}. Note that in (A.32b), only indices that sastify $T_j^{minoff} \leq 2$ are included. An example highlighting how the red-zone constraints function is illustrated in Fig. A.2.

Grid Signal Shaping Constraints

The signal corresponding to connection of the local micro grid to the external grid can be shaped if desired in the A-EMS controller. To enable peak shaving and reduction over some baseline the following inequality is employed

$$\mathbf{p}_{bat}^{gc} + \mathbf{p}_{bat}^{rc} - \mathbf{p}_{bat}^{gd} - \mathbf{p}_{bat}^{rd} + \mathbf{p}_d \leq p_g^{base}\mathbf{1} + p_g^{ob}\mathbf{1} \tag{A.33}$$

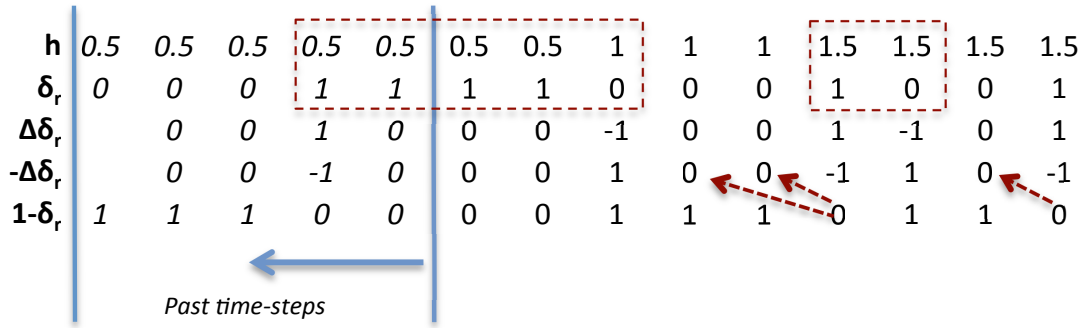

Figure A.2: Battery red zone power rates maximum-on-time/minimum-off-time constraints example that shows an allowable $\boldsymbol{\delta}_r$. The dashed boxes incite the scanning windows for the maximum on-time constraints. The dashed arrows correspond to the minimum off-time constraints. $T^{maxon} = 2.5$ h and $T^{minoff} = 2.5$ h.

where $p_g^{ob} \geq 0$.

Grid signal flattening or squeezing requires the inequalities

$$p_g^{min}\mathbf{1} \leq \mathbf{p}_s^{c_s} + \mathbf{p}_s^{c_b} - \mathbf{p}_s^{d_b} - \mathbf{p}_s^{d_s} + \mathbf{p}_d \leq p_g^{max}\mathbf{1} \tag{A.34}$$

where p_g^{min} and p_g^{max} are scalar optimization variables corresponding to minimum and maximum grid power rates.

Grid signal smoothing of successive grid power rate changes needs inequalities

$$\begin{aligned} -\mathbf{u}_{g_i} \leq \mathbf{p}_{s_i}^{c_s} + \mathbf{p}_{s_i}^{c_b} - \mathbf{p}_{s_i}^{d_b} - \mathbf{p}_{s_i}^{d_s} + \mathbf{p}_{d_i} - \mathbf{p}_{d_{i-1}} \\ -\mathbf{p}_{s_{i-1}}^{c_s} - \mathbf{p}_{s_{i-1}}^{c_b} + \mathbf{p}_{s_{i-1}}^{d_b} + \mathbf{p}_{s_{k-1}}^{d_s} \leq \mathbf{u}_{g_i} \end{aligned} \tag{A.35}$$

for $i \in [1, N_h]$ and $\mathbf{u}_g \geq \mathbf{0}$. When $i = 1$, past grid power activity and net demand from the previous time-setp or iteration of the rolling horizon controller is needed. Note that (A.33)-(A.35) can be rewritten in terms of other variables by employing

(A.9) and (A.10).

Appendix B

A-EMS: Glossary of Terms & Nomenclature

Constants

$Nh \in \mathbb{N}$	Number of time steps in horizon
$\mathbf{h} \in \mathbb{R}_{\geq 0}^{Nh}$	Vector of time step lengths in hours
$\eta_{bat}^{c} \in \mathbb{R}$	Battery charging efficiency
$\eta_{bat}^{d} \in \mathbb{R}$	Battery discharging efficiency
$\eta_{EV_k}^{c} \in \mathbb{R}$	EV charging efficiency
$\eta_{EV_k}^{d} \in \mathbb{R}$	EV discharging efficiency
$P_{bat}^{loss} \in \mathbb{R}$	Battery self discharge loss power
$P_{EV_k}^{loss} \in \mathbb{R}$	EV self discharge loss power
$E_{bat}^{min} \in \mathbb{R}$	Minimum battery energy level
$E_{bat}^{max} \in \mathbb{R}$	Maximum battery energy level
$E_{EV_k}^{min} \in \mathbb{R}$	Minimum EV energy level
$E_{EV_k}^{max} \in \mathbb{R}$	Maximum EV energy level

$p_{bat}^{min} \in \mathbb{R}$	Minimum battery discharge rate
$p_{bat}^{max} \in \mathbb{R}$	Maximum battery charge rate
$p_{EV_k}^{min} \in \mathbb{R}$	Minimum EV power rate
$p_{EV_k}^{max} \in \mathbb{R}$	Maximum EV power level
$\mathbf{c}^b \in \mathbb{R}^{Nh}$	Vector of time-of-use buy prices
$\mathbf{c}^s \in \mathbb{R}^{Nh}$	Vector of time-of-use sell prices
$\varsigma \in \mathbb{R}_{\geq 0}$	Small positive constant
$N \in \mathbb{N}$	Number of particles
$L_k \in \mathbb{N}_0$	Number of connection periods in a horizon
$K \in \mathbb{N}_0$	Number of EVs
$E_{bat}^o \in \mathbb{R}_{\geq 0}$	Battery energy at start of horizon
$M \in \mathbb{N}$	Constant used in Stochastic Optimization

Decision Variables

$\mathbf{p}_g \in \mathbb{R}^{Nh}$	Grid power (in Formulation II)
$\mathbf{p}_g^b \in \mathbb{R}^{Nh}$	Buying portion of grid power (in Formulation II)
$\mathbf{p}_{bat}^c \in \mathbb{R}^{Nh}$	Battery charging power rates
$\mathbf{p}_{bat}^d \in \mathbb{R}^{Nh}$	Battery discharging power rates
$\mathbf{p}_{bat} \in \mathbb{R}^{Nh}$	Battery power rates
$\mathbf{p}_{bat}^b \in \mathbb{R}^{Nh}$	Battery power rates while buying power
$\mathbf{p}_{bat}^s \in \mathbb{R}^{Nh}$	Battery power rates while selling power
$\boldsymbol{\delta}_{bat}^{cd} \in \{0,1\}^{Nh}$	Battery charging/discharging decisions
$\mathbf{p}_{EV_k}^c \in \mathbb{R}^{Nh}$	EV charging power rates
$\mathbf{p}_{EV_k}^d \in \mathbb{R}^{Nh}$	EV discharging power rates
$\mathbf{p}_{EV_k} \in \mathbb{R}^{Nh}$	EV power rates
$\mathbf{p}_{EV_k}^b \in \mathbb{R}^{Nh}$	EV power rates while buying power
$\mathbf{p}_{EV_k}^s \in \mathbb{R}^{Nh}$	EV power rates while selling power
$\boldsymbol{\delta}_{EV_k}^{cd} \in \{0,1\}^{Nh}$	EV charging/discharging decisions
$\boldsymbol{\delta}_{EV_k} \in \{0,1\}^{Nh}$	EV On/Off decisions
$\delta_{OB_k} \in \{0,1\}$	EV One Block Variable
$z_n \in \{0,1\}$	Binary variable corresponding to particles

Auxiliary Variables

$\mathbf{p}_{g,i} \in \mathbb{R}^{Nh}$	Grid power (in Formulation I)

System State

$E_{bat,i} \in \mathbb{R}_{\geq 0}$ Battery energy at time step i

$E_{EV,i} \in \mathbb{R}_{\geq 0}$ EV energy at time step i

Optimization Control Variables

$E_{bat}^{desired} \in \mathbb{R}_{\geq 0}$ Desired battery energy at end of horizon

$E_{EV_k}^{desired,l_k} \in \mathbb{R}_{\geq 0}$ Desired EV energy at disconnection

$p_g^{min} \in \mathbb{R}$ Minimum grid power

$p_g^{max} \in \mathbb{R}$ Maximum grid power

$\epsilon \in \mathbb{R}_{\geq 0}$ Probability of infeasibility

Uncertain System parameters

κ_{l_k} Set of connection indices in connection period

$\mathbf{p}_d \in \mathbb{R}^{Nh}$ Net demand vector

$E_{EV_k}^{o,l_k} \in \mathbb{R}_{\geq 0}$ EV initial energy at connection

Uncertain System parameters for Notational Convenience

$\mathbf{p}_d^b \in \mathbb{R}^{Nh}$ Net demand while buying power

$\mathbf{p}_d^s \in \mathbb{R}^{Nh}$ Net demand while selling power

Appendix C

Distributed EMS: Glossary of Terms & Nomenclature

Constants

$Nh \in \mathbb{N}$	Number of time steps in horizon
$\mathbf{h} \in \mathbb{R}_{\geq 0}^{Nh}$	Vector of time step lengths in hours
$\eta_{bat}^{c} \in \mathbb{R}$	Battery charging efficiency
$\eta_{bat}^{d} \in \mathbb{R}$	Battery discharging efficiency
$P_{bat}^{loss} \in \mathbb{R}$	Battery self discharge loss power
$E_{bat}^{min} \in \mathbb{R}$	Minimum battery energy level
$E_{bat}^{max} \in \mathbb{R}$	Maximum battery energy level
$p_{bat}^{min} \in \mathbb{R}$	Minimum battery discharge rate
$p_{bat}^{max} \in \mathbb{R}$	Maximum battery charge rate
$\rho \in \mathbb{R}_{\geq 0}$	Lagrangian penalty parameter
$\mathbf{c}_g^b \in \mathbb{R}^{Nh}$	Vector of time-of-use grid buy prices

$\mathbf{c}_g^s \in \mathbb{R}^{Nh}$	Vector of time-of-use grid sell prices
$\mathbf{c}_l^b \in \mathbb{R}^{Nh}$	Vector of time-of-use local buy prices
$\mathbf{c}_l^s \in \mathbb{R}^{Nh}$	Vector of time-of-use local sell prices
$\epsilon \in \mathbb{R}_{\geq 0}$	Small positive constant
$E_{bat}^o \in \mathbb{R}_{\geq 0}$	Battery energy at start of horizon

Decision Variables

$\mathbf{p}_g \in \mathbb{R}^{Nh}$	Grid power
$\mathbf{p}_g^b \in \mathbb{R}^{Nh}$	Buying portion of grid power
$\mathbf{p}_l \in \mathbb{R}^{Nh}$	Local power
$\mathbf{p}_l^b \in \mathbb{R}^{Nh}$	Buying portion of local power
$\mathbf{p}_{bat}^c \in \mathbb{R}^{Nh}$	Battery charging power rates
$\mathbf{p}_{bat} \in \mathbb{R}^{Nh}$	Battery power rates

System State

$E_{bat,i} \in \mathbb{R}_{\geq 0}$	Battery energy at time step i

Optimization Control Variables

$E_{bat}^{desired} \in \mathbb{R}_{\geq 0}$	Desired battery energy at end of horizon
$p_g^{min} \in \mathbb{R}$	Minimum grid power
$p_g^{max} \in \mathbb{R}$	Maximum grid power
$\mathcal{U} \in \mathbb{R}^{Nh}$	Utopia vector
$\alpha \in \mathbb{R}_{\geq 0}$	Stopping criterion

Bibliography

[1] R. Lasseter, A. Akhil, C. Marnay, J. Dagle, R. Guttromson, A. Meliopoulous, R. Yinger, and J. Eto, "The CERTS microgrid concept," *White Paper*, 2002.

[2] R. Lasseter, "Smart distribution: Coupled microgrids," *Proceedings of the IEEE*, vol. 99, no. 6, pp. 1074–1082, Jun. 2011.

[3] H. Farhangi, "The path of the smart grid," *IEEE Power Energy Mag.*, vol. 8, no. 1, pp. 18–28, Jan./Feb. 2010.

[4] R. Lasseter, "MicroGrids," *Proceedings of IEEE Power Engineering Society Winter Meeting.*, vol. 1, pp. 305–308 vol.1, 2002.

[5] H. Liang, A. Tamang, W. Zhuang, and X. Shen, "Stochastic information management in smart grid," *IEEE Commun. Surveys Tuts.*, vol. 16, no. 3, pp. 1746–1770, Third Quarter 2014.

[6] A. Ravichandran, P. Malysz, S. Sirouspour, and A. Emadi, "The critical role of microgrids in transition to a smarter grid: A technical review," in *Proc. ITEC 2013*, Dearborn, MI, Jun. 2013, pp. 1–7.

[7] D. Olivares *et al.*, "Trends in microgrid control," *IEEE Trans. Smart Grid*, vol. 5, no. 4, pp. 1905–1919, Jul. 2014.

[8] X. Wang, J. Guerrero, F. Blaabjerg, and Z. Chen, "A review of power electronics based microgrids," *J. Power Electron.*, vol. 12, no. 1, pp. 181–192, Jan. 2012.

[9] R. Zamora and A. Srivastava, "Controls for microgrids with storage: Review, challenges, and research needs," *Renewable and Sustain. Energy Rev.*, vol. 14, no. 7, pp. 2009–2018, Sep. 2010.

[10] S. Suryanarayanan, F. Mancilla-David, J. Mitra, and Y. Li, "Achieving the smart grid through customer-driven microgrids supported by energy storage," in *Proceedings of IEEE International Conference on Industrial Technology (ICIT)*, 2010, pp. 884–890.

[11] X. Yu, Y. Xue, S. Sirouspour, and A. Emadi, "Microgrid and transportation electrification: A review," in *Proceedings of IEEE Transportation Electrification Conference and Expo (ITEC)*, 2012, pp. 1–6.

[12] J. Carrasco, L. Franquelo, J. Bialasiewicz, E. Galvan, R. Guisado, M. Prats, J. Leon, and N. Moreno-Alfonso, "Power-electronic systems for the grid integration of renewable energy sources: A survey," *IEEE Trans. Ind. Electron.*, vol. 53, no. 4, pp. 1002–1016, Jun. 2006.

[13] A. Rabiee, H. Khorramdel, and J. Aghaei, "A review of energy storage systems in microgrids with wind turbines," *Renewable and Sustainable Energy Reviews*, vol. 18, no. 0, pp. 316–326, Feb. 2013. [Online]. Available: http://www.sciencedirect.com/science/article/pii/S1364032112005412

[14] X. Tan, Q. Li, and H. Wang, "Advances and trends of energy storage technology in microgrid," *International Journal of Electrical Power & Energy*

Systems, vol. 44, no. 1, pp. 179–191, Jan. 2013. [Online]. Available: http://www.sciencedirect.com/science/article/pii/S0142061512003754

[15] S. Beer, T. Gomez, D. Dallinger, I. Momber, C. Marnay, M. Stadler, and J. Lai, "An economic analysis of used electric vehicle batteries integrated into commercial building microgrids," *IEEE Trans. Smart Grid*, vol. 3, no. 1, pp. 517–525, Mar. 2012.

[16] F. Diaz-Gonzalez, A. Sumper, O. Gomis-Bellmunt, and R. Villafafila-Robles, "Modeling and validation of a flywheel energy storage lab-setup," in *Proceedings of 3rd IEEE PES International Conference and Exhibition on Innovative Smart Grid Technologies (ISGT Europe)*, 2012, pp. 1–6.

[17] H. Xuemei, "Implementing intelligence and distributed execution mechanism for flywheel energy storage system in micro grid," in *Proceedings of International Conference on Electronic and Mechanical Engineering and Information Technology (EMEIT)*, vol. 1, 2011, pp. 413–416.

[18] C. Abbezzot, T. Tran, P. Poggi, P. Serre-Combe, M. Perrin, and M. Muselli, "Using a flywheel associated to PV power plant in order to increase the integration of PV into island electrical grid," in *Proceedings of International Conference on Renewable Energies and Power Quality (ICREPQ)*, Bilbao, Spain, Mar. 2013. [Online]. Available: http://www.icrepq.com/icrepq'13/370-abbezzot.pdf

[19] M. Dali, J. Belhadj, and X. Roboam, "Hybrid solarwind system with battery storage operating in grid-connected and standalone mode: Control and energy management experimental investigation," in *Proceedings of*

The 7th International Conference on Sustainable Energy Technologies, vol. 35, no. 6, Jun. 2010, pp. 2587–2595. [Online]. Available: http://www.sciencedirect.com/science/article/pii/S0360544210001234

[20] R. Majumder, S. Chakrabarti, G. Ledwich, and A. Ghosh, "Control of battery storage to improve voltage profile in autonomous microgrid," 2011, pp. 1–8.

[21] C. S. Hearn, M. C. Lewis, S. B. Pratap, R. E. Hebner, F. M. Uriarte, D. Chen, and R. G. Longoria, "Utilization of optimal control law to size grid-level flywheel energy storage," *IEEE Trans. Sustain. Energy*, vol. PP, no. 99, pp. 1–8, 2013.

[22] S. Chen, H. Gooi, and M. Q. Wang, "Sizing of energy storage for microgrids," *IEEE Trans. Smart Grid*, vol. 3, no. 1, pp. 142–151, Mar. 2012.

[23] T. Weiqing, S. Wen, and D. Chen, "Research on super-capacitor and battery hybrid energy storage system applied in micro-grid," in *Proceedings of International Conference on Control Engineering and Communication Technology (ICCECT)*, 2012, pp. 157–160.

[24] Z. Guoju, T. Xisheng, and Q. Zhiping, "Research on battery supercapacitor hybrid storage and its application in MicroGrid," in *Proceedings of Asia-Pacific Power and Energy Engineering Conference (APPEEC)*, 2010, pp. 1–4.

[25] A. Etxeberria, I. Vechiu, H. Camblong, and J. Vinassa, "Hybrid energy storage systems for renewable energy sources integration in microgrids: A review," in *IPEC 2010 Conference Proceedings*, 2010, pp. 532–537.

[26] A. Etxeberria, I. Vechiu, H. Camblong, and J.-M. Vinassa, "Comparison of three topologies and controls of a hybrid energy storage system for

microgrids," *Energy Conversion and Management*, vol. 54, no. 1, pp. 113–121, Feb. 2012. [Online]. Available: http://www.sciencedirect.com/science/article/pii/S0196890411002779

[27] J.-H. Jeon, J.-Y. Kim, S.-K. Kim, and J.-M. Kim, "Unified compensation control of a hybrid energy storage system for enhancing power quality and operation efficiency in a diesel and wind-turbine based stand-alone microgrid," in *Proceedings of The 3rd IEEE International Symposium on Power Electronics for Distributed Generation Systems (PEDG)*, 2012, pp. 264–270.

[28] B. Liu, F. Zhuo, and X. Bao, "Fuzzy control for hybrid energy storage system based on battery and ultra-capacitor in micro-grid," in *Proceedings of the 7th International Power Electronics and Motion Control Conference (IPEMC)*, vol. 2, 2012, pp. 778–782.

[29] L. Baoquan, Z. Fang, and B. Xianwen, "Control method of the transient compensation process of a hybrid energy storage system based on battery and ultra-capacitor in micro-grid," in *Proceedings of IEEE International Symposium on Industrial Electronics (ISIE)*, 2012, pp. 1325–1329.

[30] R. Kamel, A. Chaouachi, and K. Nagasaka, "Three control strategies to improve the microgrid transient dynamic response during isolated mode: A comparative study," *IEEE Trans. Ind. Electron.*, vol. 60, no. 4, pp. 1314–1322, Apr. 2013.

[31] L. Xiaoping, D. Ming, H. Jianghong, H. Pingping, and P. Yali, "Dynamic economic dispatch for microgrids including battery energy storage," in *Proceedings of 2nd IEEE International Symposium on Power Electronics for Distributed Generation Systems (PEDG)*, 2010, pp. 914–917.

[32] L. Wei, C. Guang-tang, and Q. Xiao-yan, "Optimal load distribution of microgrid including vanadium redox flow battery," in *Proceedings of Asia-Pacific Power and Energy Engineering Conference (APPEEC)*, 2012, pp. 1–4.

[33] M. Erickson and R. Lasseter, "Integration of battery energy storage element in a CERTS microgrid," in *Proceedings of IEEE Energy Conversion Congress and Exposition (ECCE)*, 2010, pp. 2570–2577.

[34] S. Mohammadi, B. Mozafari, S. Solimani, and T. Niknam, "An adaptive modified firefly optimisation algorithm based on hong's point estimate method to optimal operation management in a microgrid with consideration of uncertainties," *Energy*, vol. 51, no. 0, pp. 339–348, Mar. 2013. [Online]. Available: http://www.sciencedirect.com/science/article/pii/S0360544212009255

[35] D. Velasco de la Fuente, C. Rodríguez, G. Garcerá, E. Figueres, and R. Gonzalez, "Photovoltaic power system with battery backup with grid-connection and islanded operation capabilities," *IEEE Trans. Ind. Electron.*, vol. 60, no. 4, pp. 1571–1581, Apr. 2013.

[36] A. Chaouachi, R. Kamel, R. Andoulsi, and K. Nagasaka, "Multiobjective intelligent energy management for a microgrid," *IEEE Trans. Ind. Electron.*, vol. 60, no. 4, pp. 1688–1699, Apr. 2013.

[37] S. Bando, Y. Sasaki, H. Asano, and S. Tagami, "Balancing control method of a microgrid with intermittent renewable energy generators and small battery storage," in *Proceedings of the IEEE Power and Energy Society General Meeting*

- *Conversion and Delivery of Electrical Energy in the 21st Century*, 2008, pp. 1–6.

[38] F. Mohamed and H. Koivo, "Online management of MicroGrid with battery storage using multiobjective optimization," in *Proceedings of International Conference onPower Engineering, Energy and Electrical Drives. POWERENG.*, 2007, pp. 231–236.

[39] M. I. Marei and M. H. Soliman, "A coordinated voltage and frequency control of inverter based distributed generation and distributed energy storage system for autonomous microgrids," *Electric Power Components and Systems*, vol. 41, no. 4, pp. 383–400, Jan. 2013. [Online]. Available: http://dx.doi.org/10.1080/15325008.2012.749550

[40] Y. Levron, J. M. Guerrero, and Y. Beck, "Optimal power flow in microgrids with energy storage," *IEEE Trans. Power Syst.*, vol. PP, no. 99, pp. 1–9, 2013.

[41] L. Xu and D. Chen, "Control and operation of a DC microgrid with variable generation and energy storage," *IEEE Trans. Power Del.*, vol. 26, no. 4, pp. 2513–2522, Oct. 2011.

[42] J. Vasiljevska, J. Peças Lopes, and M. Matos, "Integrated micro-generation, load and energy storage control functionality under the multi micro-grid concept," *Electric Power Systems Research*, vol. 95, no. 0, pp. 292–301, Feb. 2013. [Online]. Available: http://www.sciencedirect.com/science/article/pii/S0378779612002969

[43] J.-Y. Kim, J.-H. Jeon, S.-K. Kim, C. Cho, J.-H. Park, H.-M. Kim, and K.-Y. Nam, "Cooperative control strategy of energy storage system and microsources for stabilizing the microgrid during islanded operation," *IEEE Trans. Power Electron.*, vol. 25, no. 12, pp. 3037–3048, Dec. 2010.

[44] H. Zhou, T. Bhattacharya, D. Tran, T. Siew, and A. Khambadkone, "Composite energy storage system involving battery and ultracapacitor with dynamic energy management in microgrid applications," *IEEE Trans. Power Electron.*, vol. 26, no. 3, pp. 923–930, Mar. 2011.

[45] A. A. Moghaddam, A. Seifi, T. Niknam, and M. R. Alizadeh Pahlavani, "Multi-objective operation management of a renewable MG (micro-grid) with back-up micro-turbine/fuel cell/battery hybrid power source," *Energy*, vol. 36, no. 11, pp. 6490–6507, Nov. 2011. [Online]. Available: http://www.sciencedirect.com/science/article/pii/S0360544211006141

[46] M. Molina and P. Mercado, "Power flow stabilization and control of microgrid with wind generation by superconducting magnetic energy storage," *IEEE Trans. Power Electron.*, vol. 26, no. 3, pp. 910–922, Mar. 2011.

[47] S. Manfredi, M. Pagano, and R. Raimo, "Ultracapacitor-based distributed energy resources to support time-varying smart-grid power flows," in *Proceedings of International Symposium on Power Electronics, Electrical Drives, Automation and Motion (SPEEDAM)*, 2012, pp. 1148–1153.

[48] H. Kanchev, D. Lu, F. Colas, V. Lazarov, and B. Francois, "Energy management and operational planning of a microgrid with a PV-Based active generator

for smart grid applications," *IEEE Trans. Ind. Electron.*, vol. 58, no. 10, pp. 4583–4592, Oct. 2011.

[49] J. Liang and C. Feng, "Stability improvement of micro-grids with coordinate control of fuel cell and ultracapacitor," in *Proceedings of IEEE Power Electronics Specialists Conference. PESC 2007.*, 2007, pp. 2472–2477.

[50] J. Guerrero, M. Chandorkar, T. Lee, and P. Loh, "Advanced control architectures for intelligent MicrogridsPart i: Decentralized and hierarchical control," *IEEE Trans. Ind. Electron.*, vol. 60, no. 4, pp. 1254–1262, Apr. 2013.

[51] J. Guerrero, P. C. Loh, T.-L. Lee, and M. Chandorkar, "Advanced control architectures for intelligent MicrogridsPart II: power quality, energy storage, and AC/DC microgrids," *IEEE Trans. Ind. Electron.*, vol. 60, no. 4, pp. 1263–1270, Apr. 2013.

[52] A. K. Srivastava, B. Annabathina, and S. Kamalasadan, "The challenges and policy options for integrating plug-in hybrid electric vehicle into the electric grid," *The Electricity Journal*, vol. 23, no. 3, pp. 83–91, Apr. 2010. [Online]. Available: http://www.sciencedirect.com/science/article/pii/S1040619010000606

[53] B. K. Sovacool and R. F. Hirsh, "Beyond batteries: An examination of the benefits and barriers to plug-in hybrid electric vehicles (PHEVs) and a vehicle-to-grid (V2G) transition," *Energy Policy*, vol. 37, no. 3, pp. 1095–1103, Mar. 2009. [Online]. Available: http://www.sciencedirect.com/science/article/pii/S0301421508005934

[54] S. J. Skerlos and J. J. Winebrake, "Targeting plug-in hybrid electric vehicle policies to increase social benefits," *Energy Policy*, vol. 38, no. 2, pp. 705–708, Feb. 2010. [Online]. Available: http://www.sciencedirect.com/science/article/pii/S030142150900843X

[55] S. Huang, B.-M. S. Hodge, F. Taheripour, J. F. Pekny, G. V. Reklaitis, and W. E. Tyner, "The effects of electricity pricing on PHEV competitiveness," *Energy Policy*, vol. 39, no. 3, pp. 1552–1561, Mar. 2011. [Online]. Available: http://www.sciencedirect.com/science/article/pii/S0301421510009298

[56] D. M. Hill, A. S. Agarwal, and F. Ayello, "Fleet operator risks for using fleets for V2G regulation," *Modeling Transport (Energy) Demand and Policies*, vol. 41, no. 0, pp. 221–231, Feb. 2012. [Online]. Available: http://www.sciencedirect.com/science/article/pii/S030142151100824X

[57] S.-L. Andersson, A. Elofsson, M. Galus, L. Gransson, S. Karlsson, F. Johnsson, and G. Andersson, "Plug-in hybrid electric vehicles as regulating power providers: Case studies of sweden and germany," *Energy Policy: The Role of Trust in Managing Uncertainties in the Transition to a Sustainable Energy Economy, Special Section with Regular Papers*, vol. 38, no. 6, pp. 2751–2762, Jun. 2010. [Online]. Available: http://www.sciencedirect.com/science/article/pii/S0301421510000121

[58] W. Kempton and J. Tomić, "Vehicle-to-grid power fundamentals: Calculating capacity and net revenue," *Journal of Power Sources*, vol. 144, no. 1, pp. 268–279, Jun. 2005. [Online]. Available: http://www.sciencedirect.com/science/article/pii/S0378775305000352

[59] W. Kempton and J. Tomic, "Vehicle-to-grid power implementation: From stabilizing the grid to supporting large-scale renewable energy," *Journal of Power Sources*, vol. 144, no. 1, pp. 280–294, Jun. 2005. [Online]. Available: http://www.sciencedirect.com/science/article/pii/S0378775305000212

[60] M. D. Galus, M. Zima, and G. Andersson, "On integration of plug-in hybrid electric vehicles into existing power system structures," *Energy Efficiency Policies and Strategies with regular papers.*, vol. 38, no. 11, pp. 6736–6745, Nov. 2010. [Online]. Available: http://www.sciencedirect.com/science/article/pii/S0301421510005070

[61] J. Lopes, F. Soares, and P. Almeida, "Integration of electric vehicles in the electric power system," *Proceedings of the IEEE*, vol. 99, no. 1, pp. 168–183, Jan. 2011.

[62] J. Peças Lopes, P. Almeida, and F. Soares, "Using vehicle-to-grid to maximize the integration of intermittent renewable energy resources in islanded electric grids," in *Proceedings of International Conference on Clean Electrical Power*, 2009, pp. 290–295.

[63] D. Benzai and W. Zhiqiang, "Research on electric-vehicle charging station technologies based on smart grid," in *Proceedings of Asia-Pacific Power and Energy Engineering Conference (APPEEC)*, 2011, pp. 1–4.

[64] C. Silva, M. Ross, and T. Farias, "Evaluation of energy consumption, emissions and cost of plug-in hybrid vehicles," *Energy Conversion and Management*, vol. 50, no. 7, pp. 1635–1643, Jul. 2009. [Online]. Available: http://www.sciencedirect.com/science/article/pii/S0196890409001186

[65] R. C. Green II, L. Wang, and M. Alam, "The impact of plug-in hybrid electric vehicles on distribution networks: A review and outlook," *Renewable and Sustainable Energy Reviews*, vol. 15, no. 1, pp. 544–553, Jan. 2011. [Online]. Available: http://www.sciencedirect.com/science/article/pii/S1364032110002674

[66] K. Clement-Nyns, E. Haesen, and J. Driesen, "The impact of vehicle-to-grid on the distribution grid," *Electric Power Systems Research*, vol. 81, no. 1, pp. 185–192, Jan. 2011. [Online]. Available: http://www.sciencedirect.com/science/article/pii/S0378779610002063

[67] R. Sioshansi, R. Fagiani, and V. Marano, "Cost and emissions impacts of plug-in hybrid vehicles on the ohio power system," *Energy Policy: Energy Efficiency Policies and Strategies with regular papers.*, vol. 38, no. 11, pp. 6703–6712, Nov. 2010. [Online]. Available: http://www.sciencedirect.com/science/article/pii/S0301421510005045

[68] C. Quinn, D. Zimmerle, and T. H. Bradley, "The effect of communication architecture on the availability, reliability, and economics of plug-in hybrid electric vehicle-to-grid ancillary services," *Journal of Power Sources*, vol. 195, no. 5, pp. 1500–1509, Mar. 2010. [Online]. Available: http://www.sciencedirect.com/science/article/pii/S0378775309015195

[69] J. Pillai and B. Bak-Jensen, "Integration of vehicle-to-grid in the western danish power system," *IEEE Trans. Sustain. Energy*, vol. 2, no. 1, pp. 12–19, Jan. 2011.

[70] C. Guille and G. Gross, "A conceptual framework for the vehicle-to-grid (V2G) implementation," *Energy Policy*, vol. 37, no. 11, pp. 4379–4390, Nov.

2009. [Online]. Available: http://www.sciencedirect.com/science/article/pii/S0301421509003978

[71] S. Han, S. Han, and K. Sezaki, "Development of an optimal vehicle-to-grid aggregator for frequency regulation," *IEEE Trans. Smart Grid*, vol. 1, no. 1, pp. 65–72, Jun. 2010.

[72] M. Shafie-khah, M. Parsa Moghaddam, M. K. Sheikh-El-Eslami, and M. Rahmani-Andebili, "Modeling of interactions between market regulations and behavior of plug-in electric vehicle aggregators in a virtual power market environment," *Energy*, vol. 40, no. 1, pp. 139–150, Apr. 2012. [Online]. Available: http://www.sciencedirect.com/science/article/pii/S0360544212001144

[73] B. Lunz, Z. Yan, J. B. Gerschler, and D. U. Sauer, "Influence of plug-in hybrid electric vehicle charging strategies on charging and battery degradation costs," *Energy Policy*, vol. 46, no. 0, pp. 511–519, Jul. 2012. [Online]. Available: http://www.sciencedirect.com/science/article/pii/S0301421512003175

[74] S. B. Peterson, J. Apt, and J. Whitacre, "Lithium-ion battery cell degradation resulting from realistic vehicle and vehicle-to-grid utilization," *Journal of Power Sources*, vol. 195, no. 8, pp. 2385–2392, Apr. 2010. [Online]. Available: http://www.sciencedirect.com/science/article/pii/S0378775309017443

[75] C. Weiller, "Plug-in hybrid electric vehicle impacts on hourly electricity demand in the united states," *Energy Policy*, vol. 39, no. 6, pp. 3766–3778, Jun. 2011. [Online]. Available: http://www.sciencedirect.com/science/article/pii/S0301421511002886

[76] S. Vachirasricirikul and I. Ngamroo, "Robust controller design of heat pump and plug-in hybrid electric vehicle for frequency control in a smart microgrid based on specified-structure mixed H2/H∞ control technique," *Applied Energy*, vol. 88, no. 11, pp. 3860–3868, Nov. 2011. [Online]. Available: http://www.sciencedirect.com/science/article/pii/S0306261911002911

[77] S. Vachirasricirikul and I. Ngamroo, "Robust controller design of microturbine and electrolyzer for frequency stabilization in a microgrid system with plug-in hybrid electric vehicles," *International Journal of Electrical Power & Energy Systems*, vol. 43, no. 1, pp. 804–811, Dec. 2012. [Online]. Available: http://www.sciencedirect.com/science/article/pii/S0142061512002918

[78] I. Cvetkovic, T. Thacker, D. Dong, G. Francis, V. Podosinov, D. Boroyevich, F. Wang, R. Burgos, G. Skutt, and J. Lesko, "Future home uninterruptible renewable energy system with vehicle-to-grid technology," in *Proceedings of IEEE Energy Conversion Congress and Exposition. ECCE 2009.*, 2009, pp. 2675–2681.

[79] P. Venkataraman, *Applied Optimization with MATLAB Programming.* John Wiley & Sons, 2009.

[80] J. W. Chinneck, *Practical Optimization: A Gentle Introduction.* [Online]. Available: http://www.sce.carleton.ca/faculty/chinneck/po.html

[81] I. Maros, *Computational Techniques of the Simplex Method.* Kluwer Academic Publishers, 2003. [Online]. Available: http://books.google.ca/books?id=dnwWBcKaBRsC

[82] N. Karmarkar, "A new polynomial-time algorithm for linear programming," *Combinatorica*, vol. 4, no. 4, pp. 373–395, Dec. 1984. [Online]. Available: http://dx.doi.org/10.1007/BF02579150

[83] "Branch-and-bound methods: A survey," *Operations Research*, vol. 14, no. 4, pp. 699–719, 1966. [Online]. Available: http://dx.doi.org/10.1287/opre.14.4.699

[84] S. Boyd and L. Vandenberghe, *Convex optimization*. Cambridge university press, 2004.

[85] X. Liu, P. Wang, and P. C. Loh, "A hybrid AC/DC microgrid and its coordination control," *IEEE Trans. Smart Grid*, vol. 2, no. 2, pp. 278–286, Jun. 2011.

[86] S. Dasgupta, S. Mohan, S. Sahoo, and S. Panda, "A plug and play operational approach for implementation of an autonomous-micro-grid system," *IEEE Trans. Ind. Informat.*, vol. 8, no. 3, pp. 615–629, Aug. 2012.

[87] S. Thale and V. Agarwal, "Controller area network (CAN) based smart protection scheme for solar PV, fuel cell, ultra-capacitor and wind energy system based microgrid," in *Proceedings of 38th IEEE Photovoltaic Specialists Conference (PVSC)*, 2012, pp. 000 580–000 585.

[88] M. G. Bosman, V. Bakker, A. Molderink, J. L. Hurink, and G. J. Smit, "Controlling a group of microchps: planning and realization," in *First International Conference on Smart Grids, Green Communications and IT Energy-aware Technologies, ENERGY 2011*. International Academy,

Research, and Industry Association, May 2011, pp. 179–184. [Online]. Available: http://doc.utwente.nl/78083/

[89] G. K. Venayagamoorthy, K. Rohrig, and I. Erlich, "One step ahead," *IEEE Power and Energy Magazine*, pp. 70–78, Oct. 2012.

[90] G. Kyriakarakos, D. D. Piromalis, A. I. Dounis, K. G. Arvanitis, and G. Papadakis, "Intelligent demand side energy management system for autonomous polygeneration microgrids," *Applied Energy*, vol. 103, no. 0, pp. 39–51, Mar. 2013. [Online]. Available: http://www.sciencedirect.com/science/article/pii/S0306261912007155

[91] C.-X. Dou and B. Liu, "Multi-agent based hierarchical hybrid control for smart microgrid," *IEEE Trans. Smart Grid*, vol. PP, no. 99, pp. 1–8, 2013.

[92] F. Delfino, R. Minciardi, F. Pampararo, and M. Robba, "A multilevel approach for the optimal control of distributed energy resources and storage," *IEEE Trans. Smart Grid*, vol. 5, no. 4, pp. 2155–2162, Jul. 2014.

[93] Y. Zhang, N. Gatsis, and G. Giannakis, "Robust energy management for microgrids with high-penetration renewables," *IEEE Trans. Sustain. Energy*, vol. 4, no. 4, pp. 944–953, Oct. 2013.

[94] M. Beaudin, H. Zareipour, A. Bejestani, and A. Schellenberg, "Residential energy management using a two-horizon algorithm," *IEEE Trans. Smart Grid*, vol. 5, no. 4, pp. 1712–1723, Jul. 2014.

[95] A. Fakhrazari, H. Vakilzadian, and F. Choobineh, "Optimal energy scheduling for a smart entity," *IEEE Trans. Smart Grid*, vol. 5, no. 6, pp. 2919–2928, Nov. 2014.

[96] P. Malysz, S. Sirouspour, and A. Emadi, "An optimal energy storage control strategy for grid-connected microgrids," *IEEE Trans. Smart Grid*, vol. 5, no. 4, pp. 1785–1796, July 2014.

[97] X. Guan, Z. Xu, and Q. Jia, "Energy-efficient buildings facilitated by microgrid," *IEEE Trans. Smart Grid*, vol. 1, no. 3, pp. 243–252, Dec. 2010.

[98] W. Su, J. Wang, and J. Roh, "Stochastic energy scheduling in microgrids with intermittent renewable energy resources," *IEEE Trans. Smart Grid*, vol. 5, no. 4, pp. 1876–1883, Jul. 2014.

[99] L. Igualada, C. Corchero, M. Cruz-Zambrano, and F.-J. Heredia, "Optimal energy management for a residential microgrid including a vehicle-to-grid system," *IEEE Trans. Smart Grid*, vol. 5, no. 4, pp. 2163–2172, Jul. 2014.

[100] L. Zhu, F. Yu, B. Ning, and T. Tang, "Optimal charging control for electric vehicles in smart microgrids with renewable energy sources," in *Proc. IEEE 75th VTC, Spring 2012*, Yokohama, May 2012, pp. 1–5.

[101] M. Tushar, C. Assi, M. Maier, and M. Uddin, "Smart microgrids: Optimal joint scheduling for electric vehicles and home appliances," *IEEE Trans. Smart Grid*, vol. 5, no. 1, pp. 239–250, Jan. 2014.

[102] J. Tan and L. Wang, "Integration of plug-in hybrid electric vehicles into residential distribution grid based on two-layer intelligent optimization," *IEEE Trans. Smart Grid*, vol. 5, no. 4, pp. 1774–1784, Jul. 2014.

[103] H. Liang, B. Choi, W. Zhuang, and X. Shen, "Optimizing the energy delivery via V2G systems based on stochastic inventory theory," *IEEE Trans. Smart Grid*, vol. 4, no. 4, pp. 2230–2243, Dec. 2013.

[104] M. Zhang and J. Chen, "The energy management and optimized operation of electric vehicles based on microgrid," *IEEE Trans. Power Del.*, vol. 29, no. 3, pp. 1427–1435, Jun. 2014.

[105] E. Sortomme and M. El-Sharkawi, "Optimal scheduling of vehicle-to-grid energy and ancillary services," *IEEE Trans. Smart Grid*, vol. 3, no. 1, pp. 351–359, Mar. 2012.

[106] M. Shaaban, M. Ismail, E. El-Saadany, and W. Zhuang, "Real-time pev charging/discharging coordination in smart distribution systems," *IEEE Trans. Smart Grid*, vol. 5, no. 4, pp. 1797–1807, Jul. 2014.

[107] Y. He, B. Venkatesh, and L. Guan, "Optimal scheduling for charging and discharging of electric vehicles," *IEEE Trans. Smart Grid*, vol. 3, no. 3, pp. 1095–1105, Sep. 2012.

[108] G. Calafiore and M. Campi, "The scenario approach to robust control design," *IEEE Trans. Autom. Control*, vol. 51, no. 5, pp. 742–753, May 2006.

[109] K. Margellos, P. Goulart, and J. Lygeros, "On the road between robust optimization and the scenario approach for chance constrained optimization problems," *IEEE Trans. Autom. Control*, vol. 59, no. 8, pp. 2258–2263, Aug. 2014.

[110] A. Nemirovski and A. Shapiro, "Scenario approximations of chance constraints," in *Probabilistic and Randomized Methods for Design under Uncertainty*, G. Calafiore and F. Dabbene, Eds. Springer London, 2006, pp. 3–47.

[111] B. Pagnoncelli, S. Ahmed, and A. Shapiro, "Sample average approximation method for chance constrained programming: Theory and applications," *J. Optimization Theory Appl.*, vol. 142, no. 2, pp. 399–416, 2009.

[112] M. Branda, "Sample approximation technique for mixed-integer stochastic programming problems with several chance constraints," *Operations Res. Lett.*, vol. 40, no. 3, pp. 207 – 211, 2012.

[113] S. Tarim, S. Manandhar, and T. Walsh, "Stochastic constraint programming: A scenario-based approach," *Constraints*, vol. 11, no. 1, pp. 53–80, 2006.

[114] L. Blackmore, M. Ono, A. Bektassov, and B. Williams, "A probabilistic particle-control approximation of chance-constrained stochastic predictive control," *IEEE Trans. Robot.*, vol. 26, no. 3, pp. 502–517, Jun. 2010.

[115] H. Zhang and P. Li, "Chance constrained programming for optimal power flow under uncertainty," *IEEE Trans. Power Syst.*, vol. 26, no. 4, pp. 2417–2424, Nov. 2011.

[116] D. Bienstock, M. Chertkov, and S. Harnett, "Chance-constrained optimal power flow: Risk-aware network control under uncertainty," *SIAM Rev.*, vol. 56, no. 3, pp. 461–495, 2014.

[117] M. Vrakopoulou, K. Margellos, J. Lygeros, and G. Andersson, "A probabilistic framework for reserve scheduling and n-1 security assessment of systems with high wind power penetration," *IEEE Trans. Power Syst.*, vol. 28, no. 4, pp. 3885–3896, Nov. 2013.

[118] KYOCERA to start exclusive sales in japan of new residential-use energy management system combining solar power with li-ion battery storage unit. [Online]. Available: http://global.kyocera.com/news/2012/0102_qpaq.html

[119] vehicle to home electricity supply system | NISSAN | TECHNOLOGICAL DEVELOPMENT ACTIVITIES. [Online]. Available: http://www.nissan-global.com/EN/TECHNOLOGY/OVERVIEW/vehicle_to_home.html

[120] DENSO develops vehicle-to-home power supply system for electric vehicles. [Online]. Available: http://www.densocorp-na.com/newsroom/show/id/433

[121] Energy solutions for homes | panasonic's solutions | panasonic. [Online]. Available: http://panasonic.net/es/solution-works/HouseEnergy/

[122] Eatons smart energy management could be a mid-market winner. [Online]. Available: http://greentechadvocates.com/2011/09/14/eaton%E2%80%99s-smart-energy-management-could-be-a-mid-market-winner/

[123] Energy management systems: Intel powers smart grid efficiency. [Online]. Available: http://www.intel.

com/content/www/us/en/intelligent-systems/energy-applications/energy-management-systems-intel-powers-smart-grid-efficiency.html

[124] Nest | the learning thermostat | home. [Online]. Available: http://www.nest.com/

[125] Nokia-Siemens, "Zero CO2 off-grid solution for e-plus," *White Paper*, 2011. [Online]. Available: http://www.nokiasiemensnetworks.com/sites/default/files/document/en_zero_co2_site_solution_for_e-plus_-_whitepaper_versmold_1.3.pdf

[126] Lockheed martin intelligent microgrid solutions. [Online]. Available: http://www.lockheedmartin.com/us/products/intelligentmicrogridsolutions.html

[127] ENBALA | demand-side energy management. [Online]. Available: http://www.enbala.com/

[128] Learn more | vivint smart home security systems. [Online]. Available: http://www.vivint.com/en/company/about-us

[129] Energy management: Save money & energy with alarm.com. [Online]. Available: http://www.alarm.com/productservices/energy_management.aspx

[130] Demand response - utility demand side management. [Online]. Available: https://opower.com/products/demand-response/

[131] Icontrol networks. [Online]. Available: https://www.icontrol.com

[132] Tendril - changing the way the world uses energy. [Online]. Available: //www.tendrilinc.com/

[133] C. Yuen and A. Oudalov, "The feasibility and profitability of ancillary services provision from multi-MicroGrids," in *Proceedings of IEEE Power Tech, Lausanne*, 2007, pp. 598–603.

[134] J. Vasiljevska, J. Peas Lopes, and M. Matos, "Evaluating the impacts of the multi-microgrid concept using multicriteria decision aid," *Electric Power Systems Research*, vol. 91, no. 0, pp. 44–51, Oct. 2012. [Online]. Available: http://www.sciencedirect.com/science/article/pii/S037877961200123X

[135] C. Yuen, A. Oudalov, and A. Timbus, "The provision of frequency control reserves from multiple microgrids," *IEEE Trans. Ind. Electron.*, vol. 58, no. 1, pp. 173–183, Jan. 2011.

[136] N. J. Gil and J. P. Lopes, "Exploiting automated demand response, generation and storage capabilities for hierarchical frequency control in islanded multi-microgrids," in *Proceedings of PSCC2008, 16th Power System Computation Conference, Glasgow, Scotland*, 2008. [Online]. Available: http://www.pscc-central.org/uploads/tx_ethpublications/pscc2008_66.pdf

[137] D. Rua, L. Pereira, N. Gil, and J. Lopes, "Impact of multi-microgrid communication systems in islanded operation," in *Proceedings of 2nd IEEE PES International Conference and Exhibition on Innovative Smart Grid Technologies (ISGT Europe)*, 2011, pp. 1–6.

[138] H. Dagdougui, R. Minciardi, A. Ouammi, and R. Sacile, "Optimal control of a regional power microgrid network driven by wind and solar energy," in *Proceedings of IEEE International Systems Conference (SysCon)*, 2011, pp. 86–90.

[139] M. Sofla and R. King, "Control method for multi-microgrid systems in smart grid environmentStability, optimization and smart demand participation," in *Proceedings of IEEE PES Innovative Smart Grid Technologies (ISGT)*, 2012, pp. 1–5.

[140] W. Shi, X. Xie, C.-C. Chu, and R. Gadh, "Distributed optimal energy management in microgrids," *IEEE Trans. Smart Grid*, vol. 6, no. 3, pp. 1137–1146, May 2015.

[141] W. Shi, N. Li, C.-C. Chu, and R. Gadh, "Real-time energy management in microgrids," *IEEE Trans. Smart Grid*, pp. 1–1, 2015.

[142] C. Wouters, E. S. Fraga, and A. M. James, "An energy integrated, multi-microgrid, MILP (mixed-integer linear programming) approach for residential distributed energy system planning a south australian case-study," *Energy*, vol. 85, pp. 30–44, Jun. 2015.

[143] E. Ng and R. El-Shatshat, "Multi-microgrid control systems (MMCS)," in *Proceedings of IEEE Power and Energy Society General Meeting*, 2010, pp. 1–6.

[144] A. Dimeas and N. Hatziargyriou, "Operation of a multiagent system for microgrid control," *IEEE Trans. Power Syst.*, vol. 20, no. 3, pp. 1447–1455, Aug. 2005.

[145] H. Kumar Nunna and S. Doolla, "Multiagent-based distributed-energy-resource management for intelligent microgrids," *IEEE Trans. Ind. Electron.*, vol. 60, no. 4, pp. 1678–1687, Apr. 2013.

[146] Y. Chen and J. Chang, "EMaaS: Cloud-Based Energy Management Service for Distributed Renewable Energy Integration," *IEEE Trans. Smart Grid*, vol. 6, no. 6, pp. 2816–2824, Nov. 2015.

[147] A. Ouammi, H. Dagdougui, L. Dessaint, and R. Sacile, "Coordinated Model Predictive-Based Power Flows Control in a Cooperative Network of Smart Microgrids," *IEEE Trans. Smart Grid*, vol. 6, no. 5, pp. 2233–2244, Sep. 2015.

[148] N. Nikmehr and S. Ravadanegh, "Optimal Power Dispatch of Multi-Microgrids at Future Smart Distribution Grids," *IEEE Trans. Smart Grid*, vol. 6, no. 4, pp. 1648–1657, Jul. 2015.

[149] W. Chiu, H. Sun, and H. Poor, "A Multiobjective Approach to Multimicrogrid System Design," *IEEE Trans. Smart Grid*, vol. 6, no. 5, pp. 2263–2272, Sep. 2015.

[150] K. Rahbar, C. C. Chai, and R. Zhang, "Real-time energy management for cooperative microgrids with renewable energy integration." Proceedings of the IEEE International Conference on Smart Grid Communications (SmartGridComm), Nov. 2014, pp. 25–30.

[151] X. Wang, X. Qiu, R. Jiang, D. Li, G. Wang, and L. Qian, "Economic operation of multi-microgrids containing energy storage system." Proceedings of International Conference on Power Systems Technology, Oct. 2014, pp. 1712–1716.

[152] S. Manshadi and M. Khodayar, "Resilient Operation of Multiple Energy Carrier Microgrids," *IEEE Trans. Smart Grid*, vol. 6, no. 5, pp. 2283–2292, Sep. 2015.

[153] Z. Wang, B. Chen, J. Wang, and J. kim, "Decentralized energy management system for networked microgrids in grid-connected and islanded modes," *IEEE Trans. Smart Grid*, vol. 7, no. 2, pp. 1097–1105, Mar. 2016.

[154] Z. Wang, B. Chen, J. Wang, M. M. Begovic, and C. Chen, "Coordinated energy management of networked microgrids in distribution systems," *IEEE Trans. Smart Grid*, vol. 6, no. 1, pp. 45–53, Jan. 2015.

[155] L. Che, M. Shahidehpour, A. Alabdulwahab, and Y. Al-Turki, "Hierarchical coordination of a community microgrid with AC and DC microgrids," *IEEE Trans. Smart Grid*, vol. 6, no. 6, pp. 3042–3051, Nov. 2015.

[156] S. Belhaiza and U. Baroudi, "A Game Theoretic Model for Smart Grids Demand Management," *IEEE Trans. Smart Grid*, vol. 6, no. 3, pp. 1386–1393, May 2015.

[157] A. Sheikhi, M. Rayati, S. Bahrami, and A. Ranjbar, "Integrated Demand Side Management Game in Smart Energy Hubs," *IEEE Trans. Smart Grid*, vol. 6, no. 2, pp. 675–683, Mar. 2015.

[158] L. Du, S. Grijalva, and R. Harley, "Game-Theoretic Formulation of Power Dispatch With Guaranteed Convergence and Prioritized BestResponse," *IEEE Trans. Sustain. Energy*, vol. 6, no. 1, pp. 51–59, Jan. 2015.

[159] M. Mahmoodi, P. Shamsi, and B. Fahimi, "Economic Dispatch of a Hybrid Microgrid With Distributed Energy Storage," *IEEE Trans. Smart Grid*, vol. 6, no. 6, pp. 2607–2614, Nov. 2015.

[160] K. Worthmann, C. Kellett, P. Braun, L. Grune, and S. Weller, "Distributed and Decentralized Control of Residential Energy Systems Incorporating Battery Storage," *IEEE Trans. Smart Grid*, vol. 6, no. 4, pp. 1914–1923, Jul. 2015.

[161] A. Werth, N. Kitamura, and K. Tanaka, "Conceptual Study for Open Energy Systems: Distributed Energy Network Using Interconnected DC Nanogrids," *IEEE Trans. Smart Grid*, vol. 6, no. 4, pp. 1621–1630, Jul. 2015.

[162] Mou, Y., Xing, H., Lin, Z., and Fu, M., "Decentralized Optimal Demand-Side Management for PHEV Charging in a Smart Grid," *IEEE Trans. Smart Grid*, vol. 6, no. 2, pp. 726–736, Mar. 2015.

[163] H. Lu, M. Zhang, Z. Fei, and K. Mao, "Multi-Objective Energy Consumption Scheduling in Smart Grid Based on Tchebycheff Decomposition," *IEEE Trans. Smart Grid*, vol. 6, no. 6, pp. 2869–2883, Nov. 2015.

[164] A. Sharma, D. Srinivasan, and A. Trivedi, "A Decentralized Multiagent System Approach for Service Restoration Using DG Islanding," *IEEE Trans. Smart Grid*, vol. 6, no. 6, pp. 2784–2793, Nov. 2015.

[165] P. McNamara and S. McLoone, "Hierarchical Demand Response for Peak Minimization Using DantzigWolfe Decomposition," *IEEE Trans. Smart Grid*, vol. 6, no. 6, pp. 2807–2815, Nov. 2015.

[166] L. J.H. and C. Chu, "Iterative Distributed Algorithms for Real-Time Available Transfer Capability Assessment of Multiarea Power Systems," *IEEE Trans. Smart Grid*, vol. 6, no. 5, pp. 2569–2578, Sep. 2015.

[167] P. Srikantha and D. Kundur, "Distributed Optimization of Dispatch in Sustainable Generation Systems via Dual Decomposition," *IEEE Trans. Smart Grid*, vol. 6, no. 5, pp. 2501–2509, Sep. 2015.

[168] I. Khan, Z. Li, Y. Xu, and W. Gu, "Distributed control algorithm for optimal reactive power control in power grids," *International Journal of Electrical Power & Energy Systems*, vol. 83, pp. 505–513, Dec. 2016.

[169] H. Nguyen, A. Khodaei, and Z. Han, "A big data scale algorithm for optimal scheduling of integrated microgrids," *IEEE Trans. Smart Grid*, pp. 1–1, 2016.

[170] J. Wu and X. Guan, "Coordinated multi-microgrids optimal control algorithm for smart distribution management system," *IEEE Trans. Smart Grid*, vol. 4, no. 4, pp. 2174–2181, Dec. 2013.

[171] W.-J. Ma, J. Wang, V. Gupta, and C. Chen, "Distributed energy management for networked microgrids using online alternating direction method of multipliers with regret," *IEEE Trans. Smart Grid*, pp. 1–1, 2016.

[172] S.-C. Tsai, Y.-H. Tseng, and T.-H. Chang, "Communication-efficient distributed demand response: A randomized ADMM approach," *IEEE Trans. Smart Grid*, pp. 1–1, 2015.

[173] R. Verschae, H. Kawashima, T. Kato, and T. Matsuyama, "Coordinated energy management for inter-community imbalance minimization," *Renewable Energy*, vol. 87, pp. 922–935, Mar. 2016.

[174] M. Doostizadeh, F. Aminifar, H. Lesani, and H. Ghasemi, "Multi-area market clearing in wind-integrated interconnected power systems: A fast parallel decentralized method," *Energy Conversion and Management*, vol. 113, pp. 131–142, Apr. 2016.

[175] G. Hug, S. Kar, and Wu, C, "Consensus + Innovations Approach for Distributed Multiagent Coordination in a Microgrid," *IEEE Trans. Smart Grid*, vol. 6, no. 4, pp. 1893–1903, Jul. 2015.

[176] Xu, Y., Zhang, W., G. Hug, S. Kar, and Li, Z., "Cooperative Control of Distributed Energy Storage Systems in a Microgrid," *IEEE Trans. Smart Grid*, vol. 6, no. 1, pp. 238–248, Jan. 2015.

[177] K. Meng, Z. Dong, Z. Xu, and S. Weller, "Cooperation-Driven Distributed Model Predictive Control for Energy Storage Systems," *IEEE Trans. Smart Grid*, vol. 6, no. 6, pp. 2583–2585, Nov. 2015.

[178] M. Ahmadi, J. Rosenberger, W.-J. Lee, and A. Kulvanitchaiyanunt, "Optimizing Load Control in a Collaborative Residential Microgrid Environment," *IEEE Trans. Smart Grid*, vol. 6, no. 3, pp. 1196–1207, May 2015.

[179] M. Fathi and H. Bevrani, "Statistical cooperative power dispatching in interconnected microgrids," *IEEE Trans. Sustain. Energy*, vol. 4, no. 3, pp. 586–593, Jul. 2013.

[180] "Canadian vehicle survey: Annual 2009," *Canadian social trends*, vol. 86, no. 1, p. 4957, 2010. [Online]. Available: http://www.statcan.gc.ca/pub/11-008-x/2008002/article/10689-eng.pdf

[181] R. Srinivasan, *Importance sampling: Applications in communications and detection*. Springer-Verlag Berlin Heidelberg, 2002.

[182] "Electricity prices," Ontario Energy Board, Ontario, Canada, 2014. [Online]. Available: http://www.ontarioenergyboard.ca/OEB/Consumers/Electricity/Electricity+Prices

[183] M. R. Sandgani and S. Sirouspour, "Energy management in a network of grid-connected microgrids/nanogrids using compromise programming," *IEEE Transactions on Smart Grid*, vol. PP, no. 99, pp. 1–1, 2016. [Online]. Available: http://ieeexplore.ieee.org/abstract/document/7563871/

[184] S. Boyd, N. Parikh, E. Chu, B. Peleato, and J. Eckstein, "Distributed optimization and statistical learning via the alternating direction method of multipliers," *Foundations and Trends in Machine Learning*, vol. 3, no. 1, pp. 1–122, 2011.